Title
High Transference Number Polymer-Based Electrolytes for Lithium Batteries

Author
Diederichsen, Kyle M

Publication Date
2019

Peer reviewed|Thesis/dissertation

High Transference Number Polymer-Based Electrolytes for Lithium Batteries

By

Kyle M. Diederichsen

A dissertation submitted in partial satisfaction
of the requirements for the degree of

Doctor of Philosophy

in

Chemical Engineering

in the

Graduate Division

of the

University of California, Berkeley

Committee Members

Professor Bryan McCloskey, Chair
Professor Susan Muller
Professor Nitash Balsara
Professor Kristin Persson

Summer 2019

High Transference Number Polymer-Based Electrolytes for Lithium Batteries

Abstract

High Transference Number Polymer-Based Electrolytes for Lithium Batteries

By

Kyle M. Diederichsen

Doctor of Philosophy in Chemical Engineering

University of California, Berkeley

Professor Bryan D. McCloskey, Chair

The composition of modern electrolytes is key to the performance of lithium ion batteries. State-of-the-art electrolytes are based on lithium hexafluorophosphate ($LiPF_6$) dissolved in a liquid carbonate solvent with stabilizing additives, which provide a sufficient combination of conductivity and stability towards the highly reactive electrode components. This electrolyte composition has been developed, and continues to evolve, to meet materials design and engineering requirements for high-performance energy storage, but work remains to enable the next generation of high energy density, fast charging batteries. While there are still challenges in electrode formulations and cell management, this dissertation focuses on an important remaining problem involving the electrolyte: concentration polarization as a result of the low lithium transference number (t_+) of the electrolyte. t_+ characterizes the relative motion of cations to anions within an electric field and is unity for an electrolyte where only lithium ions are mobile, and zero for the opposite case where only anions migrate. The standard liquid electrolyte discussed above has a transference number below 0.5, indicating the bulky anions move faster than lithium ions as a result of the large solvation shell of lithium ions. This high anion motion allows concentration gradients to form within a cell, limiting energy density and charge rates. In this dissertation, polymers are utilized in an effort to create higher transference number electrolytes by attaching the anion to the polymer backbone. This method has suffered from the key drawback of low conductivity for many years, and thus a primary concern of each section herein is improving electrolyte conductivity.

To study this class of electrolytes, initially a new polymer was synthesized based on polysulfone (PSF) condensation chemistry. This polymer allows incorporation of ion conducting poly(ethylene glycol) (PEG) segments, and ion containing sulfonate groups. This synthesis was an extension of existing sulfonated polysulfone and polysulfone-co-poly(ethylene glycol) polymers, but had never been combined into a single polymer before. This polymer, though not an ideal homogenous, low dispersity polymer, allows a wide range of compositions to be formed that could then be used in a variety of electrolytes.

In the first section, the wide accessible composition window of sulfonated PSF-co-PEG is employed to study the fundamentals of ion conduction in dry polymer electrolytes that have appended ions. Conductivity as a function of both PEG and sulfonate content is studied, demonstrating a tradeoff between ion content and segmental motion of the polymer backbone. This tradeoff has been observed in the past and typically in the literature is analyzed through the Vogel-Tammann-Fulcher (VTF) equation, a modified Arrhenius equation originally developed for polymer viscosity but also applied to conductivity. Here it is shown that careful fitting of this equation to conductivity data is crucial to interpret the results, and that a correlation may exist between the equation prefactor and activation energy. These parameters are usually fit to decouple the effects of ion content, related to the prefactor, and segmental motion, related to the activation

energy. This correlation was found to exist in other polymer systems and implies that this equation does not necessarily decouple these effects, complicating any analysis based on it. Further, this correlation implies that decreasing the activation energy will also decrease the prefactor, significantly limiting potential design changes to improve conductivity. Blending of a short chain PEG to the dry polymer system is found to break the correlation, further motivating this common conductivity enhancing technique.

Following this discovery, this dissertation transitions to liquid state polyelectrolyte solutions utilizing the same sulfonated PSF-co-PEG polymer. Here the polymers are dissolved in a solvent such that lithium motion may be completely disconnected from polymer segmental motion. These polymer solutions were only recently suggested for battery application, with most prior polyelectrolyte work confined to water. The work here represents the first efforts to transition polyelectrolyte solutions into battery-relevant carbonate solvents. Comparison is first made between a highly polar solvent, dimethylsulfoxide (DMSO) and a carbonate blend solvent. It is shown through NMR characterization of peak width and diffusion measurements that the lithium does not dissociate from the sulfonate group in the carbonate blend solvent even though the polymer is fully dissolved and the dielectric constant of the carbonate blend is the same as DMSO. This demonstrates that new theories which do not solely utilize the dielectric constant to dictate ion interactions in solution will be necessary to predict polyelectrolyte behavior in these nonaqueous solvents.

A further challenge in polyelectrolyte solution design for battery applications is that the vast majority of polyelectrolyte literature focuses mainly on the behavior of the polymer, particularly from a structure perspective. Design of an electrolyte must primarily take transport into account, and for a battery the primary interest is in fact the counterion transport. Existing theory must therefore be understood in a new light to inform rational design of future electrolytes. Here, a fundamental study of transport in polyelectrolyte solutions with multiple different molecular weight polymers and as a function of solvent quality is undertaken. Fully sulfonated polysulfone without PEG is employed here because it is soluble in both DMSO and water, where DMSO represents a good solvent for the backbone and ions, while water is only a good solvent for the ions. It is demonstrated that many of the fundamental theories of polyelectrolyte solutions hold for this previously unstudied system, despite the relatively short chains. By comparing the diffusion of counterions and solvent with the same data for solutions of the monomer alone, the effect of the polymeric anion can be determined. It is found that the presence of a good solvent for the backbone causes an additional slowing of the solvent and lithium in DMSO, as opposed to water. This is despite much higher viscosity in the water systems. From this, several recommendations for polyelectrolyte solution design are made.

Taking inspiration from the current state of the art electrolyte, the final work contained herein discusses the use of additives to improve ion dissociation and conductivity in the carbonate blend solvent used previously. It is shown that crown ethers, and particularly 15-crown-5, are capable of achieving an order of magnitude increase in solution conductivity with the sulfonated PSF-co-PEG previously employed. This conductivity is shown to be sufficient to fabricate a full battery with commercial lithium iron phosphate and graphite electrodes. With the optimized electrolyte, nearly 90% of the theoretical capacity is achieved, three times as high as without additives, demonstrating the potential of these new electrolytes.

Table of Contents

Abstract 1
Table of Contents i
List of Figures iv
List of Tables viii
Acknowledgements ix
1. Introduction 1
I. Drawbacks of Current Electrolytes 1
II. The Importance of a High Transference Number Electrolyte. 2
III. The Challenge of Measuring Transference Number. 3
IV. Strategies for the Development of a High Transference Number Electrolyte. 4
i. Ceramic-based single ion conductors 5
ii. Dry (Neat) Polymer Electrolytes 6
iii. Polymer electrolytes containing additives 7
iv. Swollen Ionomer Membranes 9
v. Liquid Electrolytes 10
V. Summary of Past Strategies for Increasing Transference Number 10
VI. Polyelectrolyte Solutions 10
VII. Outline of this Dissertation 13
2. Synthesis of Polysulfone-Based Polymers 15
I. Material Considerations 15
II. Reaction 16
III. NMR Characterization 17
3. The Compensation Effect in the Vogel – Tammann – Fulcher (VTF) Equation for Polymer-Based Electrolytes 20
I. Abstract 20
II. Introduction 20
III. Experimental Section 22
i. Materials 22
ii. Synthesis 22
iii. Ion Exchange 23
iv. Polymer Characterization 23
v. Polymer Blending 25
vi. Electrochemical Characterization 25
IV. Results and Discussion 26
V. Summary and Outlook 40

VI. Supporting Information 43
4. Investigation of Solvent Type and Salt Addition in High Transference Number Nonaqueous Polyelectrolyte Solutions for Lithium-Ion Batteries 45
I. Abstract 45
II. Introduction 45
III. Experimental Section 47
i. Materials 47
ii. Polymer Synthesis 47
iii. Solution Preparation 48
iv. Conductivity 48
v. Viscosity 48
vi. Pulse Field Gradient NMR 48
IV. Results and Discussion 50
V. Summary 61
VI. Supporting Information 62
5. Counterion and Solvent Transport in Nonaqueous and Aqueous Polyelectrolyte Solutions 63
I. Abstract 63
II. Introduction 63
III. Experimental Section 64
i. Materials 64
ii. Synthesis 65
iii. Polymer Characterization 65
iv. Solution Preparation 66
v. Conductivity 66
vi. Viscosity 67
vii. Diffusion Coefficients 67
IV. Results 68
V. Discussion 70
i. Scaling in DMSO-d_6 70
ii. Scaling in D_2O 75
iii. Comparison to Monomer 78
iv. Polyelectrolyte Solution Design 80
VI. Summary and Future Work 82
VII. Supporting Information 82
6. Electrolyte Additives to Enable Nonaqueous Polyelectrolyte Solutions for Lithium Ion Batteries 84
I. Abstract 84

II. Introduction 84
III. Experimental Section 85
i. Materials 85
ii. Solution Characterization 86
iii. Nuclear magnetic resonance spectroscopy (NMR) measurements 86
iv. Coin Cell Preparation 86
IV. Results and Discussion 86
V. Conclusions 91
7. Summary and Outlook 92
8. References 94

List of Figures

Figure 1.1. A) Illustration of concentration gradients as demonstrated originally by Fuller[17] B) Attainable state of change (SOC) versus charge rate for an electrolyte with σ=10 mS/cm and variable t_+ 3
Figure 1.2. Several classes of HTNE's. A) Ceramic SIC based on doped lithium thiophosphate glass, reproduced from Ref. 26 B) The neat polymer electrolyte poly(styrene trifluoromethane- sulphonylimide – co – poly(ethylene oxide), reproduced from Ref. 27 C) Mixed polymer electrolyte system based on nanoparticle/copolymer blend, reproduced from Ref. 28 D) Sketch of a solvent-filled ionomer membrane E) Sketch of a polyelectrolyte HTNE solution. 5
Figure 1.3. Conductivity of neat appended anion polymers versus the year published, the approximate magnitude of typical liquid, binary salt electrolyte conductivity is indicated. 7
Figure 2.1. Synthesis setup used for all polymerizations..... 16
Figure 2.2. ^{1}H NMR characterization of polysulfone, PSF-co-PEG (where 10% of the biphenol unit has been replaced by PEG of M_n=1000Da), and fully sulfonated polysulfone. .. 18
Figure 2.3. ^{1}H NMR Characterization in DMSO-d_6 of a series of sulfonated PSF-co-PEG, with a constant amount of PEG (70% of the biphenol replaced by PEG) and varying sulfonate content. 19
Figure 2.4. ^{1}H NMR Characterization in DMSO-d_6 of a series of sulfonated PSF-co-PEG, with a constant sulfonate content (10% of the sulfone monomer is sulfonated) and varying PEG content. 19
Figure 3.1. Thermogravimetric analysis on the polymers shown in Table 3.1 at a heating rate of 10 °C/min. Weight is normalized to the weight after drying at 100°C for 30 mins. a) Polymers with constant R_1 sulfonate mol% of 10 and b) polymers with constant R_2 PEG mol% of 70. 24
Figure 3.2. Representative dynamic scanning calorimetry (DSC) scans for three polymers at different sulfonate and PEG contents. 24
Figure 3.3. Custom Swagelok-type cell used for electrochemical measurements..... 25
Figure 3.4. Example Nyquist diagram for the sample with R_1=15 mol% sulfonate and R_2 = 100 mol% PEG during a heating scan from 30 to 110°C. 26
Figure 3.5. Glass transition temperature as a function of R_1 sulfonate mol% at a constant R_2 PEG mol% of 70 (bottom) and as a function of R_2 PEG mol% at a constant R_1 sulfonate mol% of 10% (top). Increasing PEG content drops the glass transition by ~300°C, while increasing sulfonate content increases the glass transition by ~100°C..... 28
Figure 3.6. Conductivity as a function of inverse temperature for a) increasing R_2 PEG mol% at a constant R_1 sulfonate mol% of ~10 and b) increasing R_1 sulfonate mol% at a constant R_2 PEG mol% of ~70. 29
Figure 3.7. a) Conductivity versus T-T_g for the series at an R_1 sulfonate mol% of ~10 with inset linecut at a T-T_g of 80°C. b) Conductivity versus T-T_g for the series at an R_2 PEG mol% of ~70 with inset linecut at a T-T_g of 70°C..... 30
Figure 3.8. a) VTF prefactor (A) versus R_1 sulfonate mol% for the fit routines outlined in Table 3.2. The legend in a) applies to b) and c), and the units on A are S/cm for Fit #1-2 and #4-5, and $S * K\hat{}(1/2)/cm$ for Fit #3 b) Sum Squared Residuals for the different fit

routines versus R_1 sulfonate mol%. c) $T_g - T_o$ versus R_1 sulfonate mol%, equivalent to 50°C for Fit #5 and T_g for Fit #1, but calculated from the fit for the other routines. . 33
Figure 3.9. Demonstration of the fits at low (a,c) and high (b,d) sulfonate mol%. 34
Figure 3.10. Natural log of the VTF prefactor versus the apparent activation energy for the dry PSf-co-PEG copolymers synthesized here, and blends with several of these copolymers and short chain PEG (M_n=300Da). Inset are the Arrhenius plots for conductivity versus inverse temperature of the two polymers circled (A – R_1 is 3 mol% sulfonated, R_2 is 66mol% PEG and B – 100mol% sulfonated, 77mol% PEG).. 36
Figure 3.11. Demonstration of representative Arrhenius plots for several polymer blends. a) Conductivity as a function of inverse temperature for the dry copolymer at R_1 sulfonate mol% = 3 and R_2 PEG mol% = 66 and blends of that polymer with PEG (Mn=300 Da) at 35, 66 and 91 wt% PEG300. b) The same diagram for the dry copolymer at R_1 sulfonate mol% = 64 and R_2 PEG mol% = 71 and blends at 34, 65 and 87 wt% PEG300. 37
Figure 3.12. Natural log of the VTF prefactor, A, versus the apparent activation energy, E_a, for several polymer systems. 38
Figure 3.13. A) Illustration of an attempt to increase conductivity by increasing segmental motion of the polymer. If polymer polarity is reduced, chains are able to move more freely, but ions dissolved in the polymer will pair. B) Illustration of attempts to increase charge carrier concentration by either adding ions or increasing polymer polarity. In both cases, new transient interactions between chains are introduced, increasing the T_g and thereby reducing segmental motion. 41
Figure 4.1. Example Stejskal-Tanner plots for each component of the solution at 0.1M Polymer, 0.1M LiTFSI in EC/DMC=2 (v/v). Each plot shows a linear decay, with slightly higher noise in the Lithium signal due to low signal intensity. 50
Figure 4.2. Conductivity as a function of LiTFSI added at each polymer concentration in A) DMSO and B) EC/DMC=2 (v/v). 51
Figure 4.3. Viscosity as a function of LiTFSI added to each polymer solution for EC/DMC (solid lines) and DMSO (dashed lines). Polymer free solutions are shown as squares, 0.01M polymer corresponds to triangles, and 0.1M polymer corresponds to diamonds. The 3% error estimated from the calibration is smaller than the data points in this figure..... 52
Figure 4.4. Molar conductivity (normalized using total Li^+ concentration in each solution) as a function of LiTFSI added at each polymer concentration in A) DMSO and B) EC/DMC=2(v/v). 53
Figure 4.5. Conductivity normalized to LiTFSI concentration for all solutions. 54
Figure 4.6. Diffusion coefficients of each species (polymer, Li^+, and $TFSI^-$) as a function of LiTFSI added for A) DMSO and B) EC/DMC=2 (v/v) 55
Figure 4.7. Diffusion coefficient of each species normalized to the solvent diffusion coefficient as a function of LiTFSI added for A) DMSO and B) EC/DMC=2 (v/v). 56
Figure 4.8. Viscosity ratio defined in Equation 4.3 as a function of LiTFSI added for each polymer concentration in A) DMSO and B) EC/DMC=2 (v/v). Inverse Haven Ratio as a function of LiTFSI added for each polymer concentration in C) DMSO and D) EC/DMC=2 (v/v). In each figure, reported error has been propagated from the measurements. ... 58
Figure 4.9. A) ^7Li spectra for the series of solutions at 0.01M Polymer in EC/DMC with added LiTFSI. The spectra of each solution have been overlaid, and the intensity normalized.

With added LiTFSI, the peak width narrows. B) ^{7}Li peak width at half maximum as a function of LiTFSI added for all solutions. 59
Figure 4.10. Transport number as a function of LiTFSI added at each polymer concentration in A) DMSO B) EC/DMC=2 (v/v)..... 61
Figure 4.11. Diffusion coefficient of the DMSO solvent as a function of LiTFSI added to each polymer solution. 62
Figure 4.12. Diffusion coefficient of DMC (dashed lines) and EC (solid lines) in each polymer solution as a function of LiTFSI added..... 62
Figure 5.1. A) NMR Characterization of the sulfonated polysulfone (SPSF) polymers and the sulfonated, lithium-form monomer (sulfonated bis(4-chlorophenyl) sulfone), with peak assignments noted for the polymer. Peaks associated with the end groups are denoted by a star. B) GPC of the SPSF polymers with color corresponding to the polymer in A). 66
Figure 5.2. Viscosity as a function concentration in A) DMSO-d_6 and B) D_2O. The legend in A) also applies to B). The monomer (SPSF-1) is the lithium form sulfonated bis(4-chlorophenyl) sulfone. Reported concentrations are that of the Li^+ counterion. 68
Figure 5.3. Conductivity as a function of concentration in A) DMSO-d_6 and B) D_2O. The legend in B) also applies to A). 69
Figure 5.4. Diffusion coefficients, as measured using PFG-NMR, of the solvent, lithium, and backbone as a function of concentration in A) DMSO-d_6 and B) D_2O 69
Figure 5.5. Scaling of specific viscosity with concentration for A) the monomer, B) shortest polymer, and C) longest polymer in DMSO-d_6. Numbers on the plot correspond to the slope of the fit line in that region. D) The scaling exponent (slope from A-C) plotted as a function of repeat units for each region. 70
Figure 5.6. Scaling exponent of specific viscosity with molecular weight, as a function of concentration in DMSO-d_6 71
Figure 5.7. Scaling of backbone diffusion coefficient D_b with concentration for A) the monomer, B) shortest polymer, and C) longest polymer in DMSO-d_6. Numbers on the plot correspond to the slope of the fit line in that region. D) The scaling exponent (slope from A-C) plotted as a function of repeat units for each region. 72
Figure 5.8. Scaling exponent of the backbone diffusion coefficient with molecular weight, as a function of concentration in DMSO-d_6. 72
Figure 5.9. A) Scaling of the Li diffusion coefficient (D_{Li}) with concentration for the longest polymer in DMSO-d_6. B) Scaling of the solvent diffusion coefficient (D_S) with concentration for the longest polymer in DMSO-d_6. Numbers on the plot correspond to the slope of the fit line in that region. C) The scaling exponent for Li diffusion (slope from A) plotted as a function of repeat units for each region. D) The scaling exponent for solvent diffusion (slope from B) plotted as a function of repeat units for each region. 74
Figure 5.10. Scaling of backbone diffusion coefficient with concentration for A) the monomer, B) shortest polymer, and C) longest polymer in D_2O. Numbers on the plot correspond to the slope of the fit line in that region. D) The scaling exponent (slope from A-C) plotted as a function of repeat units for each region. 75
Figure 5.11. Scaling exponent of backbone diffusion with molecular weight, as a function of concentration in D_2O..... 76

Figure 5.12. Scaling of specific viscosity with concentration for A) the monomer, B) shortest polymer, and C) longest polymer in D_2O. Numbers on the plot correspond to the slope of the fit line in that region. D) The scaling exponent (slope from A-C) plotted as a function of repeat units for each region. 77
Figure 5.13. Scaling exponent of specific viscosity with molecular weight, as a function of concentration in D_2O..... 77
Figure 5.14. Diffusion coefficients of solvent and lithium normalized to the diffusion coefficient of the same species in the monomer solution for A) DMSO-d_6 and B) D_2O. Diffusion in the monomer solutions appears as a straight line at 1 on this plot..... 79
Figure 5.15. Transport number defined in Equation 5.3 in DMSO-d_6 (A and C), and D_2O (B and D). Darker color in C) and D) corresponds to higher concentration. The legend in A) also applies to B). Error bars are propagated from the diffusion measurement. 80
Figure 5.16. Lithium conductivity as a function of concentration for A) DMSO-d_6 and B) D_2O. Points in B) that are circled use an estimated t_{+NMR} of 1 to calculate σLi 81
Figure 5.17. Specific viscosity scaling as a function of concentration in DMSO-d_6 for the three polymers not shown in the main text. 82
Figure 5.18. Scaling of backbone diffusion coefficient as a function of concentration in DMSO-d_6 for the three polymers not shown in the main text..... 83
Figure 5.19. Scaling of backbone diffusion coefficient as a function of concentration in D_2O for the three polymers not shown in the main text. 83
Figure 5.20. Scaling of specific viscosity as a function of concentration in D_2O for the three polymers not shown in the main text. 83
Figure 6.1. Conductivity and viscosity of a range of potential additives to improve conductivity of the control 0.1M polymer in 2:1(vol.) EC:DMC solution. Each additive is introduced at 0.1M, to match the lithium content of the solution. The structure of the polymer, EC and DMC in the control solution are also included. 87
Figure 6.2. Conductivity and viscosity as a function of A) 15-crown-5 content and B) water content in a 0.1M polymer in 2:1(vol.) EC:DMC solution. The total lithium concentration is maintained constant in each solution by diluting from a higher concentration with either 15-crown-5, water, or EC/DMC. Viscosity error bars taken from repeat measurements of the same sample are smaller than the data points in this plot..... 88
Figure 6.3. A) Diffusion coefficient for EC from the ^{1}H spectra, ^{7}Li diffusion coefficient, and polymer backbone diffusion coefficient measured from the ^{19}F spectra for the set of solutions in Figure 6.2A. Error bars, estimated from the diffusion calibration, are smaller than the data points. B) ^{7}Li spectra for each 15-crown-5 containing solution in Figure 6.2A and inset plot of the ^{7}Li peak location. With increasing crown ether content, the peak narrows and shifts upfield..... 89
Figure 6.4. Second charge and discharge curves for batteries fabricated with the 0.1M polymer in 2:1(vol.) EC:DMC solution containing no additives, containing stabilizing additives FEC and VC, and containing 15-crown-5 and the stabilizing additives. The calculated theoretical maximum capacity of the cell is also shown..... 90

List of Tables

Table 1.1. Summary of expected scaling relationships for polyelectrolyte solutions. 12
Table 3.1 Summary information of the polymer series at roughly R_1 = 10 mol% sulfonate, and the second at roughly R_2 = 70 mol% PEG discussed in Figure 3.5 - Figure 3.8. Weight percent PEG is the calculated weight of ethylene oxide repeat units in the overall polymer. 27
Table 3.2. Equations and fitting methods used in Figure 3.8 and Figure 3.9. Fit routine 2 was used for data presented in Figure 3.10 and Figure 3.12. 32
Table 3.3. Detailed summary information for all dry PSf-co-PEG copolymers shown in Figure 3.10. "PEG M_n" refers to the length of PEG monomer used. PEG wt% is the calculated weight percent of ethylene oxide repeat units in the overall polymer. EO/Li is the calculate ethylene oxide repeat unit to lithium ratio often referred to in the polymer electrolyte literature. The VTF parameters E_a, A and T_o are reported from Fit #2, as plotted in Figure 3.10. Samples labeled with * are the series at a R_1 sulfonate mol% of 10 and samples labeled with # are the series at a R_2 PEG mol% of 70. 43
Table 3.4. Compositions of the blend samples. Copolymer mol% reported here refers to the parent dry PSf-co-PEG copolymer used to make the blend. The dry copolymer glass transition temperature and the blend glass transition temperature are reported. Most of the blends exhibited melting behavior at a temperature (T_m) below the range of conductivity analysis. The VTF parameters reported here are those plotted in Figure 3.10, from Fit #2..... 44
Table 4.1. Dissociation constant in EC/DMC and DMSO calculated with implicit solvent and explicit solvent. 60

Acknowledgements

I would first like to thank my family, for always supporting me and giving me the foundation to succeed. Despite not always knowing what I am working on, my family has always been there for me and encouraged me to do the best that I can.

Julie has been the perfect partner in this entire experience. She has supported me no matter what and we have done so many amazing things together to keep the experience fun, be it flying around the world to go explore, or just watching Sci-Fi at home in the evenings. I imagine I would have a much worse view of grad school without her around.

My time at Berkeley has been marked by more amazing people than I ever could have imagined. It is the people here that really make it a special place, and I have been fortunate enough to live at least part time with many of them. My first roommate Pete, everyone that come through the Alligator House after that – Andy, Parry, Matt, Kristian, Jana, Sarah, Becca, Constance, Tammy – and everyone at the Hearst House – Sudi, Kristen, Danielle, Clay, Jon. The graduate students at Berkeley are an incredibly inspiring group of people, and I really hope that the tradition of community continues. Those that brought me into GSAC early on, Barbara and Rachel had a huge part in keeping that going. I am thankful to see great people taking on the next set of challenges too – Whitney, Lorena, Helen, Anthony, Julie F., Sarah Y. and so many more.

I of course have to thank my advisor for all of his advice over the years, and never falling into any of the typical bad stereotypes for assistant professors. It saddens me to hear so frequently how terrible advisors can be, and I am really thankful not to have experienced any of that. The group has been a great place to grow and learn, even if I have always been on the outskirts of what everyone else does. Hilda was the best person to start in lab with, so full of enthusiasm, but never too serious. Taking apart equipment and cleaning out labs never bothered me when you have someone fun to do it with. Colin, Jessica, Sara, Kristian, and all of the people that have come through the lab since have built a smart, but friendly culture that I hope continues. I have to thank Kara in particular for coming into our polyelectrolyte project and showing us the right way to think about things. I look forward to seeing where Kara and Helen take everything as I leave.

I also have to thank the Balsara Lab – Jacob, Mahati, Whitney, Jackie, Deep, Mike, Lorena, Katie, David, Louise, and Hee Jeung – for always welcoming my questions and not minding my nosiness. Those at JCAP, Dan, Blaine, and Sarah, have always been so welcoming and I have greatly appreciated the opportunities available there. Hasan and Nanette in the NMR facility worked far too hard to keep everything running, as does Carlet for all of the graduate students. I am happy to have been able to work in many different buildings and labs, allowing me to meet so many great people.

I am immensely thankful for my time at Berkeley and am so happy to have taken on this adventure.

1. Introduction[†]

Consumer Li-ion battery powered devices are ubiquitous in the modern world and significant growth in the electrification of vehicles, powered by advances in Li-ion batteries, has occurred in the last several years. Plug-in hybrid (PHEV) and pure electric vehicles (EVs) accounted for 0.9% of total cars purchased globally in 2016 and 2.2% in 2018, and sales of all plug-in vehicles have achieved year-over-year growth of at least 46% since 2012, with 2.1 million PHEV/EV sales (360,000 in the United States) in 2018.[1] However, current consumer electronics and EV's still suffer from a few major challenges related to their batteries: they are larger and heavier than desired, they take a long time to charge, and safety incidents continue to attract significant media attention. For Li-ion batteries to continue their impressive market penetration over the next few decades, breakthroughs in battery technology are required that continue to directly address these issues.

For this reason, significant research has targeted increased energy density, higher charge and discharge rate, and improved safety through various advances in every component of the Li-ion battery.[2,3] Electrolyte mixtures and separators have been identified that enable reasonably safe, long term use,[4,5] and cell designs and energy management technologies have enabled impressive gains in cycle life, safety, and energy density.[6] Recent work has particularly emphasized improving the energy density of Li-ion electrode materials. As relevant examples, Li alloys (Si and Sn being the most well-studied) or pure Li metal are being explored as high-capacity anode materials, and the so-called Li-rich transition metal oxides are being pursued as cathode materials.[7–11]

The focus of this work is another strategy to improve energy density and charging rates of batteries, namely the development of high Li^+ transference number electrolytes (HTNE's), those in which the ionic current is carried predominantly by the Li^+ rather than its counteranion. The definition of the Li^+ transference number in the dilute limit for a binary salt electrolyte in which both ions are univalent (a 1:1 electrolyte) relates the diffusion of Li^+ and its counterion through the following simple relationship:

$$t_+ = \frac{D_+}{D_- + D_+} \tag{1.1}$$

Where t_+ is the Li^+ transference number, D_+ is the Li^+ diffusion coefficient, and D_- is the anion diffusion coefficient.[12] In this limit the transference number can be considered as simply the fraction of the total ionic conductivity that is carried by Li^+. Despite numerous advances in porous electrode materials, improvement of electrolyte properties, including stability, ionic conductivity, σ, and t_+, remains one of the most important challenges to any further performance gains.

I. Drawbacks of Current Electrolytes

Conventional electrolytes are based on a binary lithium salt and stabilizing additives dissolved in a mixture of carbonate liquid solvents.[4] These electrolytes are then imbibed in the porous polyethylene or polypropylene separator and electrodes to create ionic contact while maintaining electronic insulation between the electrodes. This class of electrolytes imparts high lithium-ion conductivity and has been successfully commercialized for many years, but suffers from a couple of key drawbacks. First, all liquid electrolytes possess a voltage stability window,

[†] Portions of this introduction were previously published as a review in *ACS Energy Letters,* and are adapted with permission from co-author E.J. McShane and B.D. McCloskey.[18]

typically between ~1 V and ~4.5 V vs Li/Li^+, that ultimately limits battery rechargeability, safety, and high-energy active electrode materials development.[13] To address capacity fade during battery cycling, in combination with limiting the upper operating voltage to improve stability at the cathode-electrolyte interface, carbonate-based electrolytes typically contain small amounts of organic additives which are usually selected through empirical combinatorial analyses, although effort has been made to develop a deeper understanding of the topic.[5,14] During the first few discharge-charge cycles, these additives will facilitate the formation of solid, ion-conducting layers on the anode surface that otherwise substantially suppress parasitic reactions between the anode and electrolyte.[15] While commercial mixtures of additives have been realized after many years of research, understanding the influence of additives on electrode processes at a molecular level remains a poorly understood topic.

Second, although current liquid electrolytes offer high conductivity across a wide temperature range (~1-10 mS/cm) and well dissociated ions with a solubility >1 M Li^+, they have a Li^+ transference number below 0.5, indicating the majority of the total ionic conductivity is in fact the result of anion motion. This low t_+ occurs due to the strong preferential solvation of Li^+ over its counterion, resulting in a bulky solvation shell around Li^+ compared to that of typical anions.[16] Within a lithium ion battery, anions tend to migrate in the opposite direction of the lithium and eventually accumulate at the electrode surface, resulting in the buildup of a concentration gradient, as is demonstrated in Figure 1.1A specifically for the case of a lithium metal anode and polymer electrolyte. This concentration gradient limits the rate at which the battery may be charged or discharged, creates a concentration overpotential that limits the operating voltage of the cell, and limits the thickness of electrodes that may be used, all of which limit the power and energy density of the cell. All of these challenges could be substantially alleviated if a high t_+, high σ electrolyte were developed. However, as will be discussed below, the creation of organic electrolytes that provide both high t_+ and σ has been elusive due to the inherent limitations of ion transport in systems where the anion is immobilized, while inorganic electrolytes have long suffered from processability issues.

II. The Importance of a High Transference Number Electrolyte.

Doyle, Fuller, and Newman in 1994 demonstrated the importance of the lithium ion transference number, showing that a t_+ of 1 offers significant enhancement in terms of materials utilization, power, and energy density over a t_+~0.2, particularly at high rates of discharge and even with an order of magnitude decrease in conductivity.[17] These simulations focused on a poly(ethylene oxide) – based polymer electrolyte which had relatively low conductivity (~0.1 mS/cm) with $LiMn_2O_4$ and lithium metal electrodes. Our group later extended these simulations to model charging of a commercial dual lithium ion insertion cell consisting of a porous graphite anode, a porous $LiCoO_2$ cathode, and an electrolyte of varying transport properties.[18] We also focused on charge instead of discharge because EV batteries are discharged at high rates only intermittently (during acceleration), such that the salt concentration gradients that ultimately limit cell performance do not evolve to the extremes that would be expected during high rate charging. The total attainable state of charge (SOC) prior to hitting the cutoff voltage (4.2V) is shown as a function of charge rate and transference number for these cells in Figure 1.1B Although little difference is observed in the attainable SOC at low current densities (<1C), the beneficial effects of high t_+ can be clearly observed at 2C rates and above, where a precipitous increase in attainable SOC as t_+ is increased is observed. Clearly, the transference number has a dramatic effect on cell performance at EV battery-relevant rates.

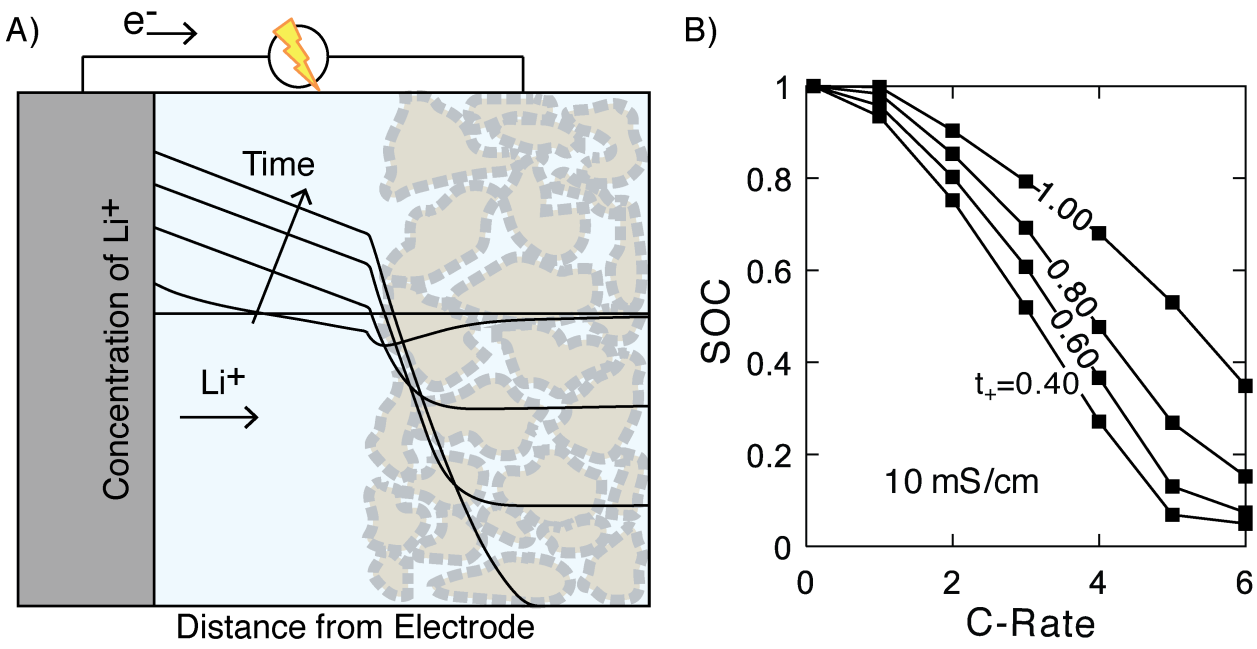

Figure 1.1. A) Illustration of concentration gradients as demonstrated originally by Fuller[17] B) Attainable state of change (SOC) versus charge rate for an electrolyte with σ=10 mS/cm and variable t_+.

III. The Challenge of Measuring Transference Number.

The measured values of the transference number, conductivity, diffusion coefficients, and activity coefficients are critical for accurately predicting battery performance. Unfortunately, measurement of these properties is entirely non-trivial and has led to most studies only measuring conductivity, as it is easily accessible via simple polarization techniques. Few studies accurately measure the true transference number, even fewer make the additional step to measure diffusion coefficients, and fewer still make any attempt to measure the activity coefficient of the salt.

The Bruce and Vincent method of transference number measurement is likely the most popular technique among those studies which focus on HTNE's. This technique compares the steady state current with the initial current measured in a lithium-electrolyte-lithium symmetric cell under a constant potential. When the potential is first applied, the current measured (I_o) will be a result of the migration of all charged species, which initially exist at uniform concentration throughout the cell. After some time, a constant current is obtained after the steady-state (I_{ss}) salt concentration profile is achieved and net anion flux is zero. Assuming that convection and instabilities at the Li electrodes can be neglected, both of which can be questionable assumptions depending on the electrolyte composition, the transference number is calculated as $t_+ = \frac{I_{SS}}{I_o}$. This relation is only strictly accurate in the dilute limit and corrections have been suggested to eliminate resistances such as those due to electrolyte decomposition at the lithium surface, though such corrections typically require interpretation of complex impedance spectra.[19] Balsara and Newman recently demonstrated the correct ratio I_{ss}/I_o for concentrated solutions, in terms of the Newman number, Ne:[20]

$$\frac{I_{ss}}{I_o} = \frac{1}{1+Ne}, \quad Ne = a\frac{\sigma RT(1-t_+)^2}{F^2 Dc}\left(1+\frac{d\ln(\gamma_\pm)}{d\ln(m)}\right) \qquad 1.2$$

Here c is the concentration of the electrolyte, R is the gas constant, T is the temperature, F is Faraday's constant, a is related to the stoichiometry of the salt, $\gamma_{\pm}$ is the mean molal activity coefficient, and m is the molality of the solution. In the dilute limit this reduces to $t_+ = \frac{I_{SS}}{I_o}$. Due to the complexity of the full relation, most studies simply make an approximate transference number measurement assuming a dilute solution.

There are several additional transference number measurement techniques that provide a complete set of transport parameters (salt diffusion coefficient, activity coefficient, transference number, and conductivity), though none are as straightforward as the simple polarization experiment and typically require specialized cell geometries. Ma et al. first measured the complete set of transport parameters for a sodium salt in polymer electrolyte.[21] To do so involved the use of three careful experiments, as well as numerical differentiation of the data from those experiments, introducing appreciable experimental error. Their results demonstrated that the dilute limit assumption in polymer electrolytes fails to accurately predict t_+, emphasizing the non-trivial nature of accurate transport property measurements. The results of Pesko et al. confirmed the results of Ma et al. for LiTFSI in PEO, using a similar method.[22] In fact, the assumption of a true dilute solution without any ion aggregates is highly questionable in most battery-relevant electrolytes, even apart from polymers.[23] In an $LiPF_6$ – carbonate mixture solution, Valøen and Reimers demonstrated the true t_+ is indeed approximately 0.3-0.4, though they also highlighted the difficulty in achieving a precise result.[24] The difficulties involved in the measurement of t_+ indicates reported values should always be considered carefully. Measured transference numbers should only be taken as truly accurate if the authors either specifically made the effort to consider concentrated solution theory or checked the dissociation of salt. Pulse field gradient NMR has proven a valuable tool to probe salt dissociation by monitoring species diffusion, but does not directly account for speciation or activity coefficients.[25] As a result of these inherent challenges, this dissertation does not actually report a transference number for any of the studied systems. This is primarily because the effort involved in measuring transference number necessitates a system in which that effort is worthwhile. Chapter 6 introduces one system in which such an effort would be appropriate, but this must be left to future work.

IV. Strategies for the Development of a High Transference Number Electrolyte.

Designing an electrolyte in which the Li^+ transference number approaches 1 has been the subject of much interest since at least 1985, with a few main research thrusts. Figure 1.2 presents several representative sketches of each class of electrolyte to clearly indicate the types of electrolyte delineated herein. Lithium-conducting ceramics may be formulated that effectively create a single ion conductor (SIC) (Figure 1.2A). Dry, non-swollen polymer electrolytes, long studied as a potential solid-state electrolyte material for use with the lithium metal anode, have been synthesized with anions appended to the polymer backbone (Figure 1.2B). As a means to improve the performance of neat polymer systems, polymer electrolyte membranes with additives ranging from small molecule solvents to nanoparticles have been studied extensively (Figure 1.2C). In addition, nonaqueous solvent filled ionomers (hard polymer membranes affixed with ions) have been studied for battery applications (Figure 1.2D). Recently, alternative methods to raise the transference number of a liquid electrolyte through the use of polymeric anions (nonaqueous polyelectrolyte solutions (Figure 1.2E)), highly concentrated electrolytes (so-called 'solvent-in-salt' electrolytes), and solutions containing nanoparticles with appended anions have been suggested. The advantages and the future research directions of each system are discussed herein.

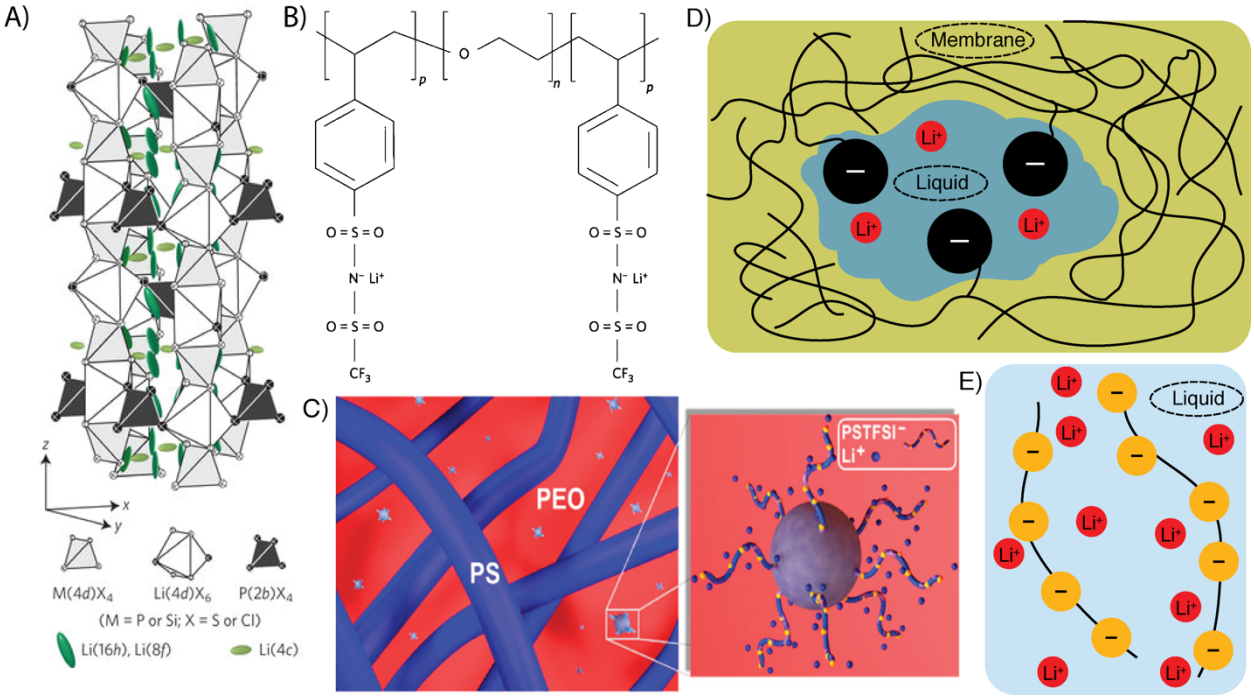

Figure 1.2. Several classes of HTNE's. A) Ceramic SIC based on doped lithium thiophosphate glass, reproduced from Ref. 26 B) The neat polymer electrolyte poly(styrene trifluoromethane- sulphonylimide – co – poly(ethylene oxide), reproduced from Ref. 27 C) Mixed polymer electrolyte system based on nanoparticle/copolymer blend, reproduced from Ref. 28 D) Sketch of a solvent-filled ionomer membrane E) Sketch of a polyelectrolyte HTNE solution.

i. Ceramic-based single ion conductors

Ion conducting inorganic ceramics are being developed as possible electrolytes to enable all solid-state battery configurations. Among these, the most actively studied materials are garnet phase metal oxides, such as those based on the $Li_7La_3Zr_2O_{12}$ structure,[29] lithium thiophosphate glasses, Li_2S-P_2S_5,[30,31] and NASICON-type conductors, such as $Li_{1+x}Al_xTi_{2-x}(PO_4)_3$.[32,33] Furthermore, recent development of new ceramics, such as Li_3OCl and Si/Cl-doped lithium thiophosphate glasses have garnered substantial interest given their high reported conductivity.[26,34] Conductivities for these ceramics have been reported to be as high as 25 mS/cm at room temperature and given that all are expected to possess unity Li^+ transference numbers, they could easily improve cell energy densities over conventional cell energy densities given the data shown in Figure 1.1. An additional advantage of ceramic electrolytes over organic liquid electrolytes is their nonflammability, such that solid-state batteries, if commercialized, may be a safer alternative to conventional organic electrolyte-based batteries.

Many challenges face ceramic ion conductors as potential battery separators; these are briefly outlined here and readers are referred to an exhaustive review article on this topic.[35] In order for batteries comprised of solid-state electrolytes to have energy densities and costs that improve upon existing Li-ion cells, the solid-state separators need to be made with exceptional homogeneity,[35] in form factors that are less than 100 μm thick (and preferably less than 20 μm) and laminated between a Li metal anode and porous cathode, all while remaining less than $5/m^2.[36] Achieving these metrics will be a challenging task given the brittle nature of ceramics and conventional solid-state synthesis procedures, which typically result in numerous grain boundaries

and a small fraction of pores between fused ceramic particles. In an attempt to improve the processability of these systems, organic-inorganic composites have also been explored, in which particles of inorganic materials are embedded in polymers in creative ways to ensure ion transport occurs through percolated inorganic particle networks.[37–40] Nevertheless, engineering interfaces in all solid-state cells, particularly the porous cathode-electrolyte interface, to provide low, stable impedances during battery operation remains a critical hurdle, and future research efforts to understand these interfaces are warranted.

ii. Dry (Neat) Polymer Electrolytes

Dry polymer electrolytes have long been proposed for use in lithium-based batteries as a significantly safer alternative to traditional flammable liquid electrolytes. In such an electrolyte, a small molecule salt is entirely dissolved by the polymer, which acts alone as a solvent, with no additional small molecule additives. In a polymer/salt complex, ions are solvated by close association of large polymer chains that are relatively immobile due to entanglement with nearby chains. As a result, ion motion is generally understood to proceed by a hopping motion in which ions transition between available solvation sites.[41] This form of ion transport proceeds significantly slower than the shuttling motion present in liquid electrolytes, where Li^+ moves freely with its solvation shell predominantly intact. As a result, all polymer electrolytes have suffered from poor conductivity at room temperature when compared to liquid electrolytes. The most conductive Li^+ polymer electrolytes known are binary lithium salts (e.g., lithium perchlorate, $LiClO_4$, or lithium bis(trifluoromethane sulfonimide), LiTFSI) dissolved in poly(ethylene oxide) (PEO), with conductivities on the order of 10^{-3} S/cm at 60-100 ºC, although room temperature conductivity often suffers due to backbone crystallization below ~60°C. Disrupting the crystallinity of PEO has been the subject of much work, and readers are referred to the review by Xue et al. for an exhaustive overview.[42] As will be discussed more completely below, PEO imparts high ion conductivity due to its unique and extensive ability to solvate ions, yet maintain high segmental backbone motion.[43,44]

These simple dry polymer electrolytes typically are found to have a transference number around 0.3 – 0.4.[45] The low transference number typically measured in these lithium electrolytes is partially due to strong solvation of the lithium relative to the bulky, charge delocalized anion by the mildly Lewis basic PEO backbone. Savoie et al. have suggested the use of strong Lewis acid polymers as a means to improve transference number because the anion would be more strongly solvated than the Li^+, though we are unaware of successful synthesis of such polymers.[46] There are few reported systems in which a high transference number electrolyte results from a simple binary salt in a dry polymer electrolyte. Perfluoropolyether polymer blended with LiTFSI has demonstrated a transference number above ~0.9 by electrochemical methods.[47] However, later publications on the same system demonstrated the ions in this system are likely poorly dissociated, and that the presence of ethoxy groups that increase conductivity actually promote anion motion and thereby lower the transference number.[48] In fact, the true transference number of this system was even later found to be negative, further demonstrating the challenges involved in designing a truly high transference number electrolyte.[49]

Affixing anions to the backbone of the polymer such that they are unable to move separate of the chain is the most common route to a HTNE. In this case, the anions are effectively immobile and so this class of polymers is often referred to as being truly single-ion conducting. The first such neat SIC polymer was reported in 1985,[50] based on a methacrylate backbone having ethylene oxide and lithiated carboxylate side chains. Similar formulations have been studied since this

original system, most often incorporating PEO either as the backbone or as a pendant side chain to act as the ion solvation medium. Other systems including polyphosphazenes,[51–54] boron containing polymers,[55,56] and siloxane polymers have also been studied, incorporating a wide variety of anion chemistries.[57]

Improved conductivity in dry SIC polymer's, however, has proven elusive – particularly at room temperature. To illustrate this point, Figure 1.3 summarizes the conductivity of 34 individual SIC polymer chemistries, based on the date of publication, at both 30 and 90°C.[27,50,52,55,56,58–82] Several example high conductivity polymers are shown, with all having the common feature of PEO incorporated as a component of the backbone or as a side chain; the [EO]/[Li] ratio is shown to identify the polymer within the reference. Generally, the highest conductivity polymer from each reference is shown. In addition, the conductivity of a typical liquid electrolyte at 10^{-2} S/cm is shown. Although conductivity has improved at higher temperatures, the best conductivity around room temperature has remained ~10^{-5} S/cm for the past ~20 years. Several recent reviews of polymer electrolytes provide further insight to the wide variety of systems that have been attempted. [42,57,83]

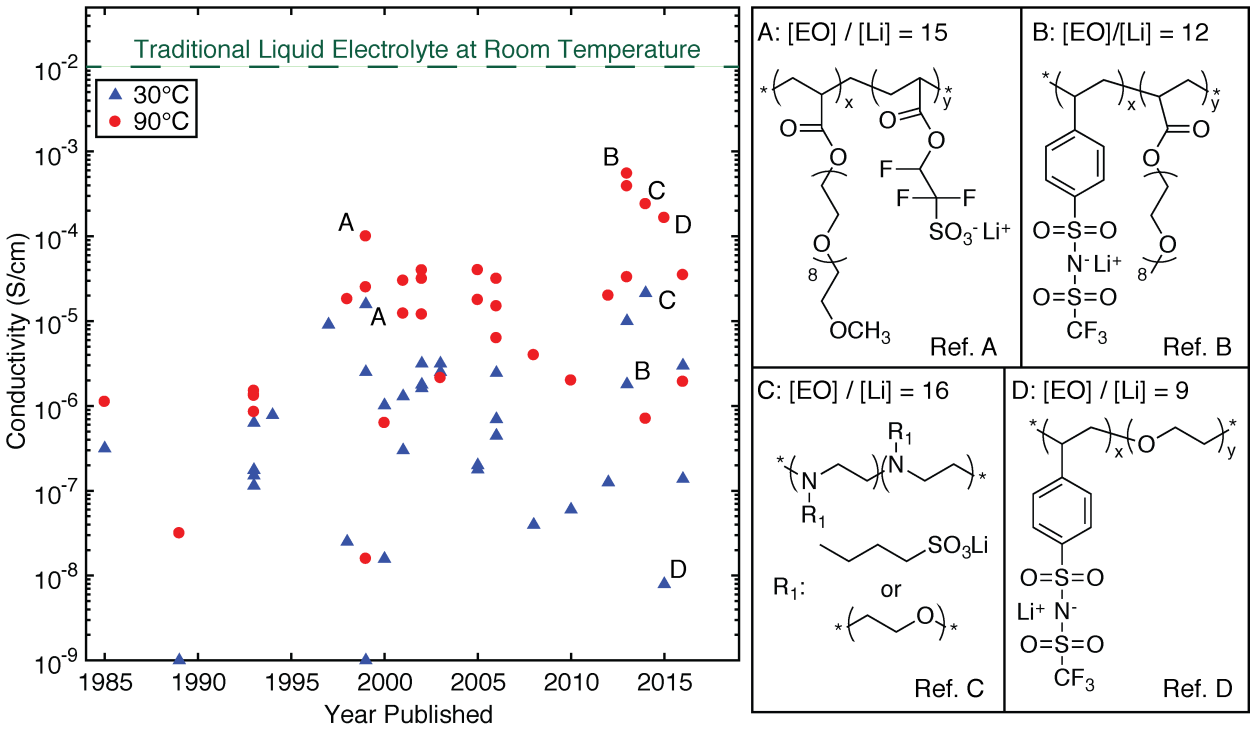

Figure 1.3. Conductivity of neat appended anion polymers versus the year published, the approximate magnitude of typical liquid, binary salt electrolyte conductivity is indicated. Each individual point corresponds to conductivity values of polymers published in the following reports: 27,50,52,55,56,58–82. Ref. A is 60, B is 73, C is 74 and D is 75.

iii. Polymer electrolytes containing additives

The significant challenges remaining in dry polymer electrolytes have led many researchers to create blended polymer electrolytes, in which small molecule solvents or particulates are added to the dry polymer in an attempt to increase conductivity. The small molecule additives typically serve to either increase polymer segmental motion through plasticization or improve ion dissociation to increase charge carrier concentration. The wide phase space of this class of

electrolytes makes significant generalizations difficult. In many cases the addition of solvent is considered after significant work on a dry system in which limited conductivity is ultimately observed, and therefore little care is taken in the choice of solvent or additive used, often with no explanation for that choice. In most cases, blends that utilize binary salts like LiTFSI have transference numbers similar to the dry polymer electrolyte case, but significantly higher conductivity due to improved segmental motion of the polymer and solvation of lithium by the small molecule additives.[84,85] Transference numbers approaching 0.8 in poly(acrylonitrile) (PAN) and poly(methyl methacrylate) (PMMA) systems blended with PC, EC, and LiTFSI have been reported due to a unique interaction of the polymer with the anion.[86] Unfortunately, PAN does not form a stable SEI against Li metal and there is little understanding of why the high transference number was found.[84]

Several reports have indicated promising results from inorganic additives.[87] Improved transference numbers were reported in ceramic composite electrolytes, but only when the ceramic occupied a significant fraction of the electrolyte.[88] Higher transference numbers have also been reported by addition of nanoparticles of TiO_2 to PEO/$LiClO_4$ electrolyte, due to the interaction of the anion with the nanoparticle.[89] These findings have thus far proven challenging to implement due to high interfacial impedance and little understanding of the complex interaction which leads to the high transference number initially. Future research must focus on understanding this interaction to suggest structure/property relationships that effectively inhibit anion motion without altering the anion.

HTNE blends are more directly formed by utilizing polymer electrolytes with affixed anions, and no added salt. There are a myriad of reported systems, and in fact such blends were first investigated prior to neat polymer SIC's.[90,91] The most recent studies often report room temperature conductivities on the order 10^{-4} S/cm, with transference numbers above 0.9.[92,93] The additives in this class of electrolytes may either be another uncharged polymer (often PEG, as in refs. [90] and [91]), nanoparticle,[28] or other small molecule additive.[94] In general, the additive must focus on improving the two key properties necessary for polymer electrolytes: improving segmental motion via plasticization, and improving ion dissociation either by directly solvating the lithium or adjusting the overall dielectric constant of the medium.

This class of electrolytes presents a vast space to explore, and significant work is still necessary to understand the additive – polymer interactions that provide the best performance. Few studies have carefully examined the effect of additive properties, with the notable exception of Klein and Runt in 2006 that suggested at low weight loadings the most important effect was the plasticization (change in glass transition) of the polymer chains.[95] Certain studies have additionally demonstrated the ability to tune ion association through the use of additives such as BF_3.[96] Unfortunately, many additives negate some of the benefits of using a polymer to begin with because most small molecule solvents are likely flammable or incompatible with current electrodes. A secondary concern with these electrolytes is the fabrication of a cell with a porous electrode. Porous electrodes are key to the high energy density of current cells as they allow a high ratio of active material to electrolyte where the pure lithium metal anode is not applicable. This implies that the polymeric membrane must be incorporated into the casting of the electrode, meaning that creating a full cell design is a daunting challenge.

Future work in mixed HTNE polymer systems must focus on understanding the complex additive – salt – polymer interactions to both optimize the segmental motion – charge carrier concentration tradeoff and maintain high transference number. There is a significant need for clear relationships between additive properties and resulting performance, though few groups have

embarked on specific studies targeting this class of electrolytes relative to the large number targeting dry electrolytes. As indicated, certain additives have displayed potential routes to HTNE's without affixing the anion in space, and researchers have clearly demonstrated high conductivity, high transference number blends. Further explicit study of the interactions that produce these promising systems is the most important work towards enabling this class of electrolytes.

iv. Swollen Ionomer Membranes

A distinct, promising class of SIC polymer-based electrolytes utilizes charged polymers formulated as a porous membrane filled with liquid solvents to allow ion motion via solvation in the more mobile liquid phase. Here, anions are bound to the polymer backbone, and as the polymer is completely fixed in space either by crosslinking or entanglement, the transference number of the resulting membrane is necessarily one. There are a wide variety of chemistries that have been explored, with conductivities that approach, or in some cases exceed, that of traditional liquids.[92,97,98] The key design parameter in these electrolytes is the dissociation of the affixed ionic species into the liquid phase, as otherwise lithium ions must hop between ionic aggregates, an unlikely phenomenon unless the aggregates are spatially close.[99] Generally, the selected solvent must have a high enough basicity such that the anion is less likely to occupy the Li^+ solvation shell than the solvent. In most cases, this has led to the use of solvents such as propylene carbonate (PC), ethylene carbonate (EC), dimethyl sulfoxide (DMSO), or n-methyl-2-pyrrolidone (NMP), all of which have either high dielectric constants, high Gutmann donor numbers (a quantitative measure of Lewis Basicity), or both. In, for example, ref. [97], the ionic conductivity of a lithiated Nafion polymer is around $10^{-6.5}$ S/cm at room temperature using a glyme or a mixture of ethylene carbonate and diethyl carbonate, but when propylene carbonate is used, conductivity improves to 10^{-4} S/cm. The conductivity and high transference number of these electrolytes is therefore quite promising for future commercial application.

There are, however, several key concerns to the future use of ionomer membranes in batteries. PC, DMSO, NMP, and most other solvents that promote high lithium ion dissociation are also well known to co-insert with Li^+ into graphite anodes, thereby exfoliating them, and suffer from poor stability at cathode-relevant potentials, leading to long-term rechargeability issues. Chemical changes to the polymer have been proposed to improve ion dissociation, for example the highly fluorinated sidechain of ref. [98] and the materials considered by Doyle et al. in 2003, which produce room temperature conductivity near 1 mS/cm in an ethylene carbonate/dimethyl carbonate blend.[100] Lithium metal has been considered with these electrolytes, but the flammability of any small molecule solvent in contact with lithium is a concern. Design of a full cell with an ionomer membrane and porous electrodes is perhaps the most important question, similar to the issue involved with blended polymer electrolytes discussed earlier. Charge neutrality dictates the ions may never migrate far from the anionic moiety on the polymer, so these anionic species must also be present throughout the electrode. Water based fuel cells incorporate this type of electrode assembly, but in water with protons as the mobile ionic species, the challenge of dissociating the anion is significantly less important, and significant effort has already been made in design of electrode assemblies with Nafion and related ionomers. These electrolytes are one of the most promising routes to a high transference number cell, but significant work remains to determine an appropriate set of solvent/electrode/polymer properties that enable the full battery cell to be implemented.

v. Liquid Electrolytes

Liquid, salt containing electrolytes are the current state of the art in lithium batteries due to conductivity on the order of 10 mS/cm across a wide temperature range, despite typically low transference numbers. In most cases these liquid electrolytes have a low transference number as a result of the large solvation shell present around lithium cations, causing the effective size of the anion to be smaller than the cation in solution. There have been few attempts to raise the transference number of liquid solutions without modification of the typically inert separator. Archer et al. in 2013 suggested a novel method of slowing anion motion by tethering them to nanoparticles, producing high transference number solutions with room temperature conductivity near 10^{-4} S/cm, limited mainly by dissociation of the anions.[101] So called solvent – in – salt electrolytes, those which are comprised of a much larger volume of salt (e.g., LiTFSI) than liquid solvent (e.g., dimethoxyethane and dioxolane), have demonstrated a transference number around 0.7.[102] It was proposed that the unique solvation structure of the lithium effectively caused the anion to be less mobile than the cation, but much work is still necessary to understand this surprising result. The relatively small body of work on raising the transference number of liquid electrolytes presents an important opportunity, if an effective means to slow the anion without losing conductivity can be found.

Our group has particularly been interested in the method first proposed by Kreuer et al., to fully dissolve polyanions in a liquid solvent to create a high conductivity, high Li^+ transference number electrolyte.[103] Here, the polymer, and hence anion, diffusion is significantly lower relative to the lithium counterion. The idea is similar to one proposed by Videa et al. to make large anions, but instead of a single bulky anion, the anions are simply tethered together.[104] Initial efforts indicated that this approach provides the ability to attain conductivity reaching 10^{-3} S/cm at room temperature with minimal system optimization,.[105] This type of electrolyte presents the possibility of incorporating a high transference number electrolyte directly to current cells without significant redesign of electrode formulations. This type of electrolyte is the subject of Chapters 4 through 6, and the polyelectrolyte literature is further reviewed in Section VI of this introduction.

V. Summary of Past Strategies for Increasing Transference Number

Improving the transference number of lithium electrolytes is clearly an important and active area of research to increase the energy density and charge rates of lithium batteries. There are many potential systems that could lead to high transference number, high conductivity electrolytes. Several classes of lithium ceramics like those of Kato et al. display a transference number of 1 with conductivity around 25mS/cm at room temperature.[26] Several ionomer filled membrane systems show significant potential.[97] Liquid solutions in particular are promising for near term application to lithium ion batteries. Salt-tethered nanoparticles dispersed in liquid solvents,[101] solvent-in-salt systems,[102] and polyelectrolyte solutions[103] present important and significantly under-researched areas to explore. Such systems all could lead to significantly enhanced lithium ion batteries in the near future.

VI. Polyelectrolyte Solutions

Polyelectrolyte solutions are a broad class of electrolytes that can generally be defined as a polymer bearing several pendant charge groups fully dissolved in a solvent. These may appear similar to swollen ionomer membranes and polymers with additives, but are more directly compared to a standard liquid electrolyte where the typical binary salt is replaced by a polyion. The literature at times also refers to partially charged polymers as ionomers (the historical

definition, no longer consistently followed, reserving "polyelectrolyte" only for polymers with an ionic group in every repeat unit) and thus solutions of ionomers also fall under this classification. In Muthukumar's 2017 perspective on such systems he states, "The description of polyelectrolytes is perhaps the most challenging subject today among all biological and chemical systems in their liquid and solid states."[106] Given this, one cannot hope to fully encompass the vast array of literature. Instead, only a brief introduction to the theory and experiments surrounding these solutions in aqueous and nonaqueous solutions will be given.

Solutions of polymers can be characterized by numerous different length scales and interactions. When dissolved, the polymer tends to take on a conformation characterized by a radius of gyration R_g, defined as the root mean square distance of each particle in the polymer chain from the center of mass of the polymer. Relative to an uncharged polymer, polyelectrolytes take on more extended, linear conformation due to the added electrostatic repulsion along the chain. These electrostatic interactions are a complex function of charge and solvation, and though numerous theories have been presented over the years, Manning's counterion condensation theory is the most often discussed.[107–109] In this theory, developed for an infinite line of point charges, counterions are said to 'condense' on the polyelectrolyte chain when the distance between charges on the chain is less than the Bjerrum length (Equation 1.3, l_B).

$$l_B = \frac{e^2}{4\pi\varepsilon_0\varepsilon kT} \qquad 1.3$$

Here, e is the elementary charge, ε_0 is the vacuum permittivity, and ε is the dielectric constant of the solvent. This can be thought of as the distance at which electrostatic energy is equal to the thermal energy. In a low dielectric constant solvent where the charges on the chain are not well screened from each other, counterions will condense on the chain to minimize the repulsion between charge groups. These condensed counterions are not necessarily bound in place, though Manning's original theories assume so. Later theories describe 'territorially bound' or 'trapped' counterions that may be mobile along the chain, but not able to move away from the chain.[110,111] Uncondensed counterions are also not truly free in solution, but instead are typically considered to exist within a cloud around the chain (the size of which would be dictated by the Debye length). To consider motion of the chain, one must therefore also consider motion of this cloud of ions, which in turn must also take into account the number of ions and charge state of the polymer. The presence of an added salt only further complicates this.

In general, three regimes are most commonly discussed in the literature: dilute solutions below an overlap concentration c^* in which intrachain interactions are much stronger than interchain; semidilute solutions where interchain interactions become important; and an entangled regime above c^e where chains are interwoven and entangled. Practically, the dilute regime is rarely accessed because $c^*$is often extremely low due to the extended conformation of a polyelectrolyte in salt free solution.[112] The entangled regime and higher are also fairly under-studied due to the challenges inherent with highly viscous samples, and thus the majority of experimental research has occurred within the semidilute regime. The solution properties within each regime have been estimated from numerous theoretical techniques, but perhaps most commonly from scaling arguments.

Building upon the work of uncharged polymer solutions, deGennes first introduced scaling theories for the solution structure (and scattering from the solution).[113] Dobrynin, Colby, Muthukumar, and others have since expanded these ideas and used them to describe dynamics, including battery-relevant properties like diffusion and viscosity.[106,112,114,115] The expected scaling

of polyion diffusion and solution viscosity with concentration and molecular weight are summarized in Table 1.1.

Table 1.1. Summary of expected scaling relationships for polyelectrolyte solutions.

Property	Dilute, $c < c^*$	Semidilute, $c^* < c < c^e$	Entangled $c > c^e$
Polyion Diffusion, D_p [112,115]	$\sim\frac{1}{N}$	$\sim\frac{c^0}{N}$	$\sim\frac{1}{c^{\frac{1}{2}}N^2}$
Solution Viscosity, $\frac{\eta-\eta_0}{\eta_0}$ [115]	$\sim cN^2$	$\sim\sqrt{c}N$	$\sim c^{1.7}N^{3.4}$

Solution conductivity has also been the subject of much work, with many approaches based on Equation 1.4.[116–118]

$$\Lambda = f(\lambda_i^0 + \lambda_p) \qquad 1.4$$

Here, Λ is the molar conductivity, f is an interaction parameter, λ_i^0 is the limiting equivalent conductivity of the counterion, and λ_p is the equivalent conductivity of the polyion. The interaction parameter f was originally considered as the fraction of free ions, but has been derived by Manning and others to be related to D_c/D_c^0, the ratio of the diffusion of the counterion in the polyelectrolyte solution to the counterion diffusion without polyelectrolyte at infinite dilution.[119,120] Wandrey later found that the parameter f only agreed with Manning's predictions when the Debye length divided by the contour length of the polymer was low. More recently others have developed more complex models for conductivity, but they are not easily simplified and can be challenging to implement for all but ideal polymers.[121,122]

Recently, the vast majority of polyelectrolyte work has considered only the polymer backbone or accounts for the counterion only to allow accurate description of the chain morphology.[123–125] In this work, where the goal is eventual implementation of a polyelectrolyte solution within a lithium-ion battery, particular emphasis must be given to counterion transport. Prabhu in 2005 reviewed the literature on counterion dynamics, focusing on the influence of the counterion on the polyion, but also discussing the counterion behavior alone.[126] In his original papers Manning covers counterion motion, beginning with a theory for a fixed charge lattice that could be extended to polyelectrolytes and extending later to his seminal limiting laws series.[108,127,128] These early theories were particularly interested in understanding counterion condensation, predicting changes in diffusion mainly as a function of charge on the polymer. More recently, several papers by Leyte utilized a Poisson-Boltzmann-Smoluchowski cell model where the polymer is described by a cylindrical cell within which counterions may move freely along the chain, but experience electrostatic interactions moving away from the chain, to describe diffusion data in a polyelectrolyte solution.[129–131] This model captured their experimental data which had a non-monotonic dependence of counterion diffusion on concentration within the dilute and semidilute range, but fails as the solution becomes more concentrated. In contrast, other coarse grain simulations have shown that counterion diffusion monotonically decreases with concentration.[132,133] The authors suggest that this discrepancy is a result of weak coupling of the counterion to the polymer. The relative motion of counterions to the polyion has also been studied at times via the transference number (usually reported as the transference number of the polyion, or $1 - t_+$ as defined in this dissertation in the absence of added salt). In 1950, using radioactive sodium, Huizenga et al reported the polyion transference number of polyacrylic acid to vary

between 0.3 and 0.5, increasing with percent neutralization (increasing sodium ion content).[134] Vink has also summarized some transference number measurements, finding values spanning 0.2 to 1.[116]

Historically, polyelectrolyte solutions have been studied almost exclusively in water due to their relevance as model biological systems and other uses such as layer by layer film deposition; however an important parameter is the solvent quality for the polymer backbone. Neutral polymers exhibit a rich array of interactions with solvent, including a variety of phase behavior and challenging to predict solubility. Charged polymers are naturally even more challenging. The most often studied polyelectrolyte solution, polystyrene sulfonate in water, contains a hydrophobic polymer without its charge groups, and thus there is a competition between collapse of the chain and electrostatic repulsion. Dobrynin has extensively described hydrophobic polyelectrolytes, and the necklace, or bead – string model is most often discussed.[112,135,136] Past a critical number of charged monomers on the chain, a collapsed polymer glob will begin to extend, and eventually form a series of smaller, dense blobs with extended monomer strings between them. This is in contrast to a polyelectrolyte in good solvent (a hydrophilic polyelectrolyte in water), which is said to take on a random walk within electrostatic blobs along the entire chain, while these electrostatic blobs take on a random walk themselves.[113] These ideas are further influenced by the stiffness of the polymer backbone, nature of the ions, and concentration. An important caveat in many of these theories is that the length of the polymer is quite long, as shorter chains simply do not have enough monomers to form complex structures.[137] Clearly these different conformations will also influence the transport properties of the polyelectrolyte solution. The theory of Bordi, Cametti, and Gili suggests that the polyion equivalent conductivity is only a function of the fraction of free ions and a solvent quality parameter, related to the theta temperature.[138] Generally, they find lower equivalent conductivity of the polyion for better solvent conditions and an increase with increasing fraction of free ions. They note, however, that counterion condensation is also a function of concentration and solvent quality, creating a complex interplay of parameters.

Polyelectrolytes have also been studied to some extent in non-aqueous solvents, as reviewed thoroughly by Hara.[139,140] In polar solvents that are able to solvate ions, polyelectrolyte behavior has been observed, and in some cases used to better understand the behavior in water. Essafi, for example, studied the influence of solvent quality with polystyrene sulfonate in water and DMSO, finding the solution in DMSO is structurally similar to a hydrophilic polyion in water.[141] It has also been shown that polyelectrolyte solution behavior can be observed in nonpolar solvents, if the ions are able to be solvated.[142] There has been relatively little theory or simulation with an explicit nonaqueous solvent, however. In most cases the solvent is modeled as a dielectric medium, or explicit water is used. The recent study by Smiatek, Wohlfarth and Holm is one of very few to directly model the ion condensation behavior of alkali metal ions in nonaqueous solvents (chloroform, DMSO), though careful investigation of the ion transport (apart from a calculation of diffusion coefficient) as a result of this behavior was not considered.[143] The theoretical foundation to predict counterion behavior in nonaqueous polyelectrolyte solutions is therefore limited, though adjustments to the theory for aqueous solutions seems a direct route to such predictions.

VII. Outline of this Dissertation

This dissertation first discusses in detail the synthesis and characterization of the class of polymers utilized throughout the following chapters, polysulfone. Specifics for the polymers used in each following chapter are included within those chapters. In Chapter 3, a variety of these polymers are employed as dry SIC polymer electrolytes and their ionic conductivity is

characterized extensively. The wide array of polymers synthesized is used to investigate the commonly used Vogel-Tammann-Fulcher equation for polymer conductivity, and the results are extended to all polymer electrolytes. In Chapter 4 the same polysulfone polymer is employed as a polyelectrolyte solution to investigate the transport properties of these solutions in typical battery-relevant carbonate solvents, finding poor performance particularly in terms of conductivity. Chapter 5 employs several different length sulfonated polysulfones for a more fundamental study of ion, solvent, and polyion transport in both aqueous and nonaqueous solutions. In Chapter 6, a method to improve conductivity using crown ether additives is demonstrated to enable a battery to charge and discharge. Together, this work sheds light on the creation of a polymer-based high transference number electrolyte in both the liquid and solid states, and particularly highlights many areas for future study.

2. Synthesis of Polysulfone-Based Polymers

Polysulfone polymers, also called poly(arylene ether sulfones), polysulphones, and many other names are a broad class of polymers based on the linkage shown in Scheme 2.1. These polymers are commercially available under several brand names including Udel and Radel, which use different linkages between sulfone units. Originally invented by Union Carbide, these polymers have found many applications due to their durability and tunability.[144] The original synthesis involved a nucleophilic aromatic substitution reaction using a strong base (NaOH). In 1985 McGrath and coworkers described a method using a weak base shown in Scheme 2.2 that was more versatile.[145] This weak base method was later extended to incorporate a wide variety of moeities into the polymer, including sulfonated monomers.[146,147] Copolymers can also be made by this method provided that the constituents have appropriate end groups.[148,149]

Scheme 2.1. The typical polysulfone linkage

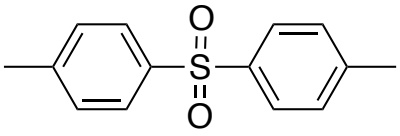

Scheme 2.2. The typical weak base polymerization of polysulfone (Radel)

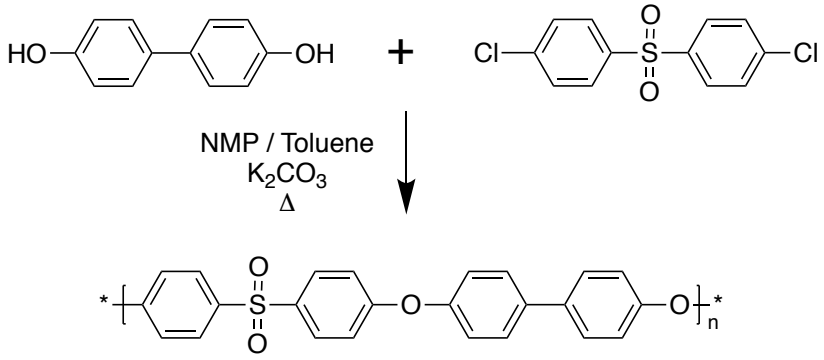

In this dissertation, sulfonated polysulfone/poly(ethylene glycol) copolymers were prepared for the first time, combining procedures for sulfonated polysulfone and the previously reported poly(ethylene glycol) copolymers.[146,149] Different formulations of this copolymer are used in the subsequent chapters, and specifics on those individual polymerizations are included there. Here, the general procedure of the polymerization is described. The polymerization is the same as that outlined in Scheme 2.2, although the sulfone monomer may be replaced by a disulfonated monomer, and the biphenol can be replaced by another difunctional hydroxyl containing species, including poly(ethylene glycol) (PEG). The original paper of McGrath contains many details on the weak base class of polysulfone synthesis reactions, including the kinetics and mechanism.[145] The thesis by Jeffrey Mecham contains many more details on the original reaction, and the reaction with sulfonated monomers including preparation of the sulfonated monomer, although this is now commercially available.[150]

I. Material Considerations

As a condensation reaction which produces water, the presence of additional water in the reaction from the monomers and solvent would limit the attainable molecular weight. In addition, obtaining a perfectly stoichiometric ratio of monomers is important, and impurities not accounted

for when weighing material can have a significant impact. Solvents should be anhydrous, and monomers should be dried prior to use. Sulfonated monomers and PEG can have significant water uptake, and thus must either be weighed quickly or weighed in a dry environment. The weak base, potassium carbonate, should also be dried, but it is used in excess and thus its weight is less important. The inherent polydispersity of PEG also introduces an error in the stoichiometric balance of end groups which cannot be entirely controlled for. N-methyl-2-pyrrolidone (NMP) is used as the reaction solvent for all reactions in this dissertation, but in principle DMSO would also function similarly. N, N- dimethylacetamide is used for polymers without sulfonate groups due to its lower boiling point, but a higher temperature is necessary for the sulfonated polymers. It has been shown that the type of biphenol monomer (BPA vs. BP vs. BPS, etc.) can have an effect on the final polymer properties, but aside from replacing biphenol with PEG, this has not been studied here.[151]

II. Reaction

The reaction is performed in a glass setup like that in Figure 2.1. Monomers and solvent are loaded directly to a straight, 3-neck flask. This reaction is typically performed at around 1-5 gram scale, at 20-30wt% solids. A nitrogen gas inlet is attached, along with a Dean Stark or Barret trap and a condenser. Heating tape is wrapped around the line going to the trap. The trap is filled with toluene until it just overflows to the reaction vessel. A 3:1 ratio of toluene:NMP is used in the reaction vessel along with the toluene in the trap to perform azeotropic removal of water in the early stages of the polymerization. Initially the temperature is raised to 110°C – 140°C, above the boiling point of toluene. This causes toluene and water to evaporate together. When the temperature is lowered in the condenser, the azeotrope breaks and water falls to the bottom of the trap while toluene is allowed to reflux to the reaction. This removes water formed as the OH groups in the reaction react with potassium carbonate. Once these have reacted, the reaction changes color (anywhere between gold, green, and purple depending on the sulfonate and PEG content). At this point, the toluene in the trap should be removed, and the toluene from the vessel will collect in the trap. This improves the solubility of reactants and salt, and allows the polymerization to proceed. The temperature can then also be raised to 190°C. At this point the heating tape on the trap should also be turned off to keep NMP within the reaction vessel.

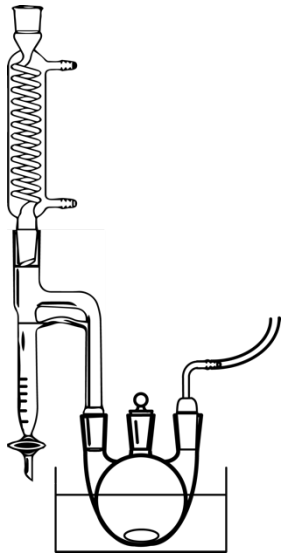

Figure 2.1. Synthesis setup used for all polymerizations.

The polymerization may take anywhere from 6 to 72 hours, with high PEG or sulfonate contents requiring more time to achieve high molecular weight. The molecular weight can be tested by precipitating a small aliquot, with high molecular weight polymers precipitating as a bead that is not easily broken. At the end of the reaction, the vessel is allowed to cool and the polymer may be precipitated. High ion content and high PEG content polymers are soluble in water and should be precipitated in isopropanol or methanol only to remove NMP, while standard polysulfone should be precipitated in water to remove salt. Salt and trace solvent is then removed by dialysis in water, either in a dialysis bag for soluble polymers or otherwise simply by soaking in water. High ion content and high PEG content polymers tend to permeate even dialysis bags with a low molecular weight cutoff relatively rapidly and thus yield is improved greatly by dialyzing in a mixture of water to alcohol. The molecular weight cutoff for most dialysis bags is determined against dextran, and as a result varies depending on the polymer contained within.

The sulfonated polymers may be ion exchanged by soaking in water, or in a dialysis bag with any lithium salt. Initially it was thought that an elevated temperature would speed the ion exchange, but the PEG containing polymers appear to hydrolyze (evidenced by a significant drop in molecular weight) in the presence of salt in water at elevated temperature. Testing several different salts found that lithium carbonate prevented this hydrolysis, although it was also determined that the rate of hydrolysis was very slow at room temperature.

III. NMR Characterization

The ^{1}H NMR characterization of sulfonated PSF-co-PEG is summarized in Figure 2.2, Figure 2.3, and Figure 2.4. In Figure 2.2, the spectra for plain polysulfone, fully sulfonated polysulfone and a copolymer with PEG and no sulfonate groups are shown. The peaks are readily assigned as shown for fully sulfonated polysulfone and plain polysulfone. In the copolymer, main chain PEG peaks are immediately apparent, and the copolymer can be confirmed by the presence of the two side peaks at ~3.8 and 4.2ppm. These peaks are from the final monomer in the short chain PEG which is next to the aromatic ring of the sulfone monomer. The aromatic region of the copolymer also contains new peaks due to the same new environment (A' and B').

The presence of these peaks due to the different neighboring monomers indicates a difficulty in analysis of the variety of compositions of this polymer. Copolymers with both PEG and sulfonate groups introduce new proton environments for each different possible neighbor monomer, and different possible end groups. Two different copolymer series are illustrated in Figure 2.3, and Figure 2.4 for a constant PEG content and constant sulfonate content, respectively. In Figure 2.3, the protons above 8 ppm all relate to the proton immediately next to the sulfonate group on the monomer. As more of the sulfonated monomer is added, this peak splits into several as there are now more possible neighbors to that same proton. The same is true for the peaks associated with the monomers at the end of the short PEG chain. Figure 2.4 also shows that new peaks within the aromatic area appear as a function of PEG content.

Despite the many overlapping peaks, it is possible to obtain the average composition of the polymer by NMR. The peaks past 8 ppm relate only to the proton next to a sulfonate group, while all of the PEG peaks are separate from any other monomer. It is also known that replacing one biphenol with PEG removes 8 protons from the aromatic region between 8 and 6.8, while replacing one sulfone unit with a sulfonate unit removes 1 proton from the same region while adding one to the peaks above 8 ppm. One can thus simply solve for the composition that would give the ratio of these unique peaks to all of the other aromatic protons which overlap.

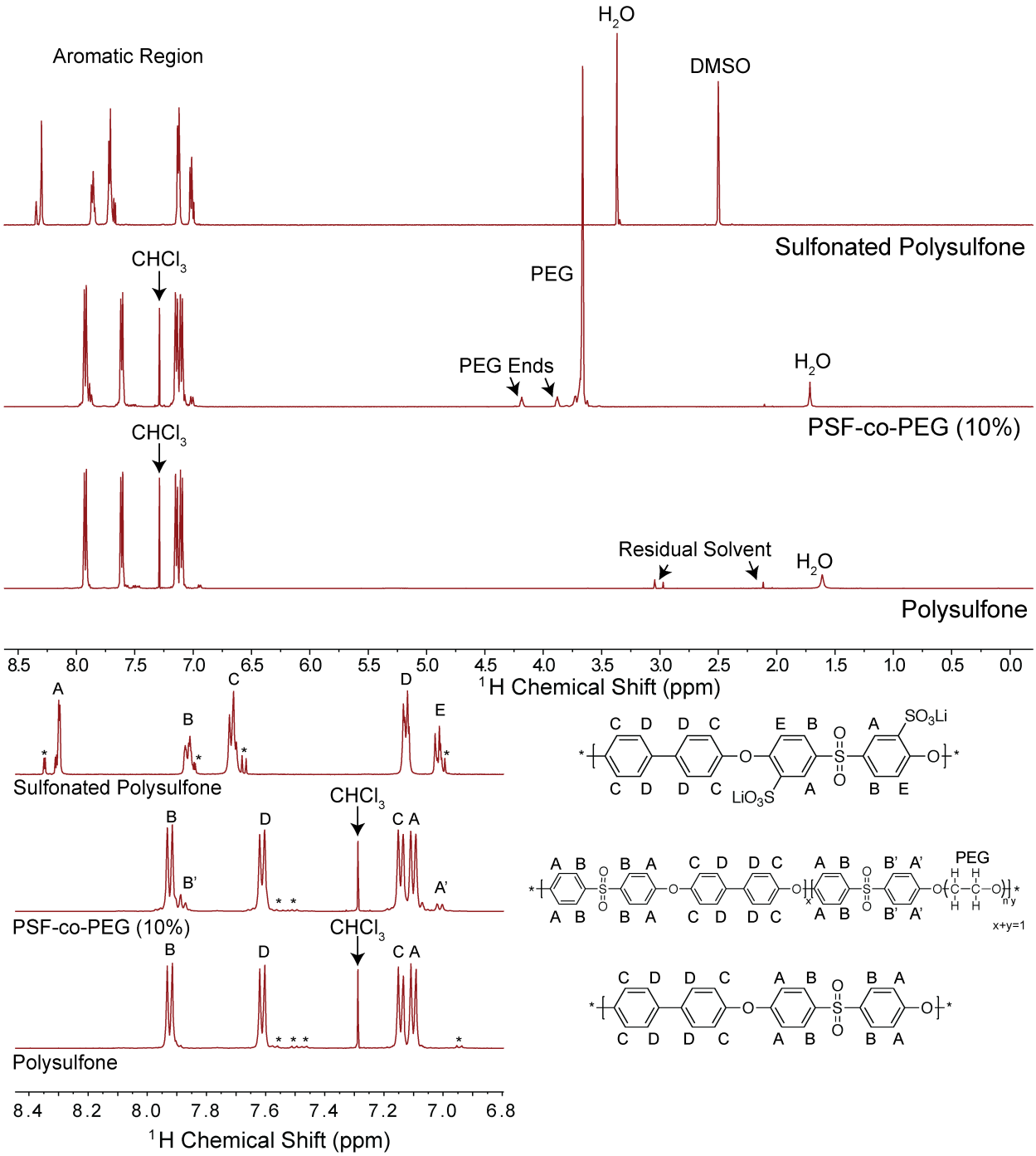

Figure 2.2. ^{1}H NMR characterization of polysulfone, PSF-co-PEG (where 10% of the biphenol unit has been replaced by PEG of Mn=1000Da), and fully sulfonated polysulfone. Sulfonated polysulfone is in DMSO-d_6 while the others are in $CDCl_3$. The aromatic region in the top spectra is expanded below. Peaks associated with end groups are marked with a star.

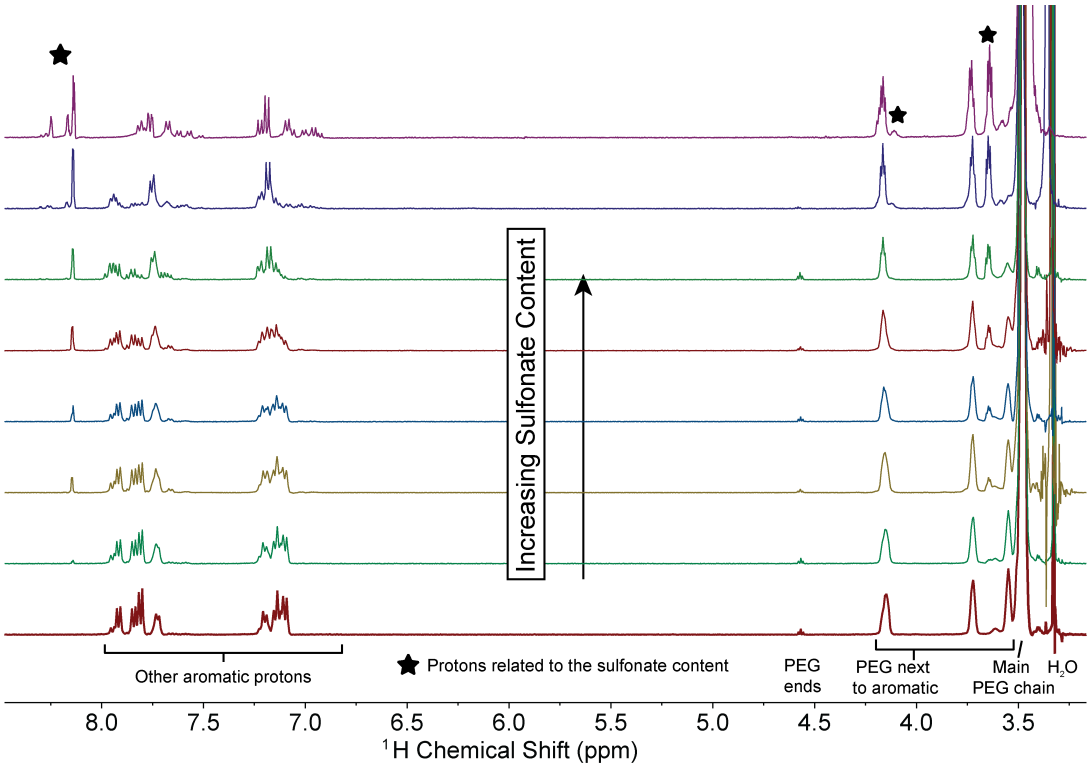

Figure 2.3. ^{1}H NMR Characterization in DMSO-d_6 of a series of sulfonated PSF-co-PEG, with a constant amount of PEG (70% of the biphenol replaced by PEG) and varying sulfonate content.

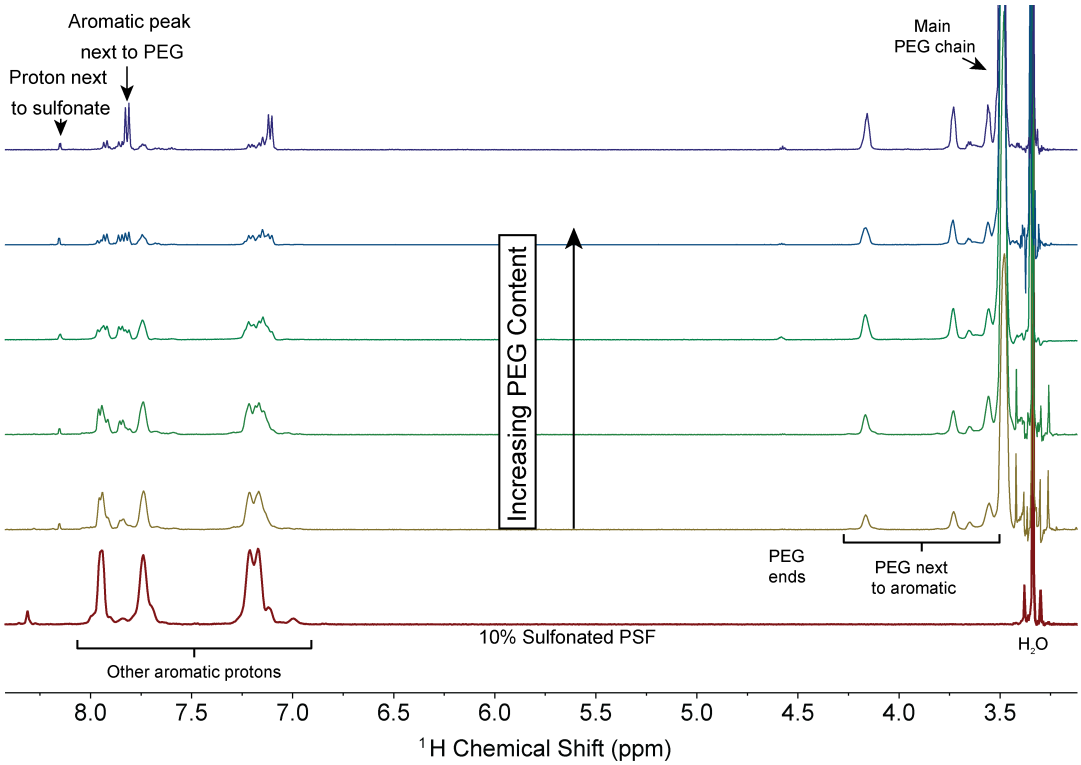

Figure 2.4. ^{1}H NMR Characterization in DMSO-d_6 of a series of sulfonated PSF-co-PEG, with a constant sulfonate content (10% of the sulfone monomer is sulfonated) and varying PEG content.

3. The Compensation Effect in the Vogel – Tammann – Fulcher (VTF) Equation for Polymer-Based Electrolytes‡

I. Abstract

Single-ion conducting polymer electrolytes have been proposed to significantly enhance lithium ion battery performance by eliminating concentration gradients within the cell. Such electrolytes have universally suffered from poor conductivity at low to moderate temperatures. In an attempt to improve conductivity, numerous studies have sought to better understand the fundamental interplay of ion content and segmental motion, with typical analyses relying on a fit of temperature-dependent conductivity data using the Vogel-Tammann-Fulcher (VTF) equation to assist in separating these effects. In this study, we leverage the large accessible composition window of a newly-synthesized, single ion conducting polysulfone-poly(ethylene glycol) (PSf-co-PEG) miscible random copolymer, to more completely understand the interrelationship of glass transition temperature, ion content, and the polymer's Li^+ conductivity. It is demonstrated here that choice of fitting procedure and Vogel temperature plays a crucial role in the observed trends and importantly, after optimization of the data fitting procedure, a strong positive correlation was observed between the VTF equation prefactor and apparent activation energy for polymers in this electrolyte class. This relationship, known as the compensation effect (among other names) for the related Arrhenius-type behavior of activated processes such as chemical kinetics and diffusion, is shown here to exist in several other polymer electrolyte classes. Given conductivity's inverse exponential dependence on the apparent activation energy, maximum conductivity within an electrolyte class is achieved in samples where the activation energy is small. For a system in which the compensation effect exists, decreasing activation energy also decreases the prefactor, highlighting the limiting nature of the compensation effect and the importance of escaping from it. Blending of small molecules is shown to break the apparent trend within the PSf-co-PEG system, suggesting a clear route to high transference number, high conductivity electrolytes.

II. Introduction

Current electrolytes utilized in commercial lithium ion batteries rely on a binary salt dissolved in a solvent (e.g., $LiPF_6$ in a liquid carbonate mixture).[15] Such systems contain both a mobile cation and anion, leading to the development of significant concentration gradients across the cell.[152] These concentration gradients and the overpotential they generate limit the rate at which the battery may be cycled, limit the thickness of electrode accessible to the chemical reaction, and have been suggested to increase the formation of dangerous dendrites with lithium metal electrodes.[153–155] The magnitude of these concentration gradients is dependent on the relative mobility of the anion and cation, and can be completely eliminated in a single-ion conductor (SIC), an electrolyte in which the anion is completely immobile.[17] Over the last 30 years, numerous attempts have been made to create a SIC, focused on either fixing the anion to the backbone of a

‡ This chapter was originally published in *Macromolecules* and is adapted with permission from co-author H.G. Buss and B.D. McCloskey.[77]

polymer chain or employing Li^+ conductive ceramics.[27,56,63,73,156] Polymer electrolytes have long been studied for their potential electrochemical and thermal stability, particularly for use with a lithium metal electrode, and offer significant advantages over ceramics in terms of processability.[41,70,157]

At room temperature, the highest reported conductivity of a SIC polymer electrolyte is around 10^{-5} S/cm, two orders of magnitude lower than any liquid electrolyte and an order of magnitude lower than the necessary conductivity suggested by Goodenough.[4,27,60] While Newman has suggested that the improvements gained from a SIC would offset an order of magnitude decrease in conductivity, the conductivities currently reported have proven too low for practical use.[17,158]

It is generally accepted that there are two important criteria necessary for the creation of a highly conductive SIC polymer. First, because the polymer acts as both the ion and the solvent, increasing segmental motion of the polymer backbone is critical. Colby and coworkers have extensively characterized a model single ion conducting electrolyte, demonstrating a close relationship between backbone relaxation and conductivity, and the significant importance of the polymer glass transition temperature on its conductivity.[70,159–161] Second, it is important to facilitate dissociation of the anion and cation to increase the number of charge carriers. To do so, to a reasonable approximation, the relative basicity of the polymer chain needs to be higher than the appended anion, such that the polymer is more likely than the anion to occupy the Li^+ solvation shell. Unfortunately, polymers comprised of relatively strong basic components (e.g., amides), have very low segmental motion due to their strong inter and intra-chain molecular interactions. Therefore, new appended anion chemistries (e.g., triflimide-based chemistries) have been developed to delocalize the negative charge and improve dissociation in polymers with high segmental motion and modest basicity (e.g., poly(ethylene oxide)).[76,162] Other methods to improve ion dissociation have focused on spatial segregation of the anion from the conducting phase.[27,69,163]

Separate from these synthetic techniques, small molecule/macromer blending has been used extensively in the literature as another method to either increase segmental motion in polymer systems through plasticization or to improve ion dissociation.[92,159,164]

Regardless of the strategy employed to improve ion dissociation and segmental motion, it is common for researchers to utilize the Vogel-Tammann-Fulcher (VTF) Equation (Equation 3.1) as a means to separate the effects of charge carrier concentration, often related to the prefactor, A, and segmental motion, related to the activation energy, E_a, on overall conductivity, σ, at a given temperature, T.[43]

$$\sigma = Aexp\left(-\frac{E_a}{R(T-T_o)}\right) \qquad 3.1$$

T_o in this equation is referred to as the Vogel temperature, equal to the glass transition in ideal glasses,[165] but typically taken as 50°C below the glass transition temperature in polymer electrolytes.[43] Though this equation is explicitly a model for the polymer matrix and not the ions themselves, it has been successfully used to fit polymer electrolyte conductivity data for many decades.

In this Chapter, a new single ion conducting polymer electrolyte based on polysulfone and poly(ethylene glycol), two miscible polymers with otherwise vastly different mechanical and thermal properties, has been synthesized and is demonstrated as a versatile platform to explore fundamental conductivity behavior. The objective of this work is to demonstrate the inherent trade-off between ion content and segmental motion in a SIC electrolyte. The coupled nature of this

problem in polymer electrolytes, and particularly in a SIC, manifests itself as a strong positive correlation of the VTF equation parameters (particularly A vs E_a), indicating the maximum in conductivity for a given system will occur at low values of the prefactor. This result is concerning for a battery electrolyte where increasing the number of charge carriers is a clear design goal. Blending of small molecules is shown to be a route to break this apparent trend, giving new motivation for a common conductivity enhancing technique.

III. Experimental Section

i. Materials

Bis(4-chlorophenyl sulfone) was purchased from Sigma Aldrich, recrystallized from toluene and dried for two days under vacuum at 80°C before use. Poly(ethylene glycol)s (Mn=300, 600, 1000, 1500, 2000, 4500 Da), anhydrous n-methyl-2-pyrrolidone and toluene were purchased from Sigma Aldrich and used as received. 4,4'-biphenol and sulfonated bis(4-chlorophenyl) sulfone were purchased from Akron Polymer Systems and were dried for two days under vacuum at 80°C before use.

ii. Synthesis

Polysulfone based polymers are synthesized via a condensation reaction in NMP, modifying procedures for PSf-co-PEG from Kim et al. and sulfonated polysulfone from Wang et al.[146,149] The reaction is outlined in Scheme 3.1 and discussed in detail in Chapter 2. Monomers are loaded to a 3-neck flask fitted with a Dean-Stark trap and nitrogen gas inlet in an oil bath on a magnetic stir plate. The mole ratio of Cl to OH is kept at one, and potassium carbonate is added such that at least 15% excess potassium is present. The trap is filled with toluene, and a 3:1 volume ratio of NMP to toluene at 35wt% dissolved solids is loaded to the reaction vessel. The reaction is stirred under nitrogen purge at 145 °C for 4 hours to perform azeotropic removal of water generated during the initial stages of the reaction. Following this phase, most end groups within the reaction have been activated (as characterized by a strong gold color) and the toluene is removed. The reaction temperature is increased to 190°C and allowed to continue until the solution becomes difficult to stir. The reaction times vary from 16 hours for low PEG content polymers to nearly 50 hours at high PEG content. For polymers where less than roughly 50% of the di-chloro monomer is sulfonated, the final mixture can be filtered after adding a small additional amount of NMP and precipitated in DI water. The same is true for polymers where less than roughly 40% of the biphenol is replaced by PEG. For higher PEG or sulfonate content polymers, the final product is either swelled strongly or completely soluble in water, making precipitation infeasible. In these cases, no additional solvent is added and instead water is directly added to the cooled reaction to dilute the NMP. This mixture is placed in a 3500 Da molecular weight cut off dialysis tube (Spectrum Labs) and soaked overnight in DI water to remove salt and NMP. The water is changed once during this time. The dialyzed polymer/water mixture is then frozen and freeze-dried under high vacuum. The final polymer is composed of sulfonated or unsulfonated sulfone linkages between either a single biphenol unit or short chain PEG. As such, these polymers are referred to by mol% sulfonated, as the ratio of SO_3Li to H in R_1 and mol% PEG, as the ratio of biphenol to PEG in R_2.

Scheme 3.1: The synthesis of the sulfonated polysulfone-co-poly(ethylene glycol) single ion conductor (PSf-co-PEG). The ratio within R_1 between lithium-neutralized sulfonate and proton groups is referred to as mol% sulfonated and the ratio within R_2 between single biphenol linkages and short chain PEG is referred to as mol% PEG. Plain polysulfone made simply from bis(4-chlorophenyl) sulfone and biphenol monomers would be referred to as R_1 = 0 mol% sulfonated and R_2 = 0 mol% PEG. A polymer made from solely short chain PEG as one monomer and sulfonated bis(4-chlorophenyl) sulfone as the other would be referred to as R_1 = 100 mol% sulfonated and R_2 = 100 mol% PEG. R_1 and R_2 composition can be independently varied and are used as studied variables throughout this article. Unless otherwise noted, 1,000 Da molecular weight PEG (m=22) is used to synthesize studied polymers.

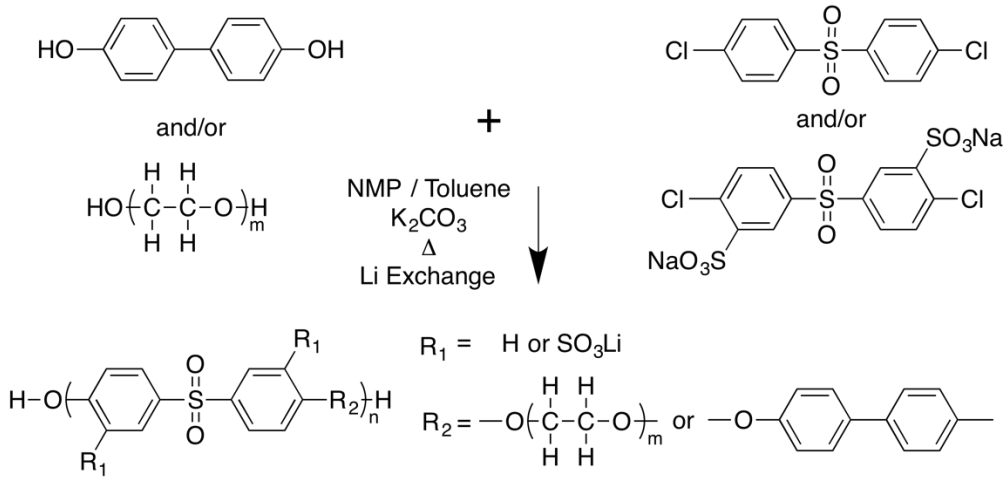

iii. Ion Exchange

The lithium form of the sulfonated polymer can be prepared by placing the polymer in a dialysis tube and soaking it in 0.1M lithium carbonate in Milli-Q water. It was found that the rate of hydrolysis at elevated temperatures was significantly reduced when using lithium carbonate, though at room temperature the rate is slow enough that other salts such as lithium bromide were also satisfactory. Complete ion exchange was verified by Inductively Coupled Plasma – Optical Emission Spectroscopy within the Molecular Foundry at Lawrence Berkeley National Lab.

iv. Polymer Characterization

The correct polymer structure was verified by 1H NMR in DMSO-d_6 on a Bruker 500MHz instrument within the Molecular Foundry. The dried polymers were characterized for thermal decomposition on a PerkinElmer Pyris 1 TGA at 10 °C/min and for glass transition on a PerkinElmer DSC 8500. All polymers are stable to 300°C, as shown in Figure 3.1. Glass transition is reported from the second heating scan at 20°C/min. Samples that were dried prior to DSC displayed the same glass transition on the first heating as those which were not dried and simply run through two heating/cooling cycles. Representative DSC scans are included in Figure 3.2. Polymer molecular weight was characterized by gel permeation chromatography on an Agilent 1260 Infinity Series fitted with Waters Styragel HR 3 and 4 columns. A mobile phase of NMP with 0.05M LiBr at 70°C was utilized and the molecular weight was calibrated to PEO standards (Fluka). It should be noted that determination of the true molecular weight of this polymer requires further study, as the highly heterogeneous, ion containing polymer may interact strongly with the GPC column; however, the values reported here should be reasonably suggestive of the polymer size.

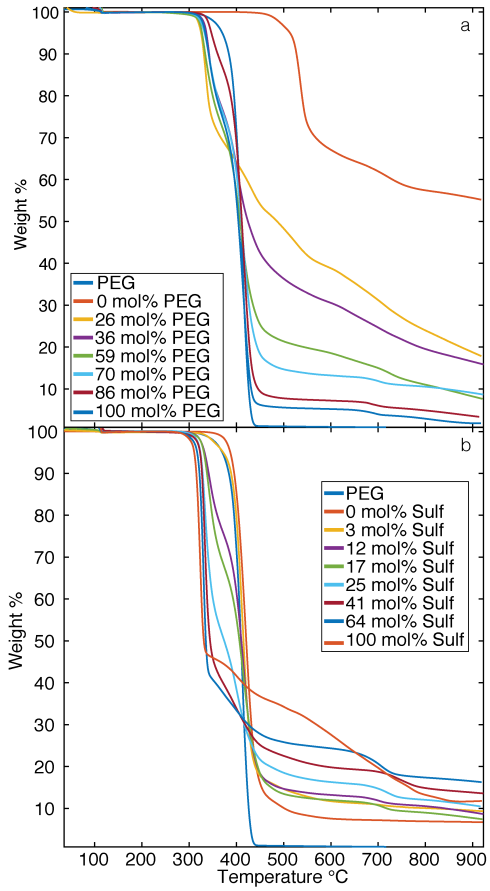

Figure 3.1. Thermogravimetric analysis on the polymers shown in Table 3.1 at a heating rate of 10 °C/min. Weight is normalized to the weight after drying at 100°C for 30 mins. a) Polymers with constant R_1 sulfonate mol% of 10 and b) polymers with constant R_2 PEG mol% of 70. All polymers are stable past 300°C. The ion containing polymers begin to degrade ~40 °C before PEG alone. Similar behavior has been reported for binary salts dissolved in PEO.[166] Sulfonated polysulfone (0 mol% PEG in a) does not degrade before 500 °C.

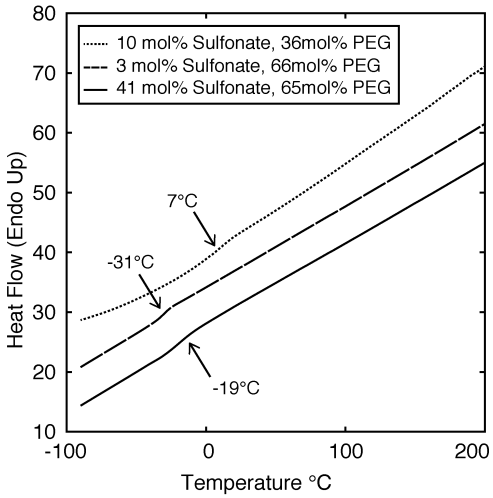

Figure 3.2. Representative dynamic scanning calorimetry (DSC) scans for three polymers at different sulfonate and PEG contents. Scans shown are the second heating scan, using liquid nitrogen cooling with a helium purge, and at a rate of 20°C/min. Only a single glass transition is observed (noted on plot), indicating no phase separation or crystallization. Scans shown are representative of all dry copolymers.

v. Polymer Blending

PEG (M_n=300) and the dry copolymer are weighed and added to a vial. The vial is then loaded to a drying oven over P_2O_5 at 70°C and allowed to mix for several days. The final dry homogenous mixture is then unloaded to an argon glovebox for electrochemical characterization.

vi. Electrochemical Characterization

A modified Swagelok cell design, in which a spring-loaded plunger is used as one of the current collectors, was selected for electrochemical measurements (schematic included in Figure 3.3). Polymers with a T_g above ambient temperature are hot pressed into a 0.005in thick insulating fiberglass/epoxy Garolite spacer at 10,000psi, 30°C above T_g, between Kapton films. The resulting film area is 0.309 in^2. The final amber colored, translucent films were placed on Nickel foil electrodes. Polymers with a T_g below ambient are hand pressed into the same spacer on nickel foil electrodes with a Teflon film. The resulting polymer films from either case are dried at 70°C over P_2O_5 under vacuum for 2 days. While still under vacuum, the polymer films are brought into the glovebox before being exposed to the dry argon atmosphere. Dry blend samples are spread on nickel foil within a 0.01in thick HT6135 silicone separator to better isolate the semi-liquid samples. Cells for conductivity measurements are made by applying a second nickel electrode to the dried nickel/polymer stack and then placing this stack in the Swagelok cell.

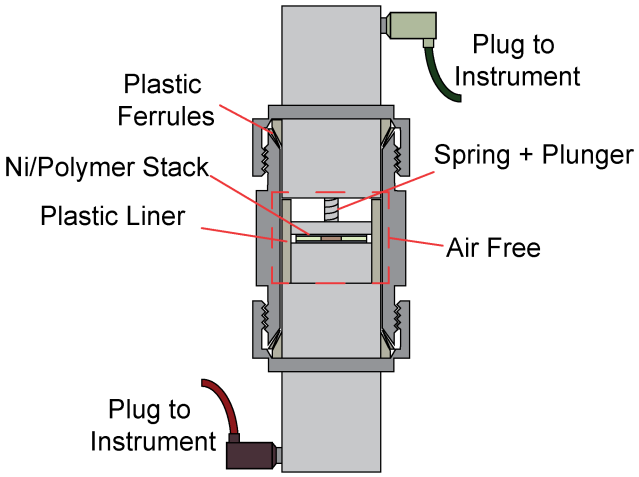

Figure 3.3. Custom Swagelok-type cell used for electrochemical measurements. The polymer is placed within a separator ring to maintain a constant area and nickel electrodes are placed on either side. This Ni/polymer stack is loaded to the bottom of the cell within an Argon glovebox. The second half of the cell contains a spring and plunger which applies a constant pressure to eliminate the possibility of delamination. The spring assembly and sample area are isolated by plastic ferrules. The cell is connected to the VMP3 potentiostat by banana plugs drilled into the stainless steel body.

Impedance measurements are performed using a Biologic VMP3 potentiostat. Cables are run into Thermotron S-1.0-3200 ovens and all samples are allowed to equilibrate for at least an hour prior to measurement at any given temperature. Conductivity is measured via AC Impedance spectroscopy (1MHz – 1 Hz, with an amplitude of 20mV), where the bulk sample conductivity is taken from the minimum of the phase angle. This value agrees with the value taken from the location at which the semicircle intersects the abscissa on the Nyquist impedance plot. An example Nyquist plot for a single polymer sample is included in Figure 3.4. Samples are first allowed to

equilibrate until their conductivity was constant at 110°C so that film thickness remained constant over successive heating. The samples are then brought to 30°C for 4.5 hours, followed by heating from 30 to 110 and back down to 30°C at 10°C increments. Temperature control was verified by an independent thermocouple placed around the samples and is always within +/- 0.5°C of the programmed value. Conductivity values at any given temperature are reported from the heating cycle after equilibration at high temperature, but these values are within error of the values from cooling. Values reported are the average of at least 3 independently made films from each independent polymer sample.

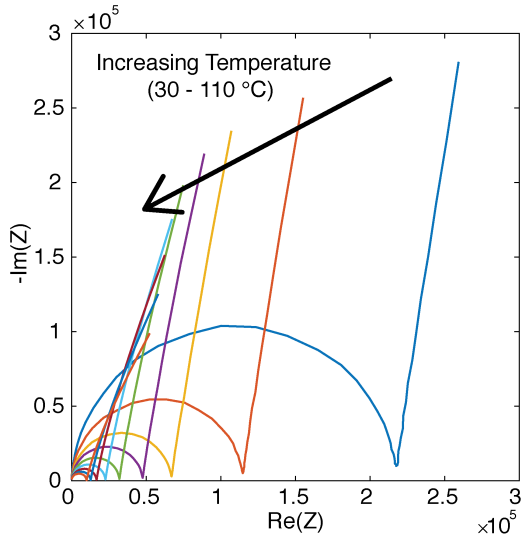

Figure 3.4. Example Nyquist diagram for the sample with R_1=15 mol% sulfonate and R_2 = 100 mol% PEG during a heating scan from 30 to 110°C. The resistance of the polymer stack is taken from the minimum of the phase angle, which corresponds to the location at which the semicircle intersects the abscissa in the Nyquist diagram.

IV. Results and Discussion

Sulfonated PSf-co-PEG (1 kDa PEG) was synthesized over a wide range of compositions and two representative series are discussed first. Table 3.1 includes the properties of a set of polymers with varied PEG content at roughly 10% degree of sulfonation (i.e., R_1 in scheme 1 is set at 1/9 SO_3^-/H, and R_2 PEG to biphenol ratio is varied over a large range) and another with varied sulfonate content at roughly 70 mol% PEG (R_1 SO_3^-/H ratio is varied over a large range, while R_2 is set at 7/3 PEG/biphenol). Ion content varies between 9 and 15 mol% for the "10% sulfonate" series, and between 66 and 77 mol% for the "70 mol% PEG" series. The trends with sulfonate content and PEG content are expected to be similar across compositions, though these two series were specifically chosen to avoid the chance of PEG crystallinity at high PEG content, and increased glass transition at high ion content. As shown in Figure 3.5, the addition of PEG to sulfonated polysulfone reduces the glass transition temperature from nearly 275°C to below –40 °C.

Table 3.1 Summary information of the polymer series at roughly R_1 = 10 mol% sulfonate, and the second at roughly R_2 = 70 mol% PEG discussed in Figure 3.5 - Figure 3.8. Weight percent PEG is the calculated weight of ethylene oxide repeat units in the overall polymer.

R_1 Mol% Sulfonate	R_2 Mol% PEG	Wt% PEG	M_n	PDI
10%	26%	41%	13,700	2.2
10%	36%	50%	11,700	1.9
12%	59%	64%	12,300	1.8
11%	70%	69%	12,500	1.9
11%	86%	75%	8,500	2.0
15%	100%	79%	4,700	1.8
3%	66%	68%	14,000	1.8
17%	71%	69%	10,100	1.9
25%	66%	66%	6,700	1.9
41%	65%	63%	6,200	1.7
64%	71%	64%	13,500	1.8
100%	77%	63%	14,200	1.8

Addition of sulfonate groups to PSf-co-PEG increases the glass transition temperature, though by a lesser degree. Ion content has been shown to affect segmental motion and the glass transition of PEO due to transient crosslinks formed by the ions, and is likely the cause of the increased T_g here; however, explicit study of this effect is beyond the scope of this paper.[167] Importantly, all samples displayed only a single glass transition, indicating the samples are not phase separated. Representative DSC scans are included in Figure 3.2. All samples except for the sample at 100 mol% PEG were completely amorphous over the temperature range studied, indicating that the typical crystallinity of PEG is disrupted by the presence of sulfone linkages and ion content. At the highest PEG content, the sample exhibited a melting temperature near 20°C, below the range of conductivity analyzed.

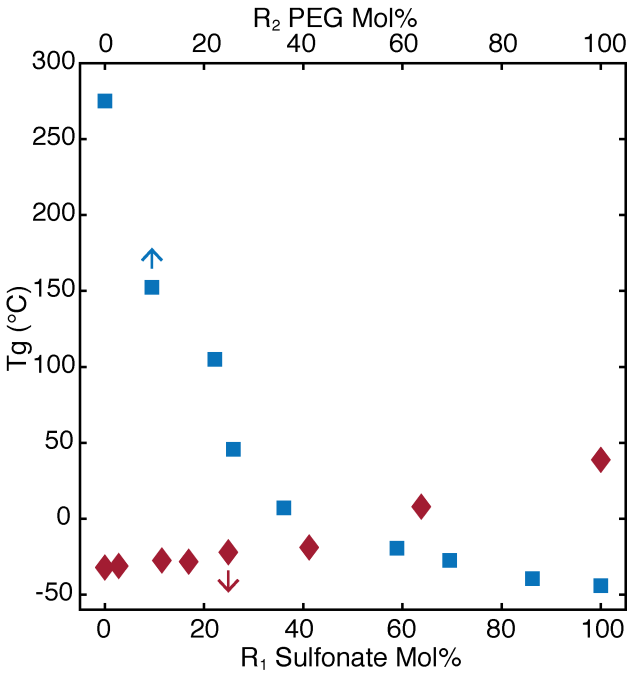

Figure 3.5. Glass transition temperature as a function of R_1 sulfonate mol% at a constant R_2 PEG mol% of 70 (bottom) and as a function of R_2 PEG mol% at a constant R_1 sulfonate mol% of 10% (top). Increasing PEG content drops the glass transition by ~300°C, while increasing sulfonate content increases the glass transition by ~100°C.

The conductivity behavior as a function of temperature and PEG content is summarized in Figure 3.6a. It is immediately evident that the addition of PEG results in a several order of magnitude increase in conductivity at any temperature and that polymers below 30 mol% PEG are essentially nonconductive below 60°C. The dependence of conductivity on sulfonate content is summarized in Figure 3.6b, indicating that a maximum in conductivity occurs around 50 mol% sulfonate at 110°C. This maximum corresponds to an EO/Li ratio of ~18, slightly lower than the maximum observed around 30 for PSTFSI-PEO.[27,75] At lower temperatures, this maximum shifts to lower sulfonate mol%, corresponding to a higher EO/Li ratio. These conductivity trends are reminiscent of most SIC polymer electrolytes and closely resemble the trends of the PEG based ionomer synthesized by Colby and coworkers in 2006.[70]

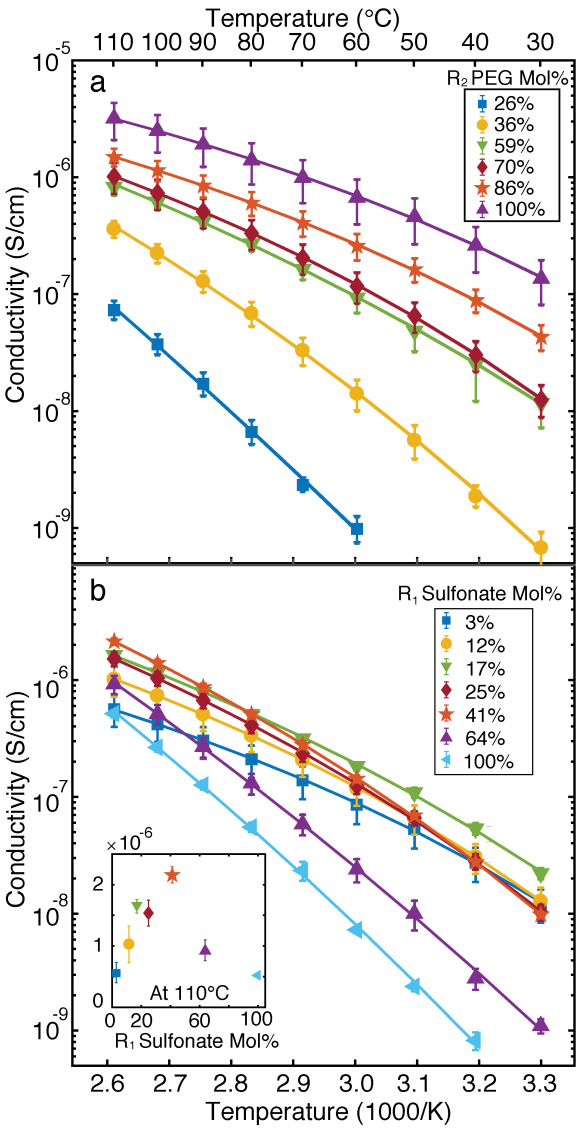

Figure 3.6. Conductivity as a function of inverse temperature for a) increasing R_2 PEG mol% at a constant R_1 sulfonate mol% of ~10 and b) increasing R_1 sulfonate mol% at a constant R_2 PEG mol% of ~70. Lines shown in a) and b) are VTF fits utilizing Fit #2, as outline in Table 3.2. Inset in b) displays the conductivity at 110°C as a function of R_1 sulfonate mol%. Error bars are the standard deviation of five independent samples. Increasing PEG content improves conductivity by several orders of magnitude at any temperature, while increasing sulfonate content exhibits a maximum around 50 mol% sulfonate at 110°C, and 25 mol% at 60°C.

Figure 3.7a demonstrates that the orders of magnitude increase in conductivity with higher PEG content can be explained by normalizing the temperature to the T_g. The conductivity of all six polymers collapse to significantly less than an order of magnitude difference such that at any given T-T_g, all polymers with similar ion content have roughly the same conductivity. This clearly confirms the known importance of segmental motion on ion transport, and mirrors the trend observed by Colby et. al.[70,168,169] Deviations here can be ascribed to variations in ion content, as the last data point in the inset figure also has the highest ion content (15 mol% sulfonate vs 10-12 mol% sulfonate for the other polymers in the series).

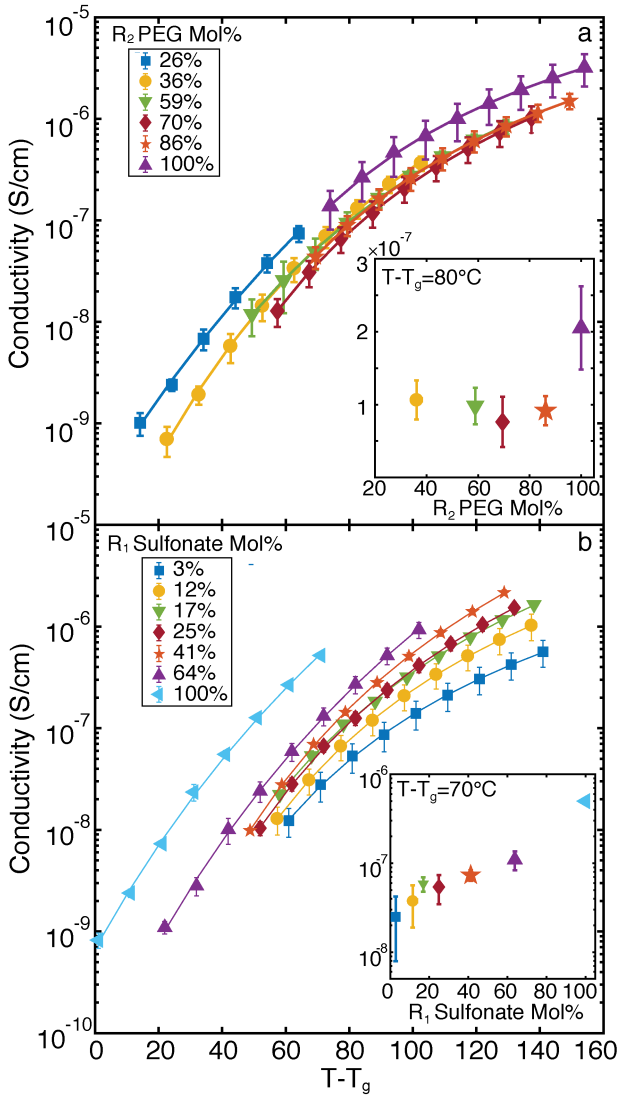

Figure 3.7. a) Conductivity versus $T-T_g$ for the series at an R_1 sulfonate mol% of ~10 with inset linecut at a $T-T_g$ of 80°C. b) Conductivity versus $T-T_g$ for the series at an R_2 PEG mol% of ~70 with inset linecut at a $T-T_g$ of 70°C. For constant ion content, the conductivity collapses when normalized to T_g. At constant PEG content, increasing ion content causes an increase in conductivity relative to T_g.

The importance of ion content is demonstrated in Figure 3.7b, where again the temperature has been normalized to the glass transition temperature of each polymer. Here, the conductivity does not collapse together, and at any given $T-T_g$, where segmental motion of each polymer is expected to be similar, the polymer with the highest ion content has the highest conductivity. Noting the trend observed in Figure 3.5, where increasing ion content increases the T_g, this ion content/segmental motion tradeoff explains the maximum in conductivity seen for the varied sulfonate content series (Figure 3.6b inset). As ion content increases, there is an initial increase in conductivity due to the addition of charge carriers, but eventually the T_g is increased to the point that conductivity begins to decrease. These trends strongly corroborate the existing understanding of SIC polymer electrolytes.[27,70,75]

The VTF equation is frequently applied at this point in similar studies to further understand the relative importance of ion content and segmental motion. The Vogel temperature T_o is often

taken as 50°C below the glass transition temperature, based on empirical evidence that conductivity data is well fit by this relation.[43] Here it was found that the choice of T_o and fitting method for the conductivity data is critical to the apparent trends of A, E_a, and T_o in Equation 3.1 as a function of polymer composition. To illustrate, the resulting value of A as a function of sulfonate content (polymers from Figure 3.6b) is plotted for several different fit routines in Figure 3.8a. Five separate fitting routines were applied to the conductivity data, as outlined in Table 3.2. Fit #1 and #5 were performed by linearizing the data according to the form of the equation while Fit #2 and #3 were achieved by a similar linearized equation, but instead T_o was varied to maximize the linearity of the resulting data. This maximization was performed utilizing the solver tool within Microsoft Excel and verified by the fminbnd function of MATLAB R2016b. Manually varying the value of T_o confirmed the local maximum in R-squared. Other potential maxima may be found at very large values of T_o (>10,000), though these results are nonphysical. Fit #4 utilized the nlinfit function of MATLAB R2016b to fit A, E_a, and T_o, which employs a Levenberg-Marquardt algorithm. It is attractive to assume the choice of Fit #1, utilizing T_g – 50°C, is correct due to the apparent maximum in A around 50% sulfonate that mirrors the maximum in the conductivity. However, examination of Figure 3.8b, where sum squared residuals (optimally zero for a perfect fit) are plotted as a function of sulfonate mol%, demonstrates that this maximum is in fact a result of poor fitting of the conductivity data at high sulfonate content. Utilizing T_g – 50°C produces successively larger residuals as ion content increases. The resulting Arrhenius plots and residuals for the cases at low and high sulfonate content are included in Figure 3.9. The squared residuals plotted in Figure 3.8b are taken from the sum of residuals over all temperatures for a given polymer, as shown for two polymers in Figure 3.9. The reason for the trend in residuals is evident in Figure 3.8c where T_g-T_o, equal to 50°C in Fit #1, T_g for Fit #5, and variable for the others, is plotted. The polymers at high sulfonate content are best fit by a T_o that is 100-200°C below T_g. It may be argued that a significantly lower T_o indicates the mechanism of conduction begins to follow a more direct Arrhenius relation, rather than the modified VTF form, but the exact cause of this difference is not as of yet clear.

Table 3.2. Equations and fitting methods used in Figure 3.8 and Figure 3.9. Fit routine 2 was used for data presented in Figure 3.10 and Figure 3.12.

Fit Routine	Equation	Vogel Temperature Used	Fitting Method
1	$\sigma = Aexp\left(-\frac{E_a}{R(T-T_o)}\right)$	$T_o = T_g - 50°C$	Linearized Data
2	$\sigma = Aexp\left(-\frac{E_a}{R(T-T_o)}\right)$	Fit T_o	Maximize Linearity
3	$\sigma = AT^{-\frac{1}{2}}exp\left(-\frac{E_a}{R(T-T_o)}\right)$	Fit T_o	Maximize Linearity
4	$\sigma = Aexp\left(-\frac{E_a}{R(T-T_o)}\right)$	Fit T_o	Nonlinear
5	$\sigma = Aexp\left(-\frac{E_a}{RT}\right)$	$T_o = 0$	Linearized Data

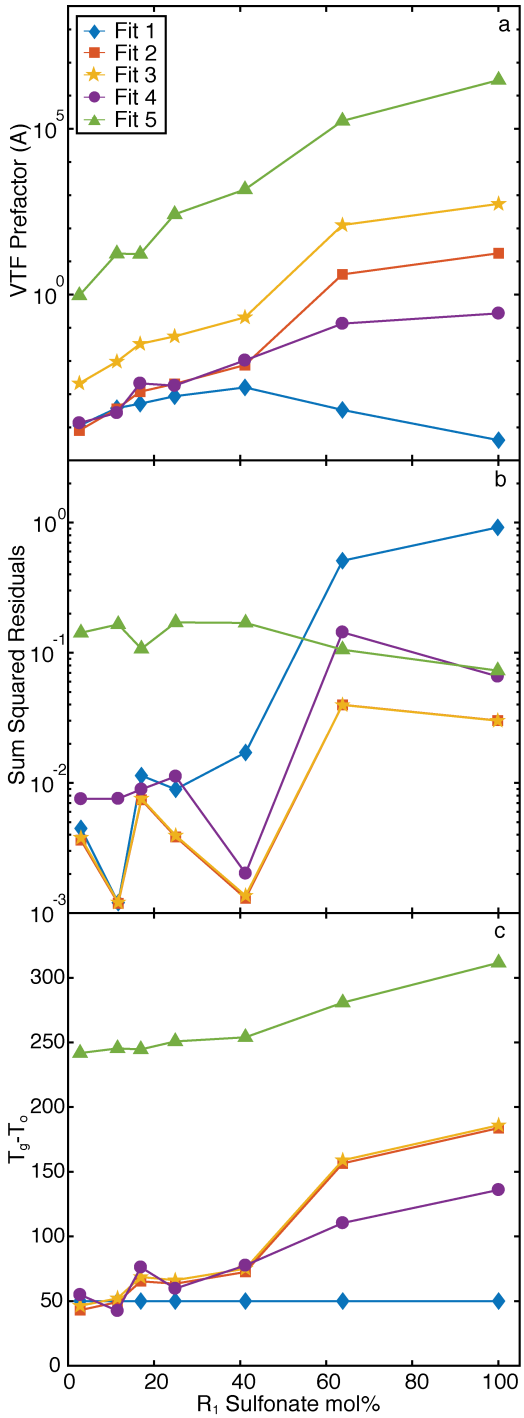

Figure 3.8. a) VTF prefactor (A) versus R_1 sulfonate mol% for the fit routines outlined in Table 3.2. The legend in a) applies to b) and c), and the units on A are S/cm for Fit #1-2 and #4-5, and $S * K^{\frac{1}{2}}/cm$ for Fit #3 b) Sum Squared Residuals for the different fit routines versus R_1 sulfonate mol%. c) $T_g - T_o$ versus R_1 sulfonate mol%, equivalent to 50°C for Fit #5 and T_g for Fit #1, but calculated from the fit for the other routines.

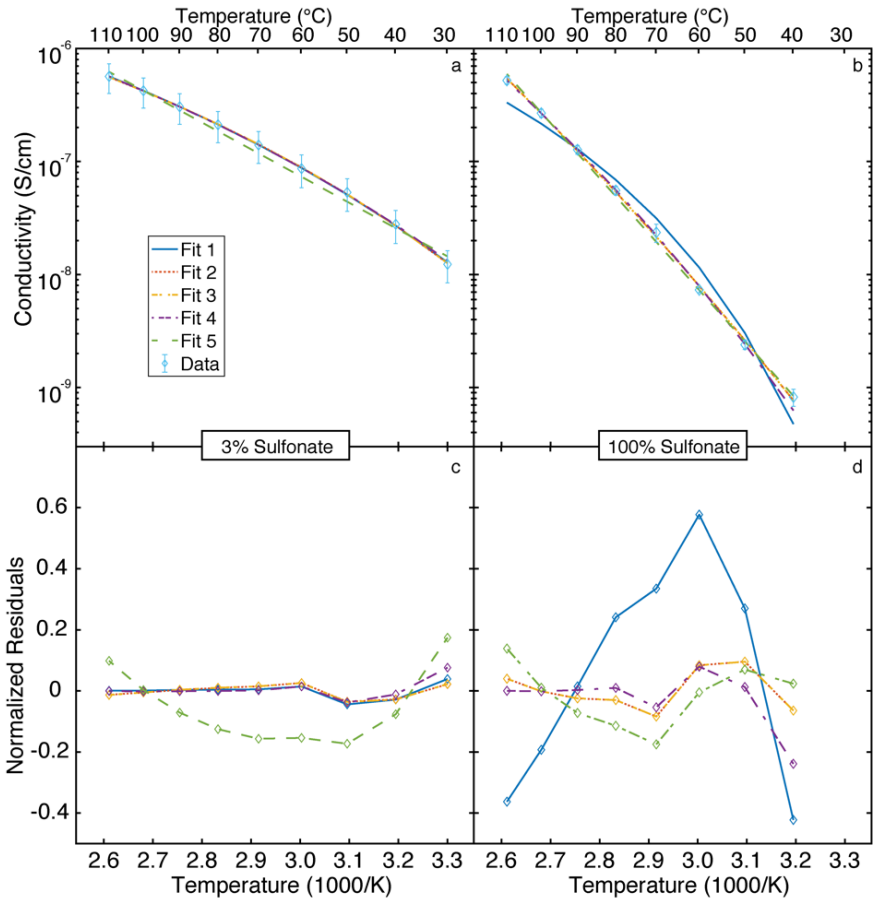

Figure 3.9. Demonstration of the fits at low (a,c) and high (b,d) sulfonate mol%. Residuals are normalized to the conductivity at each temperature to demonstrate the fit across orders of magnitude. At low R_1 sulfonate mol%, fits 1-4 all work well, with relatively random and small residuals. However, Fit #5, the Arrhenius equation, is significantly worse and clearly does not capture the curvature present in the conductivity data. At high R_2 sulfonate mol%, fits 2 and 3 are indistinguishable and are superior to the nonlinear fitting in Fit #4 as the conductivity data crosses several orders of magnitude. Importantly, use of $T_o=T_g$-50°C in Fit #1 predicts significantly more curvature at these temperatures than was experimentally observed. To adequately compare fitting parameters between these samples, either Fit #2 or #3 should be chosen. For simplicity, Fit #2 without the square root of temperature is discussed in this work, but all trends and values are completely identical with Fit #3, except the explicit value of the fitting parameters, which shifts slightly due to the temperature factor.

A factor of $T^{-1/2}$ is often included in the prefactor of the VTF, but Figure 3.8 and Figure 3.9 demonstrate that the inclusion of this factor in the VTF equation (Fit #3) produces no difference in the fit or trends in fit parameters over the analogous model in which it is omitted (Fit #2), only changing the value of A. For simplicity, this paper considers the case without the factor of $T^{-1/2}$, but all trends through the rest of this work are entirely reproducible if it were included. The choice of fitting method is also shown to affect the value of A returned, with a full nonlinear fit providing a poorer fit than the modified linearized method used for Fit #2 and #3. This is due to the scaling of the problem, where the standard nonlinear fit routine in MATLAB does not adequately account for data that spans many orders of magnitude. The most consistent residuals are produced by Fit #5, the Arrhenius equation, but this equation misses the curvature present in the polymer conductivity Arrhenius plots and therefore is a poor choice. It is clear that improper choice of T_o and fitting procedure may lead to misleading results, and as such, T_o was allowed to be a fitting

parameter (rather than set at T_g – 50 °C) for all polymers. The values reported for the remainder of this work are taken from Fit #2, producing the most consistent comparison between all polymers.

Using this fit routine, a strong correlation between the natural log of the prefactor and the apparent activation energy was observed within the PSf-co-PEG system. Figure 3.10 plots ln(A) vs E_a for 30 different polysulfone based copolymers, ranging from 25 – 100 mol% PEG and 2 to 100 mol% sulfonate. In addition, several polymers synthesized from a different length of PEG monomer are included here. The full listing of polymers included in this chart can be found in the supporting information section, Table 3.3 and covers the extent of polymers made. Error bars are shown based on the standard error generated by applying Fit #2 to the full range of data taken for each individual polymer.

In most VTF analyses, the prefactor and activation energy are considered to be related to different underlying processes and, as such, are assumed to be uncorrelated. However, a correlation between the prefactor and activation energy has been the subject of much debate with regard to processes governed by the Arrhenius equation for over 60 years. This relationship takes on many names, including the Meyer Neldel rule, the isokinetic relationship, and the compensation effect.[170–173] There are many ways in which authors have explained the relationship in the Arrhenius form, depending on the exact application, and authors have noted that a single unifying reason for the effect across all systems is unlikely.[174] In several PEO-based systems the compensation effect has been noted for polymer composites following the Arrhenius equation, but there are no reports of the effect for a polymer electrolyte that follows VTF behavior.[175,176]

The presence of a positive, linear correlation between ln(A) and E_a, as opposed to a negative one, is particularly important. In such a case, this relationship can be described by a simple line:

$$\ln(A) = mE_a + b \tag{3.2}$$

where m is the slope of the line and b is the intercept. It can then be shown by simple rearrangement of the VTF equation that the ratio of the conductivity for two different polymers described by Equation 3.2 is given in terms of the ratio of each polymer's prefactor, A, by Equation 3.3, assuming that $T - T_o$ is similar for the two polymers:

$$\frac{\sigma_2}{\sigma_1} = \left(\frac{A_2}{A_1}\right)^{1-\frac{1}{mR(T-T_o)}} \tag{3.3}$$

It is clear that the conductivity response to a change in A is strongly dependent on $mR(T - T_o)$. If $mR(T - T_o)$ is greater than one, an increase in A (*i.e.*, $A_2 > A_1$) will cause an increase in conductivity ($\sigma_2 > \sigma_1$), but, if this value is between zero and one, the conductivity of polymer 2 *will be lower* than polymer 1. If a negative correlation between ln(A) and E_a existed such that the value of m is negative, conductivity would always increase with increasing A because the power in Equation 3.3, $1-1/mR(T-T_o)$, would always be positive. The slope of the fit line to the polysulfone system is 4×10^{-4}, so $T - T_o$ must be greater than 300 to keep $mR(T - T_o)$ greater than one. None of the polymers studied here reach this value, indicating in all cases a decrease in A causes an increase in conductivity because the associated decrease in activation energy has a larger effect. Of note, it is highly unlikely for activation energy to be negative (i.e., conductivity always increases with increasing temperature), so there should be a physical lower limit for the value of E_a, resulting in a plateau in E_a at low values of A. The sample located at the point where the ln(A) vs E_a correlation breaks due to this plateau in E_a would possess the highest conductivity within an

electrolyte class that exhibits this effect, assuming the Vogel temperature similarly plateaus at some minimum value.

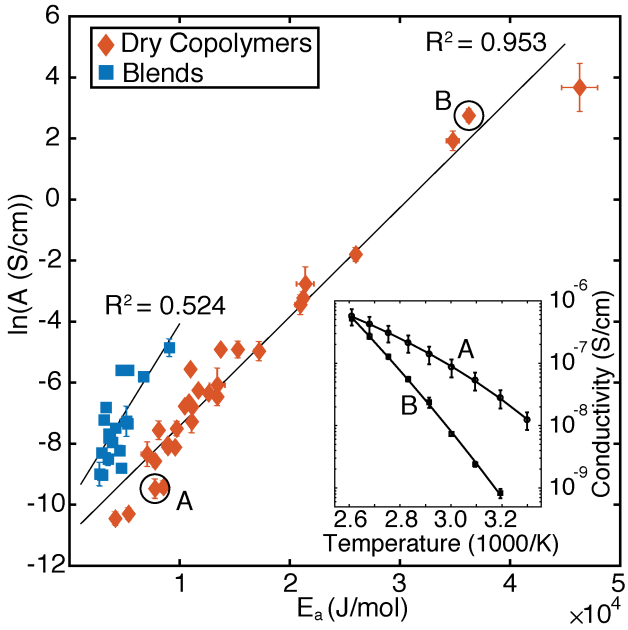

Figure 3.10. Natural log of the VTF prefactor versus the apparent activation energy for the dry PSf-co-PEG copolymers synthesized here, and blends with several of these copolymers and short chain PEG (M_n=300Da). Inset are the Arrhenius plots for conductivity versus inverse temperature of the two polymers circled (A – R_1 is 3 mol% sulfonated, R_2 is 66mol% PEG and B – 100mol% sulfonated, 77mol% PEG). High activation energy leads to a steeply sloping trend with temperature, while low activation energy allows higher conductivity at all temperatures. The PSf-co-PEG polymers display a highly linear correlation between ln(A) and E_a, while the blends lie on a significantly different trendline and display a weaker correlation.

The presence of a relationship between ln(A) and E_a might be explained in polymer electrolytes, and particularly SIC's, due to the intrinsic nature of conduction through a polymer. The prefactor is explicitly a conductivity at infinite temperature, related directly to the number of charge carriers. The number of charge carriers is often thought of as the number of ions and, borrowing from the literature of chemical kinetics, the attempt frequency for ions to transition between solvation sites. E_a is often considered a pseudo-activation energy, related to the energy of the transition state. Since ion motion in these electrolytes is intrinsically coupled to the polymer backbone, it is not unreasonable for the attempt frequency and activation energy to be coupled to segmental motion of the polymer. In such a case, E_a would increase with A in the same sense that addition of ions decreases segmental motion and so increases the glass transition temperature. The presence of this relationship here might indicate the individual fitting parameters are in reality probing the same underlying phenomena rather than probing separate contributions as is often intended. This unexpected result implies that the prefactor and activation energy cannot be separately tuned, and that design of new polymer electrolytes must always consider the inherent trade-off between segmental motion and ion concentration.

To test whether the underlying phenomena may be changed, and the apparent trend towards a limited maximum conductivity within a given polymer class can be broken, blends of several copolymer samples with 30-90wt% PEG (M_n=300Da) were made and characterized in the same manner as the dry copolymer samples, including all data analysis steps. Several representative

Arrhenius plots are included in Figure 3.11 and Table 3.4 in the supporting information section summarizes all blend samples. In all cases the conductivity of the blend sample was several orders of magnitude higher than the dry copolymer. Importantly, the blend samples exhibit a different correlation than the PSf-co-PEG polymers without added diluent (squares vs. diamonds in Figure 3.10). Short chain PEG acts as a plasticizer and facilitates much more rapid ion motion. As evident in Figure 3.10, at a given prefactor value, the apparent activation energy from the VTF equation is lower for all blends compared to the dry copolymer, as would be expected for a significantly more mobile medium. Furthermore, the strength of the ln(A) vs E_a correlation has reduced, in that the R-squared value has decreased, the slope of the correlation that does exist has increased, and the value of $mR(T - T_o)$ has moved closer to one, relative to the dry copolymer system. Taken together, these observations imply that the incorporation of a diluent, such as PEG, provides a strategy to break the deleterious ln(A) vs E_a correlation and therefore dramatically improve conductivity. It is likely that the short chain PEG diluent can solvate Li^+, thereby allowing long-range mobility of Li^+ with an intact solvation shell, as is similar to the conduction mechanism in liquids.[177,178] In the unblended PSf-co-PEG polymer, the PEG segments still act as the solvent for Li^+, but given their entanglement in the melt state, ions are required to hop between solvation sites in order to move over long ranges.[41,44,158]

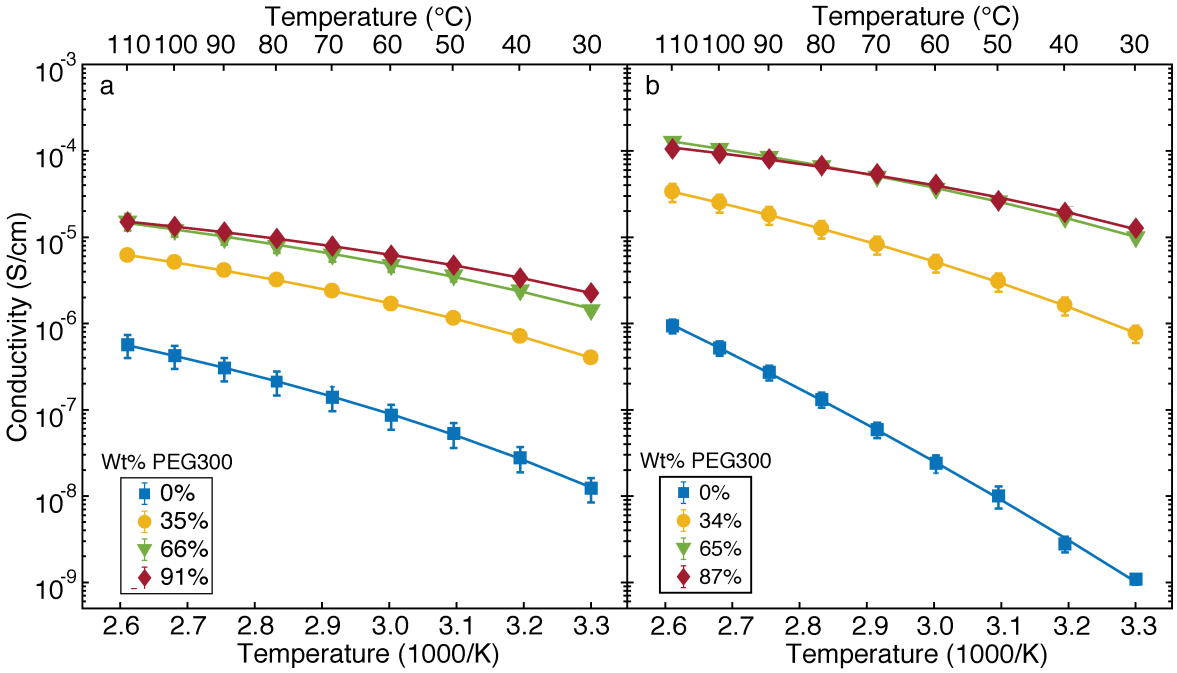

Figure 3.11. Demonstration of representative Arrhenius plots for several polymer blends. a) Conductivity as a function of inverse temperature for the dry copolymer at R_1 sulfonate mol% = 3 and R_2 PEG mol% = 66 and blends of that polymer with PEG (Mn=300 Da) at 35, 66 and 91 wt% PEG300. b) The same diagram for the dry copolymer at R_1 sulfonate mol% = 64 and R_2 PEG mol% = 71 and blends at 34, 65 and 87 wt% PEG300. Conductivity increases by several orders of magnitude on blending of PEG300. In a) the increase is less significant than in b) because the dry copolymer in a) has both a lower glass transition temperature (-31°C) and a lower ion content. The polymer in b) has a high ion content, but those ions are restricted by low segmental motion (T_g = 8°C). Addition of diluent to b) causes a larger increase in the number of free ions than in a). Notably, addition of further diluent causes the conductivity to plateau or even decrease at ~90 wt% in both cases. This is likely due to dilution of the ion content.

To investigate whether the compensation effect is isolated to the PSf-co-PEG copolymer system, conductivity data for several additional dry polymer electrolytes was obtained and fit utilizing the same routine as Figure 3.10. Figure 3.12 plots the results for these different polymer systems, with error bars removed for clarity. The data includes six SIC polymers,[52,56,60,70,75] LiTFSI in PEO[179,180] and LiTFSI in the block copolymer polystyrene-co-ethylene oxide (SEO).[179] Each system appears on a separate line in the plot of ln(A) vs E_a and some appear less correlated than others, suggesting that a change in chemical environment is sufficient to change the strength of the relationship. Importantly, none of the polymer systems studied exhibit a negative correlation between ln(A) and E_a. Also included in Figure 3.12 is data for LiTFSI in DMSO, representing the limiting case of ion in liquid.[105] Here, no relationship between the fitting parameters is evident, the apparent activation energy is significantly lower, and the prefactor is significantly higher than the polymer systems. This should represent the ideal, desired case for these fitting parameters. Polyelectrolyte solutions fall within range of the LiTFSI in DMSO case.[105] Interestingly, the most conductive known dry polymer electrolyte system PEO/LiTFSI, lies closest to this ideal case among the dry systems studied.

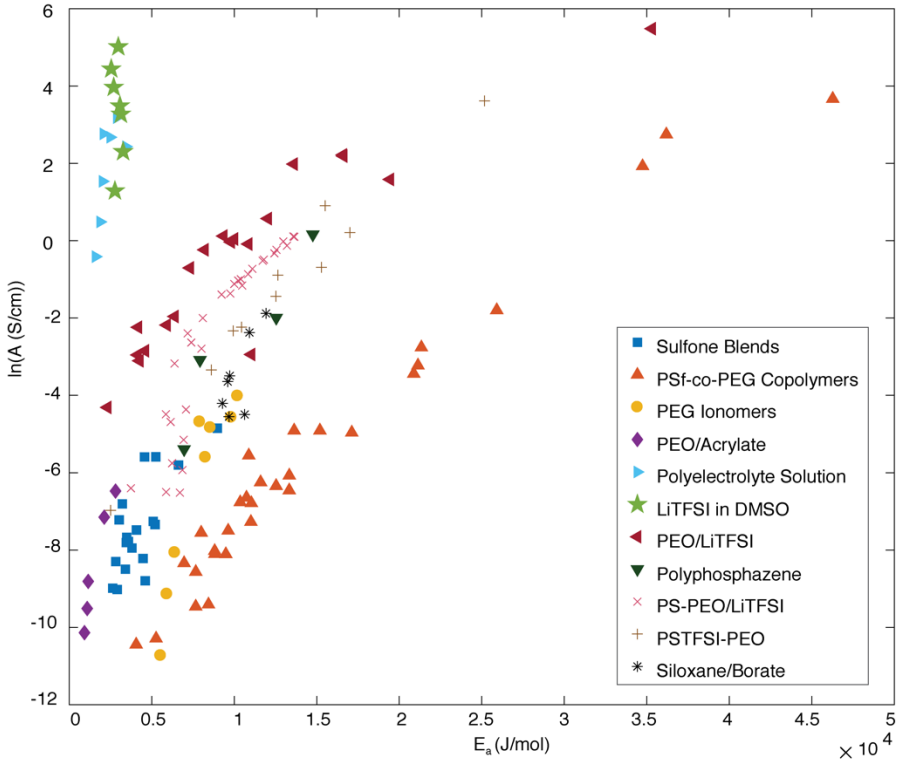

Figure 3.12. Natural log of the VTF prefactor, A, versus the apparent activation energy, Ea, for several polymer systems. PEG Ionomers are from Ref. 70, PEO/Acrylate from Ref. 60, polyelectrolyte and LiTFSI solutions from Ref. 105, PEO/LiTFSI from Refs. 179 and 180, Polyphosphazene from Ref. 52, PS-PEO/LiTFSI from Ref. 179, PSTFSI-PEO from Ref. 75, and Siloxane/Borate from Ref. 56.

Notably, the SEO copolymer system studied by Chintapalli et al. exhibits a transition from a strongly correlated region to a significantly less correlated one. The transition point in this system corresponds directly to the maximum in conductivity as a function of salt content. The Vogel temperature in the SEO system does not vary widely and so the observed maximum stems entirely from the interplay of A and E_a. This strongly supports the idea that, for an electrolyte class which exhibits the compensation effect, maximal conductivity will be obtained at the point where the

effect breaks due to a plateau at a minimum value of E_a. Due to the steep, positive correlation between A and E_a, this must occur as A tends to low values within that electrolyte class.

It should be noted that the possibility of a statistical artifact creating the relationship between ln(A) and E_a cannot be completely discounted. Researchers have described numerous experimental and statistical possibilities that could lead to this artifact within a certain system.[181–184] A simple example of this was described by Kircheim and Huang for the diffusion of hydrogen through a variety of materials.[184] If the materials are not significantly different from one another, the diffusivity might be expected to vary by a simple factor

$$\frac{D}{D_0} = f \tag{3.4}$$

where D_0 is some reference state. Rearrangement of the Arrhenius equation for this case yields

$$\ln(A) = \ln(A_o) + \ln(f) + \frac{E_a - E_{a_o}}{RT} \tag{3.5}$$

Thus, a linear dependence of the log of A on E_a should be expected if 1) f is not dependent on temperature or $\ln(f)$ is significantly smaller than the term containing the activation energy and 2) T does not vary significantly. In the present study, f would be analogous to the conductivity of any given sample relative to another sample. A similar rearrangement of the VTF equation yields

$$\ln(A) = \ln(A_o) + \ln(f) + \frac{1}{R}\left(\frac{E_a}{T - T_o} - \frac{E_{a_o}}{T - T_{o_o}}\right) \tag{3.6}$$

Here, the same assumptions would yield a linear relation between ln(A) and E_a, except the temperature is now modified by T_o. It was found that f, computed for every pair of polymers, always varied with temperature. The term containing activation energy and the term containing f, computed for every pair of polymers at each temperature studied, were also found to be on average within an order of magnitude of each other. Thus, the argument presented by Kircheim cannot explain the trend observed here because the term containing f cannot be neglected. In another statistical example, Barrie describes an artifact that results when a set of samples should actually only have a single A and E_a (i.e., all samples in the set are identical), but error results in an apparent relationship between ln(A) and E_a. It is unlikely that the wide variety of samples within each polymer system included here could have a single A and E_a, particularly in the sulfone system, given the span of nearly 80°C in glass transition and wide ranging ion content that are captured in the PSf-co-PEG polymers characterized in Figure 3.10.

There have been several attempts over the years to develop a statistical method which allows the relationship between ln(A) and E_a to be proven to result from the physical properties of the system rather than merely a statistical aberration in the Arrhenius case, but such developments have not been explored for the VTF form. Mano and Pereira described in detail the importance of careful data fitting for a glassy material's dielectric relaxation that followed the VTF form, but they only described fitting of a single sample rather than multiple unique samples within the glassy material system.[185] It is reasonable to expect that deviations from the true value for any single sample should not produce such a correlation across many samples in a given polymer class. Given the large range of T_g and ion content in polymers studied here within the PSf-co-PEG system, and the clear change upon addition of a diluent, we are confident that the relationship between ln(A) and E_a is related to the physical properties of the system rather than a statistical artifact of the fitting protocol. Development of a full statistical analysis proving the relationship between ln(A)

and E_a found here is beyond the scope of this paper, but would be necessary to be certain this effect is not statistical in nature. Even in the case that the relationship observed here is later proved a statistical artifact, the finding is still significant, as it demonstrates a failing of any analysis based on the VTF equation. Most studies include only few polymers due to the difficulty of sample preparation and synthesis, and as a result, the ability to check whether A and E_a are correlated is significantly hampered. Interpretation of the values of A and E_a is severely complicated in a system where they are related because one cannot determine if an increase is related to, for example, charge carrier concentration, when in reality any changes are simply a manifestation of segmental motion. Further, a statistical artifact would not fully explain the apparent correlation within different sets of polymer electrolytes, and, in particular, the SEO/LiTFSI system, where two different trends are observed depending on the polymer composition. The root cause of the differences between the electrolytes presented in Figure 3.12 is not clear as of yet, but should be the focus of further study.

V. Summary and Outlook[§]

This study has demonstrated that the fundamental understanding of conduction through a single ion conducting polymer electrolyte holds for a new PSf-co-PEG based system, although this new system allows access to a vast single ion conductor physical property range. Using knowledge gained from studies on this system, several shortcomings in the traditional method of analysis using the VTF equation are made clear, particularly that the choice of T_o should always be carefully considered and checked, and that a relationship between ln(A) and E_a may exist in any given system. The positive relationship between ln(A) and E_a may imply maximum conductivity for a given electrolyte class occurs at the location where E_a plateaus to a minimum value and the ln(A) vs. E_a correlation breaks. In a system that exhibits a strong compensation effect, this will occur as A tends to zero. For any electrolyte system where this trend is observed, this is a concerning result, as maximizing charge carriers is always a desired design parameter for any electrolyte. It is therefore of great importance to break the correlation between A and E_a for any polymer electrolyte class where it is present.

While it is not yet fully understood why the relationship between prefactor and activation energy exists, it is relatively straightforward to explain a tradeoff between charge carrier concentration and segmental motion as illustrated in Figure 3.13A and B. First, because the mechanism of conduction in these electrolytes is based on hopping between backbone solvation sites, fast segmental motion of the polymer is critical. However, segmental motion by itself is not the only consideration for high electrolyte conductivity, otherwise siloxanes would be the polymer-of-choice for electrolyte compositions. Even though siloxanes have extremely low T_g's, they do not form good ion conductors because they are non-polar and, hence, poor solvents for salts. The second material property necessary for high conductivity SIC polymers is the ability of the polymer to provide high ion dissociation. Achieving even modest ion dissociation is a critical limitation in SIC polymers, with studies suggesting that only a small fraction of lithium ions exist in a dissociated state.[186,187] Dissociation of ions within a neat SIC polymer is challenging for several reasons. To dissociate the ion pair, it would be expected that a section of the polymer chain should have a stronger affinity for the cation than the anion. The properties of solvents that enable such interactions to occur include high Lewis acidity or basicity, and a high dielectric constant, which, in turn, is found in strongly polar solvents. In attempting to design these features in a

[§] A portion of this section was published as part of a review in *ACS Energy Letters,* and is adapted with permission from co-author E.J. McShane and B.D. McCloskey.[18]

polymer, inclusion of polar organic groups, such as amides or sulfones, substantially reduces polymer segmental motion due to the strong polar interactions of the polymer with itself, resulting in polymers that provide poor conductivity (Figure 3.13B). Mayes and coworkers first demonstrated an alternative method to improve ion dissociation by spatially segregating the anionic moiety from the conducting moiety of a polymer backbone.[69] Recent attempts to implement this finding, have resulted in systems without any phase separation due to the significantly increased interaction of the anion with the conducting moiety relative to the same system without anions.[163]

A more direct method to increase the number of charge carriers would be to simply add ions to the system, but the addition of ions also reduces segmental motion, likely through enhanced interchain electrostatic interactions (the α-transition temperature, which is a proxy for the strength of transient electrostatic crosslinks, is known to be related to ion content, Figure 3.13B).[188] Dissociation of ions is a critical limitation in typical PEO – salt mixtures as well, but in the case that the anion is immobile and appended to the backbone, ion association necessarily reduces lithium motion significantly more than in the binary salt case where anions are still mobile and ion aggregates may still move freely.

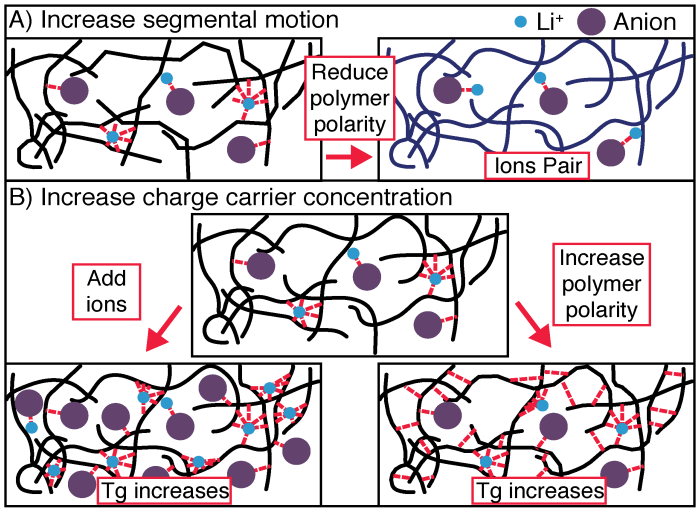

Figure 3.13. A) Illustration of an attempt to increase conductivity by increasing segmental motion of the polymer. If polymer polarity is reduced, chains are able to move more freely, but ions dissolved in the polymer will pair. B) Illustration of attempts to increase charge carrier concentration by either adding ions or increasing polymer polarity. In both cases, new transient interactions between chains are introduced, increasing the T_g and thereby reducing segmental motion.

Future design of polymer electrolytes, and particularly SIC polymer electrolytes where anions are necessarily bound to the chain, must always consider the inherent tradeoff between segmental motion and charge carrier concentration. Appending poorly basic anions to polymers with modest Lewis basicity and polarity, and hence reasonable segmental motion (such as PEO), to optimize the segmental motion/ion dissociation tradeoff is perhaps the most attractive direction for neat SIC polymer electrolytes. Significant effort has already been made to create highly charge delocalized anions, such as those that resemble $TFSI^-$, on a polymer backbone, and these ions have been shown to result in improved dissociation in a PEO matrix.[56,73] The review by Zhang et al. makes several further suggestions for such chemical modifications.[57] The optimization of the segmental motion/charge carrier concentration tradeoff in neat polymer electrolytes is still a

challenging and open question, but one that warrants further study due to the potential ease in processing and safety benefits should a high conductivity electrolyte be found. In this work, blending of short chain polymers is also shown as a potential means around this problem.

VI. Supporting Information

Table 3.3. Detailed summary information for all dry PSf-co-PEG copolymers shown in Figure 3.10. "PEG M_n" refers to the length of PEG monomer used. PEG wt% is the calculated weight percent of ethylene oxide repeat units in the overall polymer. EO/Li is the calculate ethylene oxide repeat unit to lithium ratio often referred to in the polymer electrolyte literature. The VTF parameters E_a, A and T_o are reported from Fit #2, as plotted in Figure 3.10. Samples labeled with * are the series at a R_1 sulfonate mol% of 10 and samples labeled with # are the series at a R_2 PEG mol% of 70.

PEG M_n (Da)	R_1 Mol% Sulfonate	R_2 Mol% PEG	Wt% PEG	EO/Li	T_g (°C)	M_n (Da)	PDI	E_a (J/mol)	A (S/cm)	T_o (°C)
1000	6%	28%	44%	53	40	10900	1.9	11000	6.9E-04	241
1000	10%	37%	52%	43	9	11300	2.0	17100	7.0E-03	175
1000	18%	34%	48%	23	29	11000	1.9	21300	6.3E-02	186
1000	10%	26%*	41%	29	46	13700	2.2	46300	3.9E+01	106
1000	10%	36%*	50%	41	7	11700	1.9	20900	3.2E-02	162
1000	22%	44%	54%	22	-1	7600	1.8	21100	4.0E-02	158
1000	9%	48%	59%	65	-17	7900	1.9	10400	1.2E-03	203
1000	12%	59%*	64%	58	-19	12300	1.8	13300	1.6E-03	169
1000	26%	56%	61%	25	-15	4900	1.7	13300	2.3E-03	184
1000	12% #	70%*	69%	69	-28	12500	1.9	8800	3.0E-04	198
1000	25% #	66%	66%	30	-22	6700	1.9	11600	1.9E-03	188
1000	13%	76%	71%	65	-35	11900	2.0	8800	3.3E-04	188
1000	25%	77%	70%	35	-35	6300	1.9	4100	2.9E-05	234
1000	11%	86%*	75%	93	-40	8500	2.0	7700	1.9E-04	193
1000	29%	84%	72%	33	-38	7100	1.9	8000	5.3E-04	196
1000	15%	100%*	79%	77	-44	4700	1.8	7000	2.4E-04	192
1000	28%	100%	77%	41	-43	5900	1.8	10700	1.3E-03	172
4500	11%	28%	77%	126	-48	23900	1.7	5300	3.4E-05	215
1000	41% #	65%	63%	18	-19	6200	1.7	13600	7.4E-03	182
1000	3% #	66%	68%	262	-31	14000	1.8	7700	7.8E-05	198
1000	17% #	71%	69%	48	-28	10100	1.9	11000	1.1E-03	180
1000	0%	66%	69%	-	-32	17200	1.8	8400	8.2E-05	198
300	12%	85%	47%	25	22	8200	1.8	12500	1.8E-03	229
1000	15%	74%	70%	55	-32	12700	2.1	9500	3.0E-04	189
1000	64% #	71%	64%	13	8	13500	1.8	34700	6.9E+00	119
1000	100% #	77%	63%	9	39	14200	1.8	36200	1.6E+01	130
600	10%	52%	48%	36	14	10000	3.1	15200	7.4E-03	204
1500	6%	24%	49%	73	6	12300	2.3	25900	1.7E-01	140
2000	11%	18%	48%	39	13	16700	1.9	9600	5.5E-04	208
1000	47%	100%	75%	24	-38	7800	1.4	10900	3.9E-03	180

Table 3.4. Compositions of the blend samples. Copolymer mol% reported here refers to the parent dry PSf-co-PEG copolymer used to make the blend. The dry copolymer glass transition temperature and the blend glass transition temperature are reported. Most of the blends exhibited melting behavior at a temperature (T_m) below the range of conductivity analysis. The VTF parameters reported here are those plotted in Figure 3.10, from Fit #2.

Copolymer R_1 Mol% Sulfonate	Copolymer R_2 Mol% PEG	Wt% PEG300	Dry Copolymer T_g (°C)	Blend T_g (°C)	Blend T_m (°C)	E_a (J/mol)	A (S/cm)	T_o (°C)
25%	77%	65%	-35	-69	8	3500	4.65E-04	215
10%	36%	67%	7	-70	-3	4100	5.63E-04	207
64%	71%	65%	8	-65	-4	5200	3.74E-03	197
3%	66%	66%	-31	-72	10	4500	2.69E-04	200
100%	77%	66%	39	-64	-7	4600	3.73E-03	206
100%	77%	91%	39	-75	-15	3000	7.32E-04	215
64%	71%	87%	8	-74	-15	3200	1.11E-03	217
3%	66%	35%	-31	-58	12	4600	1.52E-04	210
3%	66%	91%	-31	-75	-16	2900	1.21E-04	216
12%	70%	34%	-28	-54	None	5200	6.48E-04	206
12%	70%	64%	-28	-69	6	5100	7.03E-04	196
12%	70%	91%	-28	-75	-16	3800	3.53E-04	200
15%	100%	34%	-44	-58	19	3400	2.04E-04	221
15%	100%	67%	-44	-68	15	3600	4.19E-04	208
15%	100%	91%	-44	-78	-14	2600	1.25E-04	223
10%	36%	89%	7	-76	-16	2800	2.49E-04	219
12%	70%	69%	-28	-71	6	3500	4.07E-04	214
64%	71%	34%	8	-42	None	9000	7.83E-03	187
47%	100%	33%	-38	-55	16	6600	3.02E-03	189

4. Investigation of Solvent Type and Salt Addition in High Transference Number Nonaqueous Polyelectrolyte Solutions for Lithium-Ion Batteries**

I. Abstract

High transference number (t_+) electrolytes have attracted recent interest as a means to improve the energy density and rate capabilities of current lithium ion batteries. Here the viscosity and transport properties of a sulfonated polysulfone/polyethylene glycol copolymer that displays both high t_+ and high conductivity when dissolved in dimethylsulfoxide (DMSO) are investigated for the first time in a battery-relevant solvent of nearly equivalent dielectric constant: mixed ethylene carbonate (EC) / dimethyl carbonate (DMC). The addition of a binary salt to each solution is investigated as a means to improve conductivity, and the diffusion coefficient of each species is tracked by pulse field gradient nuclear magnetic resonance (PFG-NMR). Through the ^{7}Li NMR peak width and quantum chemistry calculations of the dissociation constant, it is shown that although the two solvent systems have nearly equivalent dielectric constants, the conductivity and transference number of the EC/DMC solutions are significantly lower as a result of poor dissociation of the sulfonate group on the polymer backbone. These results are the first study of polyelectrolyte properties in a battery-relevant solvent, and clearly demonstrate the need to consider solvent properties other than the dielectric constant in the design of these electrolytes.

II. Introduction

Lithium-ion batteries are the state-of-the-art energy storage device for portable consumer electronics and electric vehicles. Despite their widespread success, much work remains in further improving cell performance. Of particular interest is the electrolyte, which can limit a battery's energy density and rate capability through numerous issues, including concentration polarization.[17,18] Current state-of-the-art battery electrolytes are composed of a well-dissociated binary lithium salt, such as lithium hexafluorophosphate ($LiPF_6$) or lithium bis(trifluoromethanesulfonyl)imide (LiTFSI), in a blend of ethylene carbonate (EC) and a linear carbonate like dimethyl carbonate (DMC) to provide both high conductivity and favorable electrode passivation towards parasitic side reactions.[4,189] EC, which imparts a stable solid electrolyte interface at the graphite anode, is typically utilized in a mixture due to its slightly above room temperature melting point and high viscosity.[13,190]

The conductivity of these battery electrolytes is on the order 1-10 mS/cm, but the majority of this conductivity is the result of anion motion rather than motion of the electrochemically active Li^+. This high anion mobility allows concentration gradients to form within the cell, among other issues. The Li-ion transference number, t_+, characterizes the fraction of total conductivity arising from lithium motion, being roughly 0.4 in most liquid Li battery electrolytes.[24] Research in high transference number electrolytes (HTNEs), in which the anion is less mobile than the lithium, has focused on ceramic lithium conductors,[35] solid polymer electrolytes,[57] swollen gel polymer electrolytes,[191] and composite electrolytes.[192,193] In most cases there is either a trade-off between conductivity and transference number, or the need for a significant re-engineering of the standard

** This chapter was originally published in *Macromolecules* and is adapted with permission from co-authors K.D. Fong, R.C. Terrell, K.A. Persson, and B.D. McCloskey.[213]

Li-ion cell. Recently, the use of nonaqueous polyelectrolyte solutions, where a bulky polyanion is neutralized by lithium ions, has been proposed as a promising route to high transference number, high conductivity electrolytes that would not require a significant redesign of current cell configurations.[103,105]

Thus far, the only studies that have specifically investigated Li-ion transport through a nonaqueous polyelectrolyte solution have used dimethylsulfoxide (DMSO), a highly polar solvent that is able to solubilize highly charged macromolecules.[103,105,143] Unfortunately, DMSO is unsuitable for battery applications due to co-insertion of DMSO with lithium into graphite electrodes, effectively exfoliating the graphite and destroying the electrodes.[15] It is thus important to determine the fundamental design challenges remaining to create an HTNE composed of a lithium neutralized polyanion dissolved in the battery-relevant EC/DMC blend solvent.

Polyelectrolyte solutions have been studied for many years in water due to their utility in understanding the fundamental physics of complex charged biological macromolecules such as proteins and DNA. The reader is referred to the recent perspective of Muthukumar, as well as several reviews of polyelectrolyte literature for the larger context of this work.[106,112,194,195] A battery electrolyte, however, requires a nonaqueous environment where ion pairing is typically more prevalent than in water, and solvent properties can vary significantly. Polyelectrolytes have been studied in some polar organic solvents, though to our knowledge no study has ever examined a fully dissolved polyelectrolyte in any battery-relevant carbonate solvent. Hara has twice reviewed much of the nonaqueous polyelectrolyte work, though typically the motivation has ultimately been to further understand the polyion behavior in aqueous solution.[139,140]

The motion of polyions and their counterions together has been considered extensively in the literature.[121] However, the goal of much of this work was to interpret the results of experiments such as dynamic light scattering and conductivity measurements to further understand the fundamental physics of the polyion in solution, rather than optimization of any particular transport property.[126] In designing an HTNE, the goal is ultimately to optimize the transport of the lithium counterion through the solution and thus this design necessitates a re-examination of the classical polyelectrolyte experiments and theories.

The most commonly-discussed property of counterions in polyelectrolyte solutions is their effect on charge shielding, which dictates the charge repulsion between ionic groups on the polymer backbone and thus strongly influences polymer conformation.[107,108,123,136] In discussing charge interactions in solution, most classical theories of polyelectrolyte conformation rely on the Bjerrum length $l_B = e^2/\varepsilon kT$, where e is the elementary charge, kT is the thermal energy, and ε is the dielectric constant of the solvent. Manning's original theories predict that once the distance between charges on a polymer backbone moves below a certain critical value (the Bjerrum length), ions will begin to condense on the chain to neutralize the charge.[108] Though numerous more recent results and theories have demonstrated the failings of this model for flexible, irregular polymers, the concept of counterion condensation on highly charged polymers to describe the polymer conformation and the dependence of theories on the Bjerrum length are fundamental to the field.[106,113,196] The dielectric constant is therefore typically the first property considered when examining polyelectrolyte data, particularly when using solvents other than water.

As a first step to address the fundamental lack of understanding of polyelectrolytes in battery-relevant solvents, we employ a version of the sulfonated polysulfone/poly(ethylene glycol) copolymer that is fully soluble in both DMSO and a 2:1 (v/v) mixture of EC and DMC. Here we choose a polymer that is fully soluble in EC/DMC, and contains appended sulfonate groups, a common ionic group studied in polyelectrolytes. Both solvents have a dielectric constant near 50,

and thus reasonably similar behavior would be expected from the classical theory. Here we characterize the transport properties of the polyelectrolyte with and without added LiTFSI salt. From a fundamental standpoint, added salt is frequently used in the polyelectrolyte literature as a means of varying electrostatic screening in solution and reducing viscosity.[118,197] Here it is also investigated from a performance standpoint as a means to increase polyelectrolyte solution conductivity. Additionally, previous studies have not made clear the trade off in transference number when adding a small molecule salt alongside the polyelectrolyte. This study will aid in identifying the major questions remaining in the design of an HTNE using polyelectrolytes.

III. Experimental Section

i. Materials

Poly(ethylene glycol) (M_n=1500Da), anhydrous n-methyl-2-pyrrolidone, dimethyl sulfoxide, and toluene were purchased from Sigma Aldrich and used as received. Sulfonated bis(4-chlorophenyl) sulfone was purchased from Akron Polymer Systems and dried for two days under vacuum at 80°C before use. 2,2-bis(4-hydroxyphenyl)hexafluoropropane was purchased from Chem Impex Intl. and used as received. Anhydrous ethylene carbonate, dimethyl carbonate, and lithium bis(triflouromethylsulfonyl)imide were purchased from BASF and used as received.

ii. Polymer Synthesis

The polymer employed in this study is shown in Scheme 4.1, composed of short poly(ethylene glycol) (M_n=1,500 Da) segments with sulfonated sulfone linkages. 10mol% of a fluorinated biphenol monomer is also incorporated as a tag to track the diffusion of the polymer backbone in a non-deuterated solvent. Briefly, the condensation reaction is performed by loading the three monomers to a reaction vessel with n-methyl-2-pyrrolidone and potassium carbonate, and allowed to react for 48hrs at 190°C following azeotropic removal of water with toluene for several hours. The polymer is then precipitated in isopropanol, followed by dialysis in water with lithium carbonate to exchange the appended ion to lithium, and remove residual solvent and other impurities. The final structure of the polymer was confirmed through NMR and the final ion content of the polymer was verified by inductively coupled plasma optical emission spectroscopy (ICP-OES), and no other trace metallic impurities were observed. The polymer was dried for two days at 70°C over phosphorous pentoxide before use.

Scheme 4.1. Structure of the charged polymer used in this study. The R group is ~10 mol% of the fluorinated monomer, as a tag for backbone diffusion measurement via ^{19}F NMR

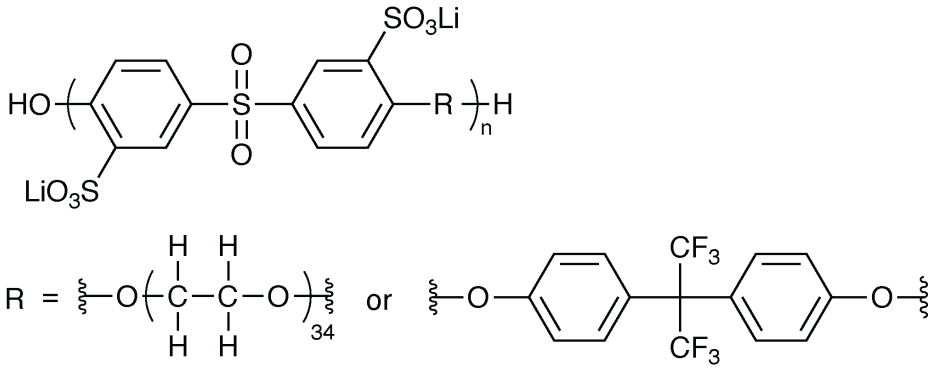

iii. Solution Preparation

Each solution was prepared in an argon glovebox (Vacuum Atmospheres) kept below 1 ppm water and oxygen. Polymer solutions were prepared and then added to weighed amounts of LiTFSI salt. No precipitation or aggregation was observed in any solutions over the course of one year. The final lithium concentration of each sample was measured by quantification with ^{7}Li NMR. Standard solutions of LiBr in D_2O were prepared, and a ^{7}Li spectrum was obtained for each using a consistent receiver gain, calibrated pulse length, and 120 second delay time. A calibration curve was then made. For each solution, the NMR spectra was shimmed on the ^{1}H signal, then a ^{7}Li spectra at the same receiver gain was obtained, enabling accurate measurement of the lithium content of each sample. The reported amount of LiTFSI added in each plot in this work is calculated from this measurement.

iv. Conductivity

To minimize the amount of solution necessary for conductivity measurement, conductivity of each solution was measured using coin cells constructed in the argon glovebox. Each cell was constructed with two stainless steel blocking electrodes and a quartz fiber (Whatman) separator that had been washed and dried prior to use. The coin cells were loaded to a temperature-controlled oven, and the temperature was maintained at 25°C throughout the measurement. AC Impedance was performed on each cell and the conductivity was determined from the minimum of the phase angle of the resulting spectra. Each value represents the average of at least four cells. The coin cell measurement was calibrated to LiTFSI in DMSO solutions measured both by the same coin cell technique and with a conductivity probe (Metrohm) inside of the glovebox.

v. Viscosity

Viscosity was measured using an electromagnetically spinning viscometer (EMS-1000, Kyoto Instruments). Achieving high accuracy measurements in low volume solutions, this technique measures viscosity based on the rotation rate and magnetically applied force to a 2-mm aluminum ball located in the testing solution. The viscometer was calibrated using known standards (Cannon Instruments Inc.), and was within 3% of the known values. 300 μL of each solution was sealed in the 13-mm diameter test tubes in the argon glovebox. At no point during the measurement, or during sample preparation, were any of the solutions exposed to ambient atmosphere, ensuring that H_2O or other atmospheric contamination was eliminated. Temperature is maintained at 25°C throughout the measurement, and the reported values represent the average of at least eight individual viscosity measurements on the same solution. Variability in these repeat measurements was also around 3%.

vi. Pulse Field Gradient NMR

Diffusion coefficients of each species were measured by pulse field gradient NMR on a Bruker Avance III 600 MHz instrument fitted with a 5mm Z-gradient broadband probe and variable temperature unit maintained at 25°C throughout the measurement. Samples were prepared in the glovebox and capped with an air free cap and parafilm. The gradient was calibrated to known values of H_2O, H_2O in D_2O,[198] H-DMSO in d6-DMSO,[199] dimethyl carbonate,[23] and 0.25M and 4M LiCl in H_2O.[198]. The T_1 of each peak monitored was measured and a recycle delay at least four times T_1 was utilized. For ^{7}Li, ^{19}F of $TFSI^-$, and the solvent, a double stimulated bipolar gradient pulse sequence (Bruker's dstebpgp3s program) was used.[200] Due to the low signal and slow

diffusion of the polymer backbone, the longitudinal eddy delay program without convection compensation (Bruker's ledbpgp2s program) was employed to monitor the diffusion of the ^{19}F peak associated with the polymer backbone.[201] The diffusion of this peak was confirmed to match the diffusion of the proton polymer peaks via a separate measurement in d6-DMSO where the polymer ^{1}H peaks are not impacted by the solvent signal. For the dstebpgp3s program, the signal intensity as a function of gradient strength was fit to

$$\frac{I}{I_0} = e^{-\gamma^2 g^2 \delta^2 D\left(\Delta - \frac{5\delta}{8} - \tau\right)} \quad 4.1$$

Where γ is the gyromagnetic ratio, g is the gradient strength, δ is the duration of the gradient pulse, D is the diffusion coefficient, Δ is the diffusion delay time, and τ is the delay for gradient recovery. The correction for sine shaped gradient pulses was included here.[202] For the ledbpgp2s program, the equation was modified to

$$\frac{I}{I_0} = e^{-\gamma^2 g^2 \delta^2 D\left(\Delta - \frac{5\delta}{16} - \frac{\tau}{2}\right)} \quad 4.2$$

Diffusion delays employed were between 0.05 and 0.25 seconds, gradient pulse lengths were between 0.8 and 5.5 milliseconds. Repeat experiments with varied diffusion delay and pulse length verified the measured diffusion coefficient was independent of experimental condition. Between 8 and 16 experiments with varying gradient strength were used for each diffusion coefficient measurement. Example Stejskal-Tanner plots are included in Figure 4.1, in all cases a linear decay in signal strength on the Stejskal-Tanner plot was observed. Variability within the gradient calibration was used to estimate a minimum error of 5% on the diffusion coefficients. For some samples the fitting error due to low signal strength was larger than this 5% error. Due to the length of repeated experiments, the maximum of the fitting error and 5% was used to determine error bars for the diffusion measurements.

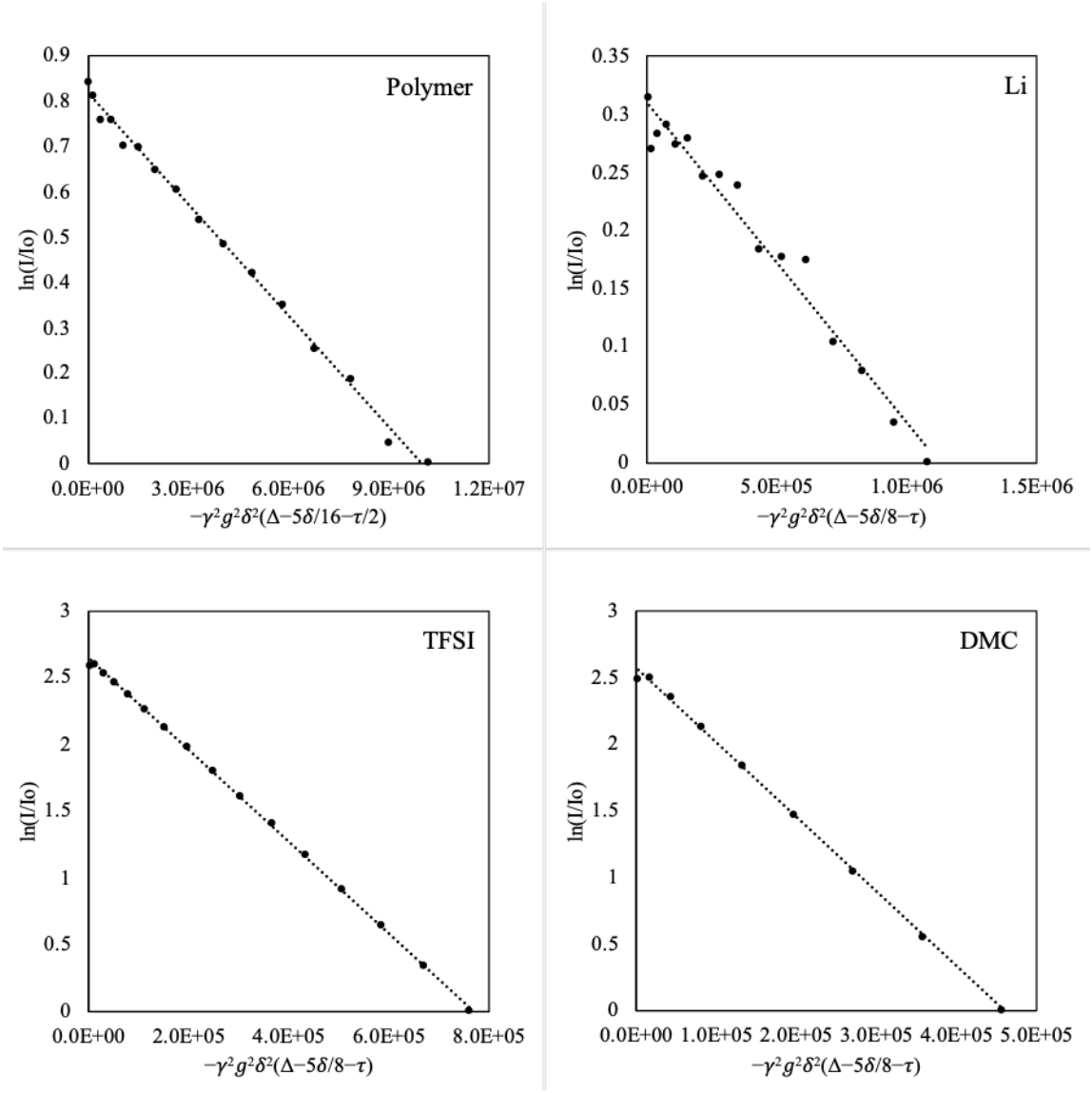

Figure 4.1. Example Stejskal-Tanner plots for each component of the solution at 0.1M Polymer, 0.1M LiTFSI in EC/DMC=2 (v/v). Each plot shows a linear decay, with slightly higher noise in the Lithium signal due to low signal intensity.

IV. Results and Discussion

Conductivity is the primary electrolyte property considered when designing a battery electrolyte. Figure 4.2 displays the conductivity of the polyion with added salt solutions using DMSO (Figure 4.2A) or EC/DMC (Figure 4.2B) as the solvent, plotted against the amount of LiTFSI added to the solution. The polymer molarity reported in all figures corresponds to the appended sulfonate ion molarity in each solution and is therefore twice the molarity of the sulfonated sulfone repeat unit (given that each sulfone repeat unit has 2 sulfonate groups). This does not, however, correspond directly to the total monomer concentration due to the additional PEG repeat units present. Without polymer (green squares in Figure 4.2), the plotted LiTFSI concentration corresponds to the total lithium concentration in solution, but for the polymer solutions the total lithium content is the LiTFSI added plus the reported polymer molarity. The

conductivity of the pure solvent, which was below 3 μS/cm, was subtracted in each case. It should be noted in all cases here, the conductivity of the polymer solutions is several orders of magnitude higher than the neat polymer in the dry state.[77] In both solvents, the conductivity of each solution increases into the range of an acceptable battery electrolyte with addition of LiTFSI, and at 0.01M polymer, the conductivity of the solution is no different from the solution without polymer at these polymer/LiTFSI concentrations.

At high polymer concentration, the conductivity behavior of solutions made from different solvents deviate. In EC/DMC, the solutions with 0.1M polymer have a lower conductivity than the solutions with no polymer at each LiTFSI concentration, even though the total lithium concentration of the polymer containing solutions is always higher. This implies that the Li^+-SO_3^- pairs appended to the polymer backbone remain substantially, if not completely, associated in EC/DMC, and hence do not contribute to conductivity. Therefore, the lower conductivity of the 0.1M polymer solutions compared to the 0M polymer solutions results from the higher viscosity imparted by the addition of polymer to the solution (see Figure 4.3). In contrast, the polyion and its lithium counterion appear to contribute to the total solution conductivity in DMSO solutions. This is particularly clear at low LiTFSI concentration, where the conductivity is significantly higher for the 0.1M polyion solutions compared to the 0M polymer solutions. The increase in conductivity on addition of more LiTFSI is less pronounced in the higher polymer concentration samples, and eventually the conductivity of the 0.1M polyion solution is equivalent to the conductivity of pure LiTFSI solutions, again despite the significantly higher total lithium concentration.

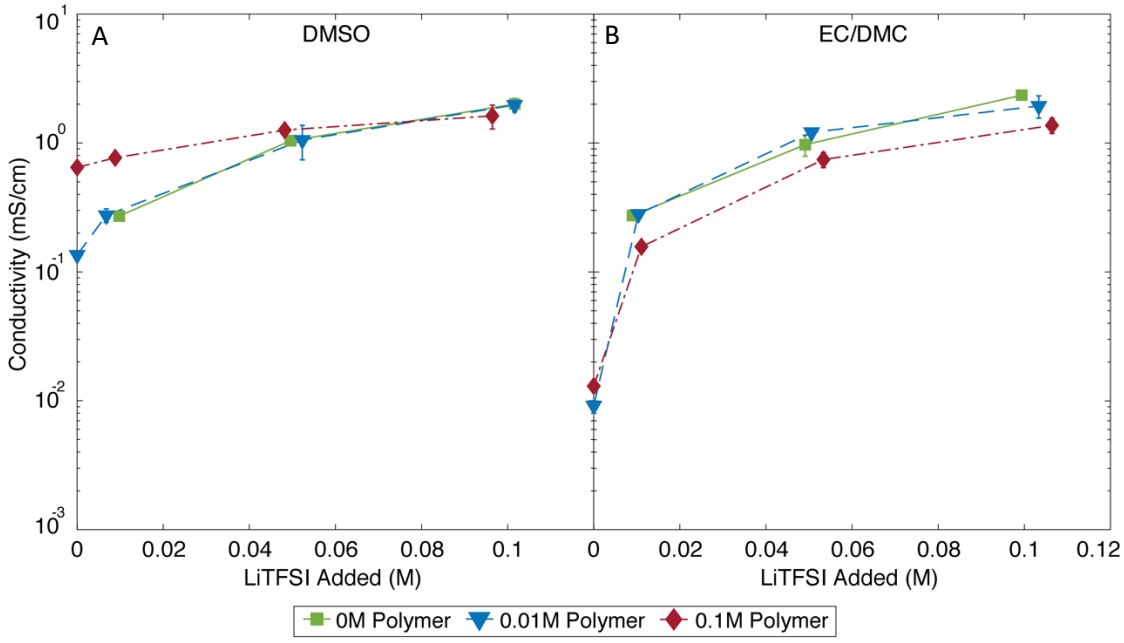

Figure 4.2. Conductivity as a function of LiTFSI added at each polymer concentration in A) DMSO and B) EC/DMC=2 (v/v).

The viscosity of each solution in Figure 4.2 is plotted in Figure 4.3 as a function of the amount of LiTFSI added. In each solvent (dashed vs solid lines), increasing polymer concentration corresponds to an increase in viscosity as would be expected. Without polymer (squares) and with 0.01M polymer (triangles), only a slight increase in viscosity is noted with addition of LiTFSI, as

the concentration of salt is relatively low. At high polymer concentration in DMSO, addition of salt causes no change in viscosity, however, in EC/DMC there is a significant decrease in viscosity with increasing salt concentration. Based on the conductivity of these solutions, these results are generally unexpected. For a charged polymer in solution, addition of small molecule salt is known to cause a decrease in the solution viscosity as a result of charge screening that allows the chain to relax into a smaller conformation.[139] Thus, we would expect that addition of salt to the polymer solutions in DMSO should cause a decrease in the solution viscosity because here the polymer contributes to the total conductivity and so must be charged. In EC/DMC, the polymer does not appear to contribute significantly to the conductivity, indicating it is not charged and that charge screening is unlikely to play a role in the viscosity.

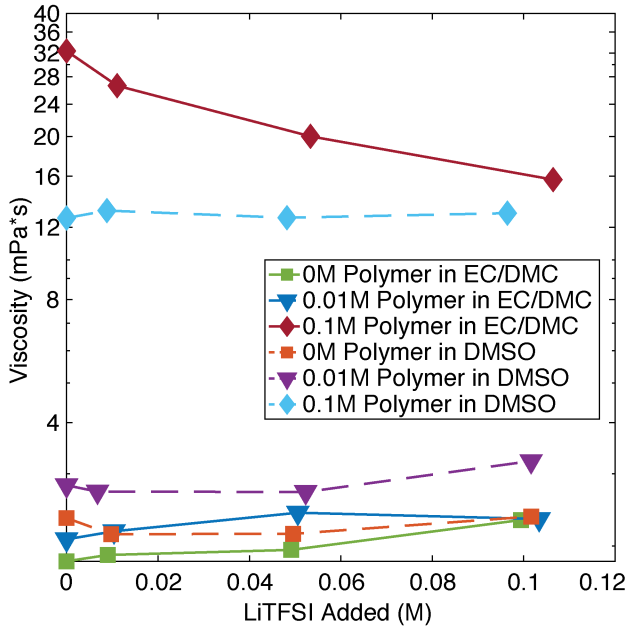

Figure 4.3. Viscosity as a function of LiTFSI added to each polymer solution for EC/DMC (solid lines) and DMSO (dashed lines). Polymer free solutions are shown as squares, 0.01M polymer corresponds to triangles, and 0.1M polymer corresponds to diamonds. The 3% error estimated from the calibration is smaller than the data points in this figure.

To further investigate these surprising results, we turn first to the molar conductivity in Figure 4.4A for DMSO and B for EC/DMC to more clearly ascertain the polymer contribution to the total conductivity. Here the conductivity is normalized to the total lithium concentration of each solution, and plotted again against the amount of LiTFSI added. In both cases, the pure LiTFSI solution molar conductivity displays negligible concentration dependence, consistent with LiTFSI being a strong electrolyte (nearly fully dissociated). In DMSO, Figure 4.4A, the polymer solutions display only a slight increase in molar conductivity with added small molecule salt. The effect of viscosity can clearly be seen here in the decreased molar conductivity with increasing polymer concentration. In Figure 4.4B, where EC/DMC solutions are presented, the polymer solutions display dramatically different behavior than DMSO solutions, with the 0.1M solution deviating the most from the pure LiTFSI case and showing an increase in molar conductivity as the concentration increases. This would be consistent with the decrease in viscosity with higher salt concentration, but could also be explained if the polyion and its counterion did not contribute to the conductivity.

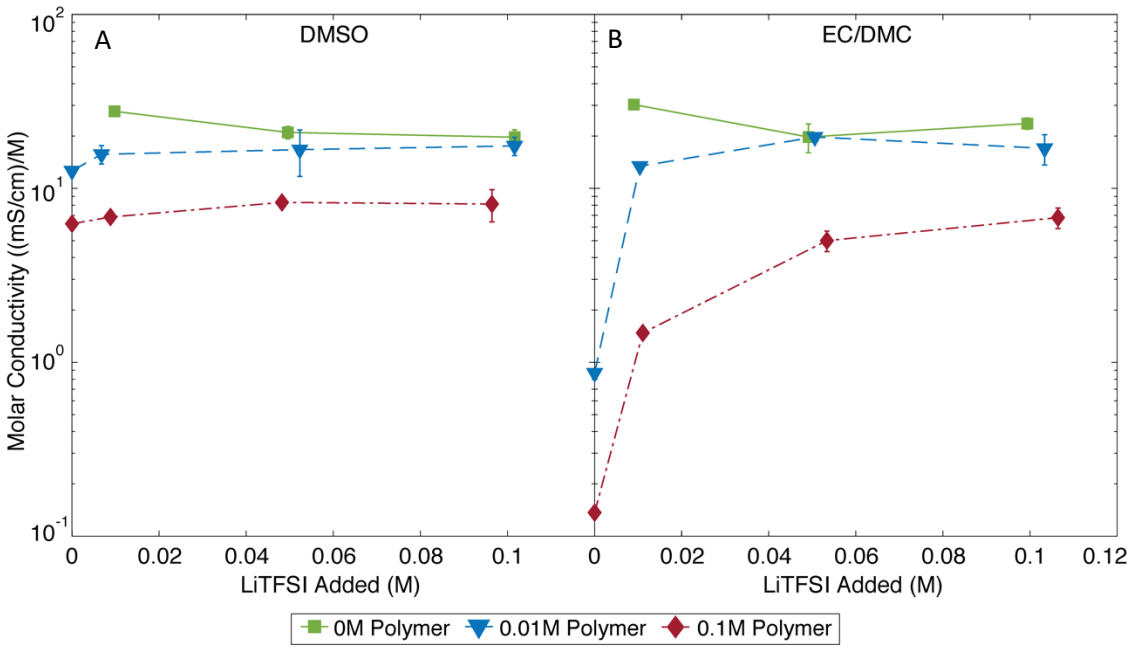

Figure 4.4. Molar conductivity (normalized using total Li^+ concentration in each solution) as a function of LiTFSI added at each polymer concentration in A) DMSO and B) EC/DMC=2(v/v).

To examine the relative contribution of LiTFSI and polyion to the conductivity, in Figure 4.5, the conductivity has been normalized to the concentration of LiTFSI rather than the total lithium concentration. Here, the molar conductivity of the pure LiTFSI and 0.01M polyion in both EC/DMC and DMSO solutions collapses to a single line that is concentration independent. At 0.1M polyion, the solution at 0.01M LiTFSI in DMSO displays dramatically higher molar conductivity, clearly indicating the polyion contributes significantly to the observed conductivity. As the concentration of salt increases, however, the [LiTFSI]-normalized conductivity falls back to similar values as the other solutions. In EC/DMC, the 0.1M polyion solution conductivity displays no concentration dependence, indicating the large increase with added LiTFSI observed in the Li^+-normalized molar conductivity (Figure 4.4B) can be explained entirely by the addition of LiTFSI, and not the decreasing viscosity shown in Figure 4.3. In this plot, increasing molar conductivity with LiTFSI concentration would be expected if the effect was a result of viscosity. Thus, the conductivity data clearly suggest that the polyion is charged in DMSO and uncharged in EC/DMC, despite the trends in viscosity. It is therefore necessary to further deconvolute each species contribution to these bulk properties.

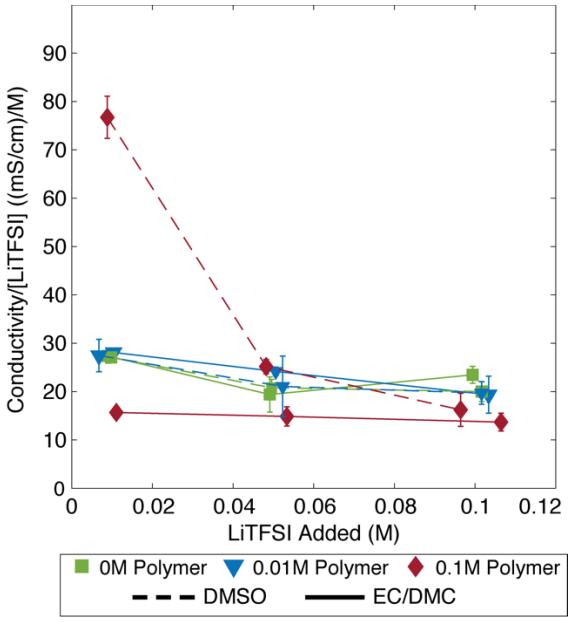

Figure 4.5. Conductivity normalized to LiTFSI concentration for all solutions.

To do so, the diffusion coefficients from PFG NMR of the polymer backbone, $TFSI^-$ anion, and Li^+ counterion, are plotted in Figure 4.6A and B for DMSO and EC/DMC, respectively. In both solvents, the diffusion of the $TFSI^-$ anion is independent of salt concentration, is higher than either other species, and appears to slightly decrease at the highest polymer concentration. This decrease in diffusion coefficient at high polymer concentration is observed for all species as a result of the increased viscosity at higher polymer concentration (Figure 4.3). The relatively higher diffusion coefficient of $TFSI^-$ compared with Li^+ is expected given the large solvation structure of Li^+ in solution.[203] The polyion backbone diffusion coefficient also does not appear to have a significant dependence on LiTFSI concentration, though is significantly slower at 0.1M polyion than 0.01M. This indicates the 0.1M polyion solution has passed the entanglement concentration, as polyelectrolyte diffusion coefficients are independent of polymer concentration within the semidilute range.[204] It is surprising that the backbone diffusion coefficient is not a function of total LiTFSI concentration in either solution, particularly in EC/DMC where a significant decrease in bulk viscosity is observed at high polymer concentration. The expansion or contraction of chain conformations that might be expected to cause this decrease in viscosity would typically be expected to also affect the diffusion of the chain.

The diffusion coefficient of the lithium is the most drastically different transport property between the two solvents, being independent of LiTFSI concentration in DMSO, but significantly increasing with LiTFSI concentration in EC/DMC. This behavior is consistent with the analysis of the molar conductivity data in EC/DMC which clearly indicates the dissociation of lithium from the polymer is very low. The lithium diffusion reported here is an average of all lithium species in solution, so addition of a fast lithium species (in the form of LiTFSI) to a solution where lithium is tightly associated with a bulky polymer would produce a slowly increasing average. Unfortunately, these different lithium species cannot be directly observed in the diffusion measurement. Given the increase in lithium diffusion with added LiTFSI in EC/DMC, it is somewhat surprising that the average lithium diffusion does not change at all on addition of LiTFSI to the DMSO-based polymer solution. There are two possible explanations for this observation in DMSO. First, the addition of a fast lithium species from LiTFSI could be perfectly balanced by

the association of an equivalent amount of lithium to the polymer (producing a slow lithium species). If these processes occur simultaneously, no change in the average Li diffusion would be seen. Such a balance might be reasonable given a dynamic equilibrium between bound and free lithium, where addition of free lithium would drive the balance back to the associated species. Similar suggestions have been made in the literature.[196,205,206] A second possible explanation is that the lithium species present in the pure polymer system diffuses at the same rate as lithium in a pure LiTFSI solution, and at these concentrations the additional ionic content does not produce any change in the species' motion. It can easily be seen from Figure 4.6A that the lithium in a 0.01M polyion solution diffuses at nearly the same rate as a lithium species in a pure LiTFSI solution, though at 0.1M polymer the lithium diffuses somewhat slower.

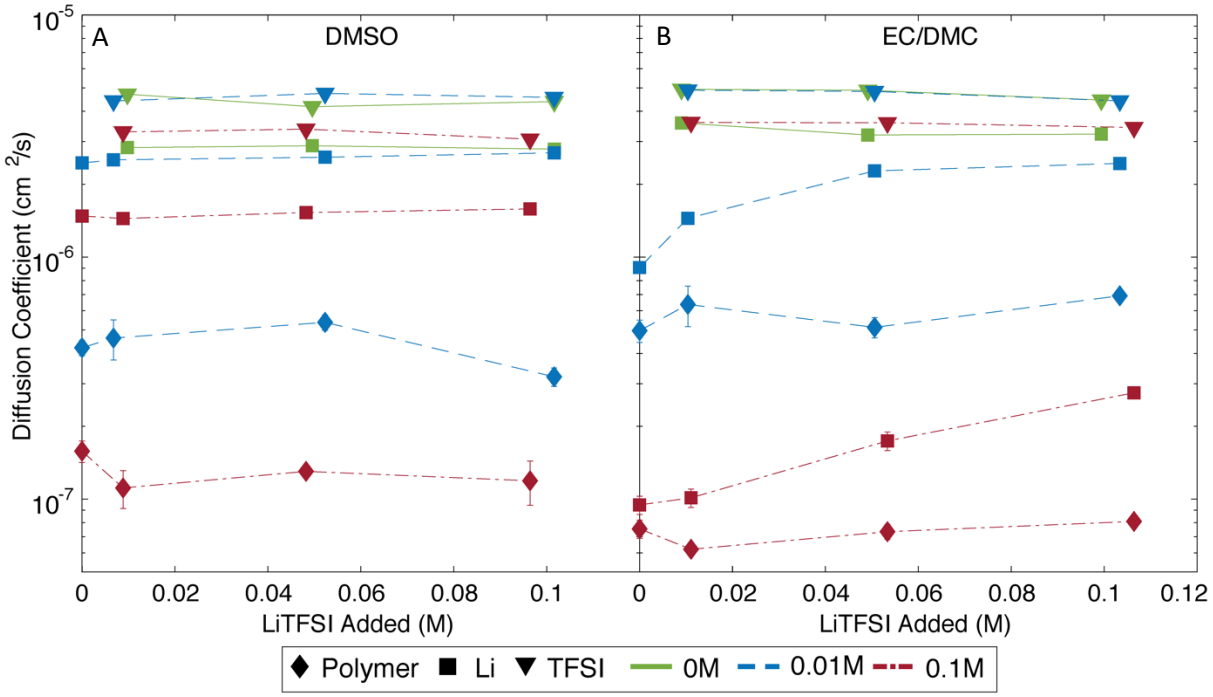

Figure 4.6. Diffusion coefficients of each species (polymer, Li^+, and $TFSI^-$) as a function of LiTFSI added for A) DMSO and B) EC/DMC=2 (v/v)

To examine the local effects of viscosity on the solution directly, we examine the diffusion coefficients relative to the solvent diffusion coefficients in Figure 4.7. The solvent diffusion coefficients are plotted alone in the Supporting Information, Section VI, Figure 4.11 and Figure 4.12. Figure 4.7 plots the diffusion coefficient of each species normalized to the diffusion coefficient of DMSO in Figure 4.7A and molar average solvent diffusion for EC/DMC in Figure 4.7B. In each case, the solvent diffusion coefficient, $D_{solvent}$, is that measured for each unique composition reported in Figure 4.6 from the ^1H spectra. In both solvents, it is immediately evident that any difference in $TFSI^-$ diffusion can be ascribed to the slightly slower solvent diffusion in the more viscous 0.1M polymer solutions, as $D/D_{solvent}$ for $TFSI^-$ collapse onto a single curve for all polymer and LiTFSI concentrations. $TFSI^-$ also appears to diffuse at the same rate in both solvents relative to the solvent diffusion. In EC/DMC, Figure 4.7B, the normalized lithium diffusion coefficients are significantly lower for the polymer solutions compared to the pure LiTFSI (0M polymer) solutions, further supporting the conclusion of poor dissociation in EC/DMC. In DMSO, Figure 4.7A, the normalized lithium diffusion coefficient is closer to the diffusion of lithium in the

pure LiTFSI solution, but does not collapse completely to a single line. Thus, it is clear that a portion of the lithium must still be associated with the polymer at 0.1M polymer in DMSO, where $D_{Li}/D_{solvent}$ is still lower at all LiTFSI concentrations than $D_{Li}/D_{solvent}$ for the 0 and 0.01M polymer cases.

Most surprisingly, the large decrease in viscosity as a function salt concentration in the 0.1M polymer in EC/DMC series is not accounted for by the diffusion coefficient of the solvent, which remains relatively constant with added salt (Figure 4.12). While at a given salt concentration there is a decrease in solvent diffusion with increasing polymer concentration that accounts for the change in $TFSI^-$ diffusion, there is no significant increase in solvent diffusion coefficient as a function of salt concentration. In fact, at this polymer concentration, the solvent diffusion coefficients appear to decrease slightly with salt concentration.

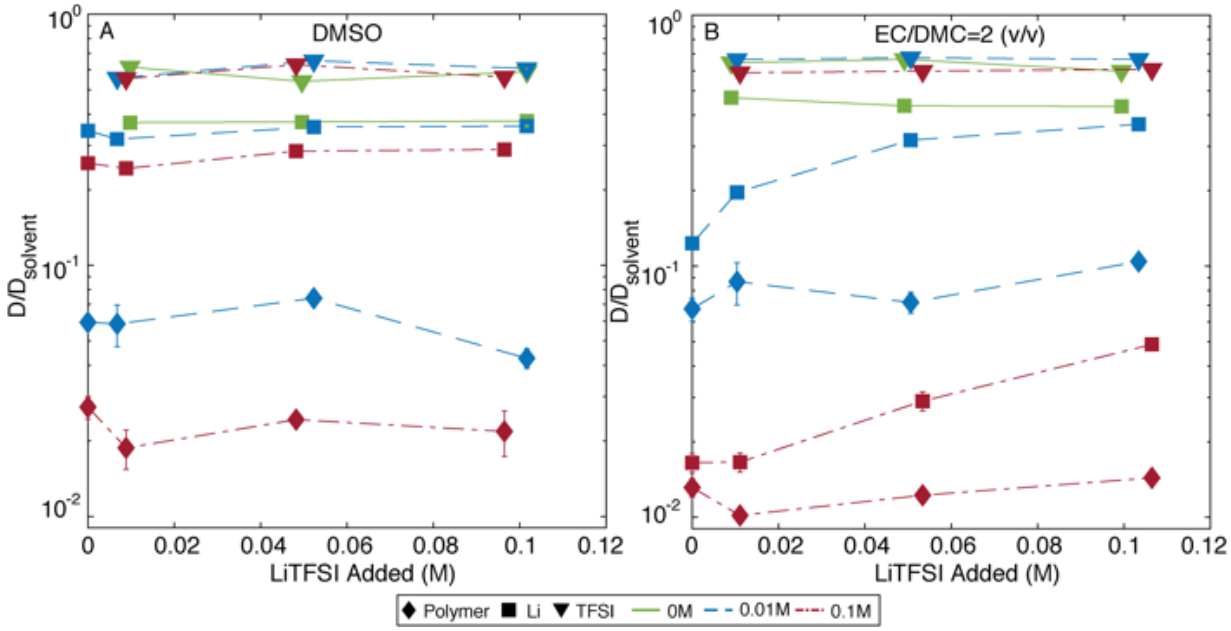

Figure 4.7. Diffusion coefficient of each species normalized to the solvent diffusion coefficient as a function of LiTFSI added for A) DMSO and B) EC/DMC=2 (v/v).

This deviation from the expected viscosity, η_{Stokes}, based on the observed solvent diffusion coefficients and assuming the molecules diffuse as Stokes spheres, can be observed most directly in Figure 4.8A and B. Here, the viscosity ratio defined in Equation 4.3 is plotted as a function of salt concentration.

$$\frac{\eta_{Stokes}}{\eta} = \frac{kT}{6\pi r_{solvent} D_{solvent} \eta} \qquad 4.3$$

Here $r_{solvent}$, the effective hydrodynamic radius of a diffusing solvent molecule, is calculated using the Stokes-Einstein equation, the measured viscosity, and PFG NMR diffusion coefficient of the pure solvent (i.e., without added salt or polymer). For EC/DMC, the diffusion coefficient of the two solvents was averaged on a molar basis to obtain an effective average solvent radius. Deviations from 1 in this ratio could therefore be a result of changes in the effective solvent radius as the solution composition changes, or other intermolecular interactions. The most apparent trend here is that the deviation from the "ideal" stokes viscosity increases with polymer concentration. This suggests that the bulk viscous effects are decoupled from the local viscosity of the solutions.

Such phenomena have been discussed in polymer solutions for some time, where it is understood that the length scale of the polymer entanglements that cause high viscosity is longer than would be felt directly by a small probe molecule.[207] Essentially, the small molecule can move around the polymer, but when a bulk shear is applied to the solution, the long chains impede this motion. This suggests that the effect that causes the decrease in viscosity at 0.1M polymer in EC/DMC occurs over a relatively long range, or that the local interaction has a stronger influence on bulk properties than local motion of small ions. This observation is important for the design of an HTNE, where the bulk viscosity might otherwise be considered a key property to minimize.

To relate local diffusion and bulk conductivity measurements directly, the Inverse Haven Ratio, H_R^{-1}, as defined in Equation 4.4, is often employed.[208]

$$H_R^{-1} = \frac{\sigma}{\frac{F^2}{RT}\left(c_{Li}D_{Li} + c_{sulfonates}D_{polymer} + c_{TFSI}D_{TFSI}\right)} \qquad 4.4$$

F is Faraday's constant, R is the gas constant, and T is the temperature (298K). Note that c_{Li} is the total lithium concentration, while the two anionic species can be treated separately. Here the measured conductivity (σ) is related to the conductivity that would be expected from the Nernst-Einstein equation if every NMR-measured diffusion coefficient ideally represented all charged species in solution. As this would only be explicitly true if every species was fully dissociated, the Haven ratio is often used to probe extent of dissociation. It should be noted that because the NMR averages all lithium species (charged, uncharged, associated, or dissociated) H_R^{-1} does not directly correspond to extent of dissociation, however it does relate to the ideality of the solution and the relationship between diffusivity and mobility.[204] In DMSO, Figure 4.8C, the ratio for the pure 0.1M polymer solution and most dilute pure LiTFSI solution is equivalent to one, within error of the measurements. The solution at 0.01M polymer appears to have an $H_R^{-1}>1$ in the pure solution, a result that was verified twice in this study (two separate multiple-replicate analyses), perhaps alluding to the complex relationship between diffusion and mobility in polyelectrolyte solutions.[115] Detailed analysis of this result is beyond the scope of this paper, but should be the subject of future work. As the LiTFSI concentration is increased, H_R^{-1} decreases, indicating the solution conductivity deviates from the conductivity that would be expected if each NMR-measured diffusion coefficient ideally translated to conductivity. Here this decrease in each solution is likely the result of ion association as concentration is increased. In EC/DMC (Figure 4.8B), H_R^{-1} of the pure polyelectrolyte solutions is very low, as would be expected for low dissociation. Interestingly, even a small amount of salt causes the Haven ratio to immediately jump to the value for pure LiTFSI. This is a result of the orders of magnitude larger diffusion coefficient of $TFSI^-$ compared to the polyanion, combined with the immediate increase in average lithium diffusion coefficient on addition of LiTFSI due to the increased dissociation of LiTFSI compared to the lithium sulfonate moieties on the polymer chain.

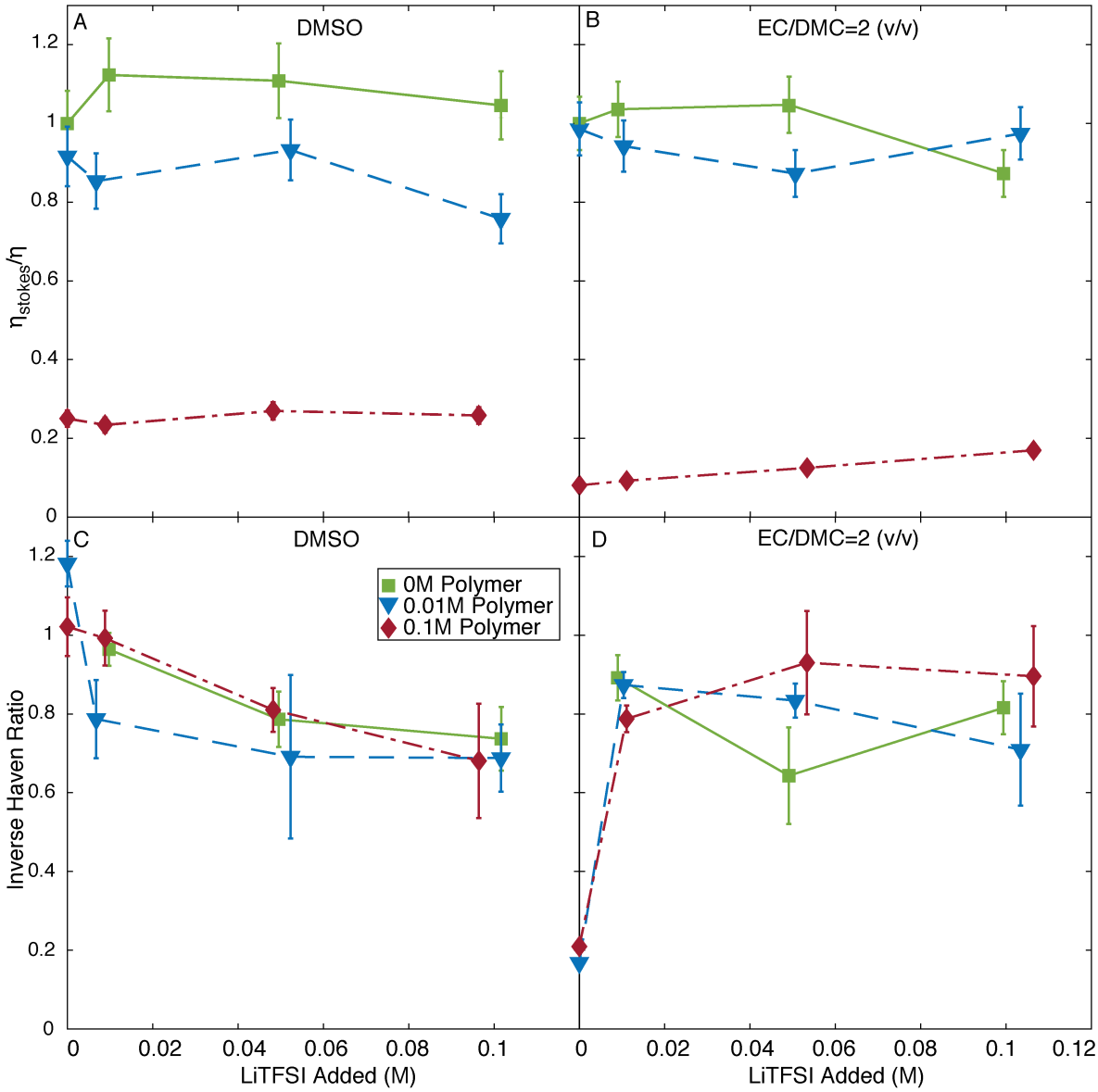

Figure 4.8. Viscosity ratio defined in Equation 4.3 as a function of LiTFSI added for each polymer concentration in A) DMSO and B) EC/DMC=2 (v/v). Inverse Haven Ratio as a function of LiTFSI added for each polymer concentration in C) DMSO and D) EC/DMC=2 (v/v). In each figure, reported error has been propagated from the measurements.

It is important to recognize the behavior reported here for the same polymer in DMSO and EC/DMC is surprising. The vast majority of literature on polyelectrolyte solutions uses the dielectric constant of the solvent as the main parameter to determine the charge of the polymer, via the Bjerrum length. The dielectric constant of DMSO at 298K is 46.7, and a 2:1 v/v mixture of EC and DMC should have a dielectric constant at least equivalent to or higher than DMSO.[209] It should be noted that a carefully measured value for EC/DMC could not be found at 298K, but has been carefully measured at 313K to be 51.[210] The dielectric constant of a blend of EC and ethyl methyl carbonate at an equivalent ratio is also near 50.[211] Based on this alone, it would be expected that the two polyelectrolyte solutions have similar ion dissociations and, ultimately, similar transport properties. Clearly this is not the case.

Evidence for low ion dissociation in EC/DMC can be observed directly from ^{7}Li NMR, as shown in Figure 4.9. Here the half width of the lithium peak is plotted for all solutions, with an example series at 0.01M polymer plotted in Figure 4.9A. The lithium peak width is significantly larger in all EC/DMC solutions with polymer, but is narrow for pure LiTFSI in EC/DMC and all DMSO solutions. NMR peak broadening or narrowing can be due to a range of potential causes, but a reasonable explanation for the data shown in Figure 4.9 is that lithium associated with a polymer would move significantly more slowly and thus its signal would be less resolved, as is typical for polymers in NMR.[212] Further, this trend cannot be explained by the bulk viscosity, as the 0.01M and 0.1M polymer in EC/DMC solutions display the same trend in peak width, despite displaying significantly different trends in viscosity. Therefore, we use the peak width here as a proxy for the relative degree of association between Li^{+} and the polyions, with a larger peak width corresponding to a higher degree of association.

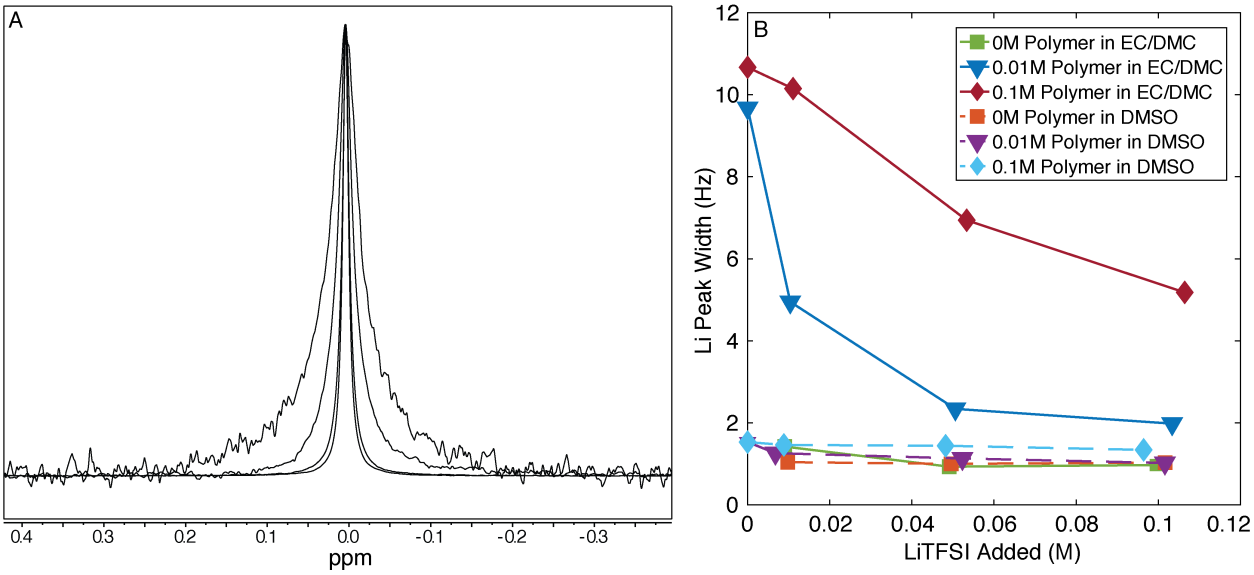

Figure 4.9. A) ^{7}Li spectra for the series of solutions at 0.01M Polymer in EC/DMC with added LiTFSI. The spectra of each solution have been overlaid, and the intensity normalized. With added LiTFSI, the peak width narrows. B) ^{7}Li peak width at half maximum as a function of LiTFSI added for all solutions.

There are two possible explanations for the apparently higher ion association in EC/DMC than DMSO. First, if the polymer conformation is coiled tightly, one might expect the lithium counterions to be trapped within some form of micellar structure. Second, despite having similar dielectric constant, EC/DMC may not provide adequate solvation of the sulfonate/Li structure. To investigate this point, a collaborator (K.D. Fong) estimated the dissociation constant of the polymer sulfonate group using quantum chemistry calculations, shown in Table 4.1. Here the dissociation constant of polymer-appended ion is calculated using both an implicit solvent model and an explicit solvent model. The details of these models are described more completely in the published article.[213] When solvation is approximated by an implicit solvent model, where the dielectric constant is the only parameter distinguishing DMSO and EC/DMC, a lower dissociation constant (corresponding to less favorable dissociation) for DMSO is observed. This is consistent with DMSO's slightly lower dielectric constant. With explicit solvent molecules included in the calculation, however, the opposite trend is apparent: dissociation is now substantially more favorable in DMSO.

Table 4.1. Dissociation constant in EC/DMC and DMSO calculated with implicit solvent and explicit solvent.

Dissociation Constants		
	Implicit Solvent	Explicit Solvent
DMSO	0.59	56.4
EC/DMC	0.86	4.38

This trend coincides with the differences in donor number of the solvent molecules, indicating that this may be a more essential parameter in determining ion association than the dielectric constant of the neat solvent. The utility of the donor number concept in describing dissociation of ions has been noted in polyelectrolytes before, though we note that others have suggested more advanced models that may be able to capture a wider range of behavior.[143,214] Note that the orders-of-magnitude differences in dissociation constants between the implicit and explicit solvent calculations are due to systematic errors in solvation energy from the implicit solvent model used, which can be on the order of 0.5 eV.[215] This error is then transferred to the exponential used to calculate the dissociation constant, yielding variations consistent with the differences between methods observed in Table 4.1. These systematic errors, however, should not affect the observed trend between solvents.

These results suggest that conventional theories of counterion condensation in polyelectrolytes, in which the solvent is only accounted for implicitly as a dielectric continuum, do not adequately capture important trends in these systems. Although polymer conformation also likely plays a role in the observed transport properties here, neutron scattering experiments that would be necessary to probe directly the polymer radius of gyration are beyond the scope of this work. As there is a clear difference in the dissociation of lithium in the two solvents, simply from the standpoint of dissociation constant, it is reasonable to infer that the deciding factor in the poor conductivity observed in EC/DMC is the dissociation of the ion appended to the polymer backbone. Further, though the viscosity measurement indicates a charge screening effect causing a decrease in viscosity on addition of salt, there is no evidence that the polymer is significantly charged in this solvent. The viscosity trend in EC/DMC might be explained instead by ionic interactions due to ion coordination with the ether functionality of the PEG segments,[216] or strong dipolar interactions between the ion pairs that would only be present in EC/DMC. Either hypothesis requires further investigation.

Ultimately, the relative motion of lithium to the other species is the desired property, as captured by the transport number, t_+, defined in Equation 4.5.

$$t_+ = \frac{c_{Li}D_{Li}}{c_{Li}D_{Li} + c_{TFSI}D_{TFSI} + c_{sulfonates}D_{polymer}} \qquad 4.5$$

Here t_+ is defined directly as the fraction of the total conductivity that would come from lithium if the Nernst-Einstein equation were valid for each species. It should be noted that this is not equivalent to the true electrochemical transference number, which would require significant electrochemical characterization that is beyond the scope of this work.[24] The transport number reported hear is still a measure of the relative motion of lithium over the other species that would contribute to the conductivity. For EC/DMC in Figure 4.10B, t_+ of the polymer solution is high without salt, but addition of any salt immediately causes a significant drop due to the very fast-moving $TFSI^-$ anion. Because a significant fraction of lithium also always diffuses slowly in this system, the t_+ of the polymer containing solutions is actually lower than the pure LiTFSI solution.

This result is only true for the case that the polyion does not dissociate because, in contrast, the t_+ remains high even as a small molecule salt is added to the DMSO polymer solutions (Figure 4.10A), where substantial Li^+-SO_3^- dissociation occurs. As salt concentration is increased, t_+ approaches the t_+ of the pure LiTFSI solution. This suggests in a well-dissociated solution there is the potential to optimize conductivity and t_+ by tuning small molecule salt content.

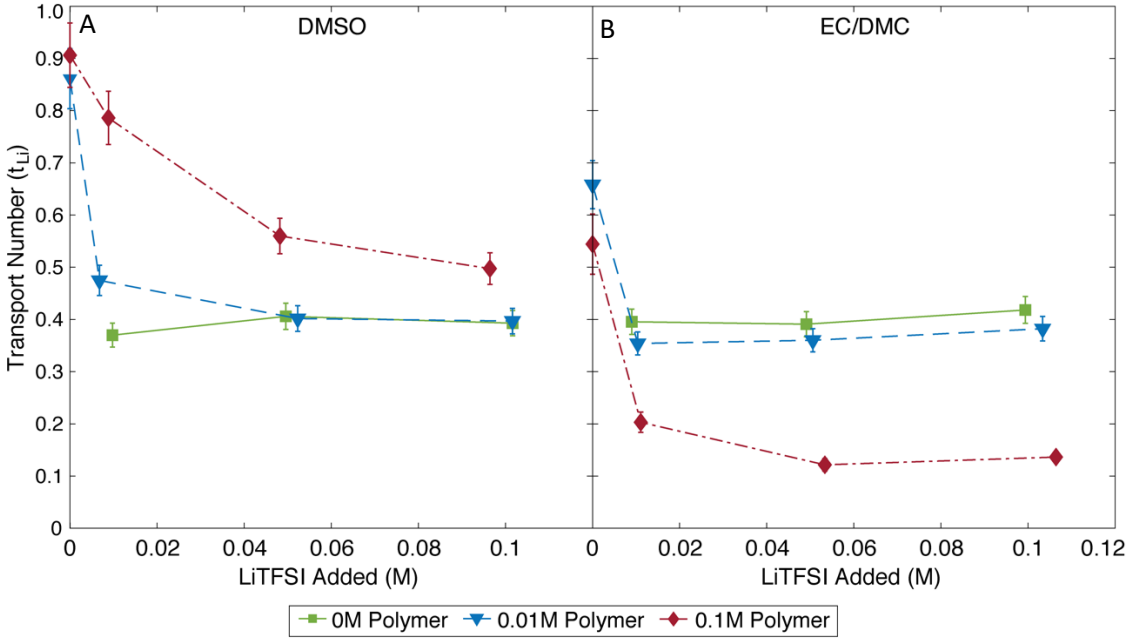

Figure 4.10. Transport number as a function of LiTFSI added at each polymer concentration in A) DMSO B) EC/DMC=2 (v/v).

V. Summary

In this work, the transport properties of solutions of sulfonated polysulfone/poly(ethylene glycol) copolymer in EC/DMC and DMSO with added LiTFSI have been investigated as a function of salt content. It is seen that the addition of salt to either solution causes an increase in solution conductivity, but that the bulk viscosity only changes as a function of salt concentration at high polymer concentration in EC/DMC. The behavior of lithium in each solution is quite different, resulting in significant differences in the final transport properties. In EC/DMC, the polymer and lithium are poorly dissociated, and adding salt does not alter the properties of the solution to significantly change lithium-polymer dissociation. Thus, the conductivity of the solution with added salt is entirely due to the added salt and changes in viscosity must be a result of another interaction, either between ether repeat units and LiTFSI or between the strong dipoles of ion pairs. In DMSO, the polymer and lithium are well-dissociated, and addition of salt causes t_+ to decrease and the conductivity not to increase as significantly as in EC/DMC. Both NMR and quantum chemistry calculations demonstrate that EC/DMC is unable to dissociate the sulfonate group on the polymer as strongly as DMSO. This alone predicts the majority of behavior observed here, suggesting the design of new HTNE polyelectrolyte solutions should strongly consider the ability of the solvent to dissociate the polyion and counterion. In the design of an HTNE for battery applications, a relatively narrow range of solvents are well-characterized, and thus structural changes to the polyion that promote dissociation are the most promising path forward, though in the next chapter additives are also shown to promote dissociation. Addition of salt is shown here

as a promising method to tune conductivity and transference number in the case that the polymer is well dissociated, an important ability that is not possible in most electrolytes.

VI. Supporting Information

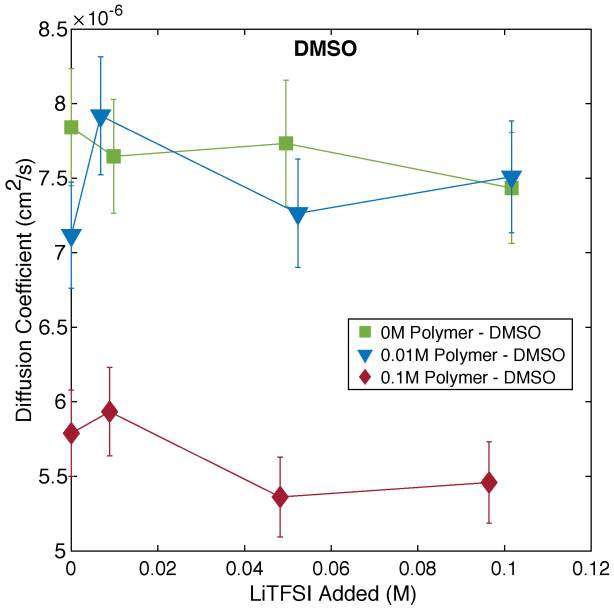

Figure 4.11. Diffusion coefficient of the DMSO solvent as a function of LiTFSI added to each polymer solution.

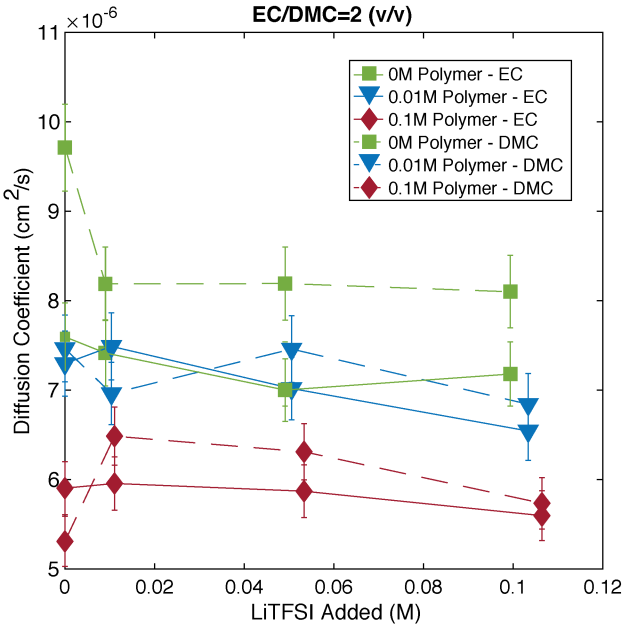

Figure 4.12. Diffusion coefficient of DMC (dashed lines) and EC (solid lines) in each polymer solution as a function of LiTFSI added.

5. Counterion and Solvent Transport in Nonaqueous and Aqueous Polyelectrolyte Solutions

I. Abstract

Nonaqueous polyelectrolyte solutions have recently been proposed as potential battery electrolytes due to the unique ability to tune the mobility of the anion relative to that of the electrochemically active lithium ion. This could potentially be used to study the effect of concentration polarization during battery charge, a major limiting factor in achieving fast charge rates that is caused by high anion mobility. An important consideration in the design of polyelectrolyte solutions for battery applications is the solubility of the polymer in battery – relevant carbonate blend solvents. Little is understood, however, about the importance of designing the polymer to be solvophillic or if it is sufficient to obtain solubility through ions alone (as with polystyrene sulfonate in water). Using a model polysulfone – based system, we investigate the conductivity, viscosity, and diffusion of polyelectrolyte solutions over a range of concentrations and molecular weights in dimethylsulfoxide (DMSO) and water. Sulfonated polysulfone is readily soluble and the charge group is known to dissociate in both solvents, but the neutral backbone polymer is only soluble in DMSO. We find marked differences in the transport behavior of polymer solutions prepared from the two solvents, particularly past the entanglement concentration. Comparing this transport behavior to that of the monomer in solution demonstrates a larger decrease in lithium motion in DMSO than in water, even though the bulk viscosity in water approaches a gel-like state. This study sheds light on the important parameters for optimizing polyelectrolyte solution transport in different solvents.

II. Introduction

Direct control of the transference number of the electrolyte, a parameter that is otherwise difficult to control in liquids, could enable high charge rate and energy dense lithium ion batteries. The transference number characterizes the relative motion of lithium to the anion in solution, and in most electrolytes is a result of the size of cation and anion (including their respective solvation shells). Polyelectrolytes present a more complex relationship between size, diffusion, and mobility in an electric field, and as a result have potential use as lithium ion electrolytes with varying transference number. An important aspect of achieving the goal of a high transference number nonaqueous polyelectrolyte solution is a full understanding of counterion and polyion motion in these systems. Given the historical motivation for study of polyelectrolyte solutions, the motion of the polyion in solution has been studied extensively, as well as the overall solution conductivity.[106,121] The transport behavior of the counterion, and solvent, however, have not been characterized to the same extent, yet are arguably more important to understand in the context of battery electrolytes.

Counterions are often taken into account in polyelectrolyte theory as a means of describing the polyion structure and dynamics. Manning's original theories on counterion condensation include D_c/D_{c_0}, the ratio of the counterion diffusion in the polyelectrolyte solution to the diffusion at infinite dilution.[108] At the time, the goal was to understand changes in counterion behavior as a function of charge on the polymer, and concentration dependence was either not discussed or not expected. The work of Schipper and Leyte from the mid 90's comprises the bulk of recent experimental characterization of counterion behavior in polyelectrolyte solutions.[129–131,217] In a

series of papers, they reported the diffusion coefficients of Li^+, Na^+, and tetramethylammonium in solutions of polymethacrylic acid, polyacrylic acid, and DNA. Through this, they examined some of the effects of counterion type, molecular weight, degree of neutralization, and concentration. Since then, computational work has found some differences in counterion behavior from these earlier experimental papers, predicting a monotonic decrease in diffusion with concentration, as opposed to non-monotonic behavior observed by Schipper.[132] Prabhu in 2005 also reviewed some of the recent work on counterion behavior, though less attention has been given to counterion dynamics in recent years.[126]

An interesting question for the design of a polyelectrolyte for a battery application is the importance of backbone solvation relative to solvation of the ions. Chapter 4 demonstrates a polymer which is soluble in carbonate based solvents, but does not dissociate the charge group in solution. At the same time, it is common to find hydrophobic polymers bearing ion groups, such as sulfonated polystyrene, dissolved in water. This fundamental idea has been the subject of significant literature, usually in terms of hydrophobic vs. hydrophilic polyelectrolytes.[112,141,218] However, no study has specifically targeted optimization of counterion transport in these two cases, and quantitative comparisons of transport between the two cases are rarely made. There are few systems where the same charged polymer is soluble in multiple solvents, and it is difficult to compare different polymers in the same solvent and still control for other possible differences due to the different polymer structure. Theory has predicted the ratio D_c/D_{c_0} to have a concentration dependence in poor solvent polyelectrolyte solutions, but not in the good solvent case.[122] Differences are thus expected, but little experimental work exists.

In this work we present results of a study of lithium-neutralized sulfonated polysulfones dissolved in dimethylsulfoxide-d_6 (DMSO-d_6), a good solvent for the polymer backbone, and D_2O, a poor solvent for the backbone. The solvents are both deuterated for NMR measurement of backbone diffusion coefficients. This polymer is chosen due to the existence of a polar, nonaqueous, good solvent for the neutral backbone, and the availability of prior simulation results for a similar sulfonated sulfone polymer in both DMSO and water.[143] This system presents an interesting case where it is known that DMSO and water dissociate the sulfonate-lithium group similarly, but the neutral backbone is insoluble in water.

Overall solution viscosity and conductivity, and pulse field gradient NMR diffusion coefficients of the solvent, lithium, and backbone are measured over a wide concentration range covering semidilute and entangled solutions. We focus on a set of short chain polymers, ranging from 7 to 30 repeat units, below the range typically considered in theories, and significantly shorter than any previous experiments. We anticipate such oligomeric chains may be the most promising to achieve a high transference number, given that the number of charges on the polymer chain appears in the denominator of the simple estimate for transference number. We also characterize solutions of the sulfonated monomer, demonstrating the effects that arise from the polymer. This Chapter is organized to first present the results as measured. In the following section, the apparent scaling with concentration and molecular weight is compared with common theory. Finally, we discuss several important observations contained within this data.

III. Experimental Section

i. Materials

Deuterium oxide (D_2O) was purchased from Sigma Aldrich and sparged with nitrogen for 30 minutes prior to being used in an Ar glovebox. Anhydrous deuterated dimethyl sulfoxide (DMSO-d_6), anhydrous n-methyl-2-pyrrolidone (NMP), toluene and the DOWEX HCR-W2 ion

exchange resin were purchased from Sigma Aldrich and used as received. Potassium carbonate was purchased from VWR and used as received. Lithium carbonate was purchased from Beantown Chemicals and used as received. 4,4'-biphenol and 4,4'-dichlorodiphenylsulfone-3,3'-disulfonic acid disodium salt were purchased from Akron Polymer Systems and were dried for two days under vacuum at 80°C before use.

ii. Synthesis

All sulfonated polysulfone polymers (SPSF), with molecular structure provided in Figure 5.1A, were synthesized with slight modifications of the typical polycondensation reaction for polysulfone.[146,147] Carefully weighed 4,4'-biphenol, sulfonated bis(4-chlorophenyl) sulfone, and potassium carbonate at 15% excess were loaded to a 3-neck flask with a Dean – Stark trap and nitrogen gas inlet in an oil bath on a magnetic stir plate. Solvent (at a 3:1 ratio of NMP to toluene) was added to produce a 20wt% dissolved solids mixture, and then the trap was filled with toluene. The reaction was stirred for 2 hours at 150°C to perform azeotropic removal of water before the temperature was increased to 190°C for approximately 20 hours. An excess of the sulfonated monomer was utilized to control for molecular weight according to the Carothers equation for the three shortest polymers.[219] The two longest polymers were produced with a 1:1 molar ratio of the monomers. The longest polymer utilized a temperature of 180°C for 20 hours, instead of 190°C. The polymer was precipitated in isopropanol, rinsed in acetone, and then redissolved in DI water. This solution was then placed in a SpectraPor 7 dialysis tube with a 1 kDa cutoff and dialyzed with an excess of lithium carbonate to replace the appended ion with lithium. The solution was then dialyzed against DI water to remove any excess salt, exchanging the water several times over several days. To ion exchange the sodium-form sulfonated monomer, DOWEX HCR-W2 ion exchange resin was first stirred with an excess of lithium carbonate in water, and then rinsed several times with water to obtain a lithiated resin. The monomer was then stirred over the lithiated resin in water, exchanging the resin four times. Ion exchange of the polymers and monomer was confirmed by ICP-OES to be at least 95 mol% lithium. After ion exchange the polymers and monomer were lyophilized before further drying for ~120 hours at 120°C under vacuum over phosphorous pentoxide.

iii. Polymer Characterization

The ^{1}H nuclear magnetic resonance (NMR) spectra of each polymer is shown in Figure 5.1A, with the structure and peak assignments noted. Gel permeation chromatography (GPC) was performed on an Agilent 1260 Infinity Series with Waters Styragel HR3 and HR4 columns and NMP with 0.05M LiBr as the mobile phase, as shown in Figure 5.1B. The number of repeat units for the shortest two polymers that were synthesized with a large excess of the sulfonated monomer were determined by end group analysis as only a single type of end group appears in the spectra. For longer polymers there is a mix of biphenol and sulfone end groups, and as such explicit determination of molecular weight is not possible by this method. Instead, the number of monomers is determined by multiplying the number for the shortest polymer by the change in M_n from GPC. This scaling method agrees well with the change between the shortest two polymers by NMR. Polymers are named SPSF-x, where x is the number of repeat units.

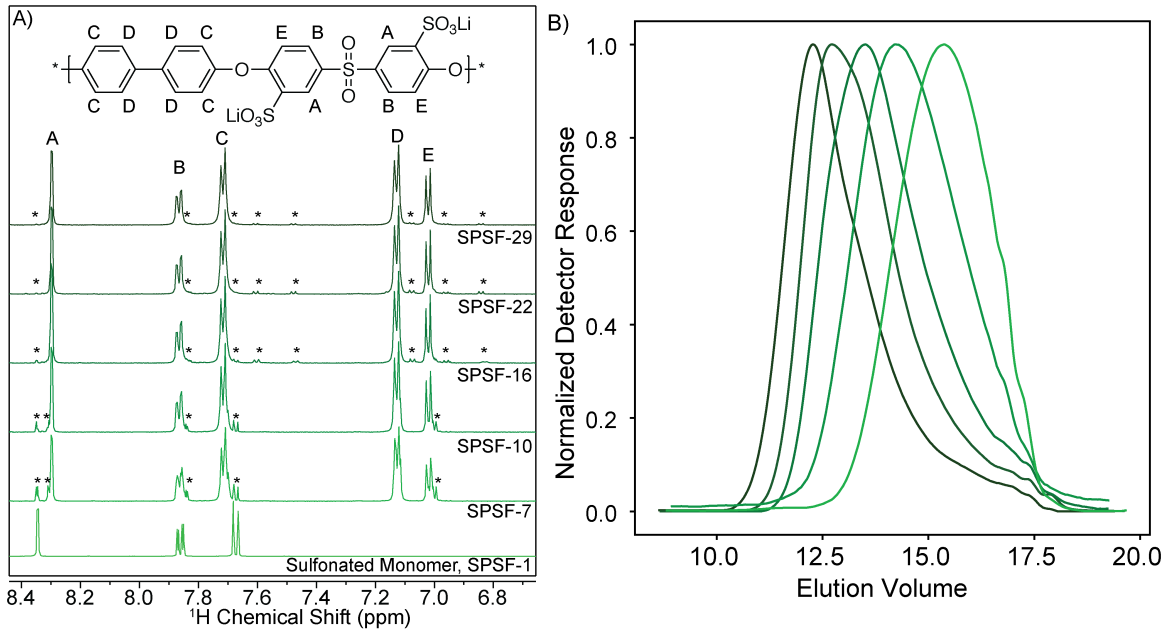

Figure 5.1. A) NMR Characterization of the sulfonated polysulfone (SPSF) polymers and the sulfonated, lithium-form monomer (sulfonated bis(4-chlorophenyl) sulfone), with peak assignments noted for the polymer. Peaks associated with the end groups are denoted by a star. B) GPC of the SPSF polymers with color corresponding to the polymer in A).

iv. Solution Preparation

Polymers were brought under vacuum from the drying oven directly into an Argon glovebox kept below 0.1ppm oxygen and water (Vac Atmospheres). Solutions in DMSO-d_6 were prepared in the same glovebox, while solutions in D_2O were prepared by weighing the polymer in the dry box before adding D_2O in an Ar filled glovebox kept free of CO_2 and O_2. NMR samples at high concentration in D_2O were prepared by weighing dry polymer stuffed directly into an NMR tube and then adding D_2O to the NMR tube. These were capped with an air tight cap, sealed with parafilm, and kept at 50°C for several weeks to allow the polymer to dissolve and slowly move to the bottom of the tube. To verify this method aligns with solutions prepared outside of the tube, the same samples were diluted from the high concentration to 0.2M, and all values aligned closely with the previously measured values. The concentration of each solution is measured by quantification with ^{7}Li NMR. A calibration curve for the ^{7}Li intensity recorded from a single scan was made with standard solutions of LiCl in D_2O. The single scan was taken after shimming on ^{1}H and optimizing the 90° pulse length, with a consistent receiver gain and a 120 second delay prior to the scan.

v. Conductivity

Solution conductivity was measured with a Mettler Toledo InLab 751-4mm conductivity probe in a dry block (Torrey Pines) kept at 25°C inside of an Argon glovebox kept below 10ppm O_2 and 1ppm H_2O. Measurement of water samples was carried out in the same box to eliminate the possibility of CO_2 contamination, and exposure of water samples to the glovebox environment was minimized to prevent evaporation. Solution temperature was verified by a temperature sensor inside of the conductivity probe, and was always within 0.5°C of the set point. The conductivity probe was calibrated against known standards (Mettler Toledo) at 84 µS/cm, 1413 µS/cm and

12.88 mS/cm in water, and also verified against previous LiTFSI in DMSO measurements.[105] A 5% error in conductivity is estimated from several repeat measurements on the same sample.

vi. Viscosity

Viscosity was measured using an electromagnetically spinning viscometer (EMS-1000, Kyoto Instruments). This technique measures the viscosity by measuring the rotation rate of an aluminum ball sitting inside of the solution as it is spun by a magnetic field. A rotation rate of 1000 rpm was used for all samples, and no change in viscosity as a function of rotation rate (within instrument capability) was observed for several test samples. The instrument maintains temperature at 25°C throughout the measurement, and vials are capped within the Argon glovebox. 10 repeats of the measurement were performed on each sample and error is reported from this variability.

vii. Diffusion Coefficients

Diffusion coefficients for the polymer backbone and solvent were measured from ^{1}H pulse field gradient NMR (PFG-NMR) diffusometry, while the lithium diffusion coefficient was measured from ^{7}Li PFG-NMR. Measurements were performed on Bruker Avance III 600 and 500 MHz instruments fitted with 5mm Z-gradient broadband probes and variable temperature units maintained at 25°C throughout the measurement. The gradient of each instrument was calibrated to known values of H_2O in D_2O,[198] H-DMSO in DMSO-d_6,[199] and 0.25M and 4M LiCl in H_2O[198]. Error in the diffusion measurement was estimated to be at minimum 5% based on variability in this calibration. The double stimulated echo pulse sequence with convection compensation was used for all measurements (Bruker's dstebpgp3s program).[200] For the 600 MHz instrument, the signal attenuation as a function of gradient strength was fit to Equation 5.1, which includes corrections for the sine shape pulse.[202]

$$\frac{I}{I_0} = e^{-\gamma^2 g^2 \delta^2 D\left(\Delta - \frac{5\delta}{8} - \tau\right)} \qquad 5.1$$

The 500 MHz instrument uses TopSpin 3.5, which has a slight adjustment to the delays in the dstebgp3s pulse program, and thus the fit equation is modified to Equation 5.2.

$$\frac{I}{I_0} = e^{-\gamma^2 g^2 \delta^2 D\left(\Delta - \frac{5\delta}{3} - 3\tau\right)} \qquad 5.2$$

Here γ is the gyromagnetic ratio, g is the gradient strength, δ is the gradient pulse duration, D is the diffusion coefficient, Δ is the diffusion delay, and τ is the delay for gradient recovery. In DMSO-d_6 δ varied from 0.6 to 8.5 milliseconds and Δ varied from 0.08 to 0.4 seconds while in D_2O δ varied from 0.6 to 3.5 milliseconds and Δ varied from 0.06 to 0.3 seconds. 16 experiments of varying gradient strengths were utilized for all samples, and a single exponential decay in signal strength was observed for all samples. For some samples, noise in the fitting due to low signal is larger than the 5% error estimated from the calibration and thus the standard error of the fit is reported as the error.

Due to the number of samples and the extremely long T_1 of relevant peaks in both D_2O and DMSO-d_6, experiment time was minimized by utilizing a short recycle delay much less than T_1, and employing 16 dummy scans to operate in a steady state mode. While errors introduced by this method have been acknowledged,[220,221] several samples utilizing a full delay of 4 x T_1 found diffusion coefficients within 5% of the steady state measurement. This, combined with the

consistency of the data shown here between different solutions using different polymers over a wide concentration range indicates the possibility of significant steady state errors is small.

IV. Results

The viscosity of each length SPSF between 0.0001M and 1M in both DMSO-d_6 and D_2O is reported in Figure 5.2. In this work molarity refers to lithium ion concentration, and the concentration plotted is taken from NMR measurement of the concentration. This accounts for the volume of the polyelectrolyte at high concentrations, and error due to weighing and dilution at low concentrations. In DMSO-d_6, viscosity increases with increasing concentration and increasing molecular weight as expected. In D_2O, the same is true, except the increase in viscosity occurs extremely rapidly. SPSF-7 at the highest concentration was the largest polymer at that concentration with a viscosity that could be measured by the EMS technique employed (which has an upper limit around $1x10^6$ mPa·s). The other samples at this concentration form effectively a gel which can be handled with forceps.

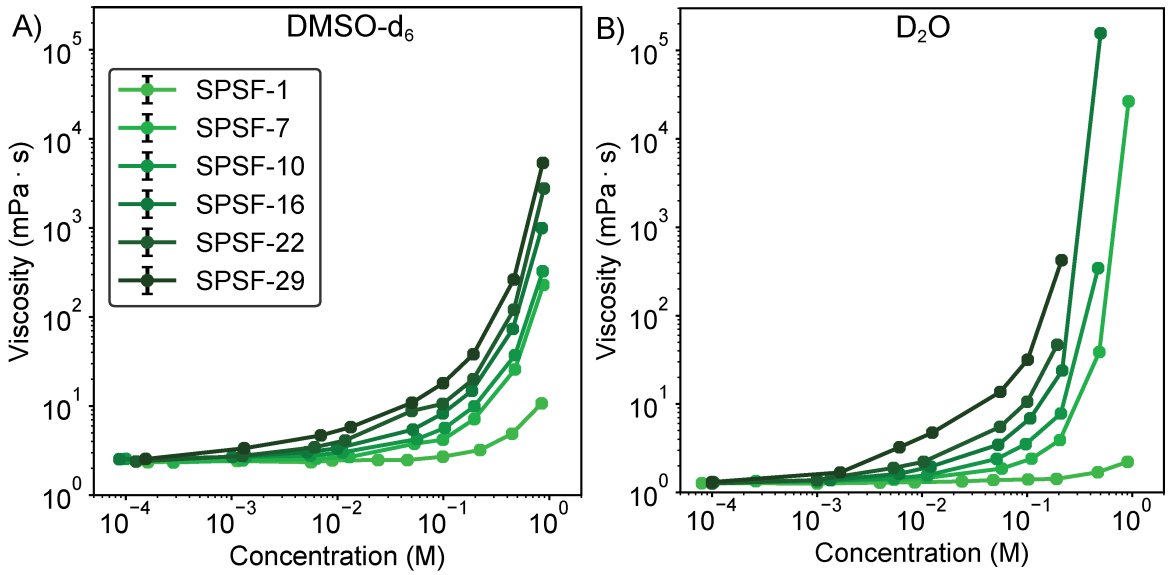

Figure 5.2. Viscosity as a function concentration in A) DMSO-d_6 and B) D_2O. The legend in A) also applies to B). The monomer (SPSF-1) is the lithium form sulfonated bis(4-chlorophenyl) sulfone. Reported concentrations are that of the Li^+ counterion.

The conductivity of the same solutions from Figure 5.2 is reported in Figure 5.3. The conductivity of high concentration D_2O samples for all but the monomer and SPSF-7 could not be consistently measured due a combination of evaporation and the highly viscous nature of these samples. Included on the same figures is the conductivity of the lithium-form sulfonated monomer. In DMSO-d_6 this is notably higher than the conductivity of the polyelectrolyte solutions, although the peak in conductivity occurs at the same concentration. In D_2O, however, the monomer is only marginally more conductive. Aside from the difference from the monomer to SPSF-7, there is no molecular weight dependence of the conductivity in D_2O, either.

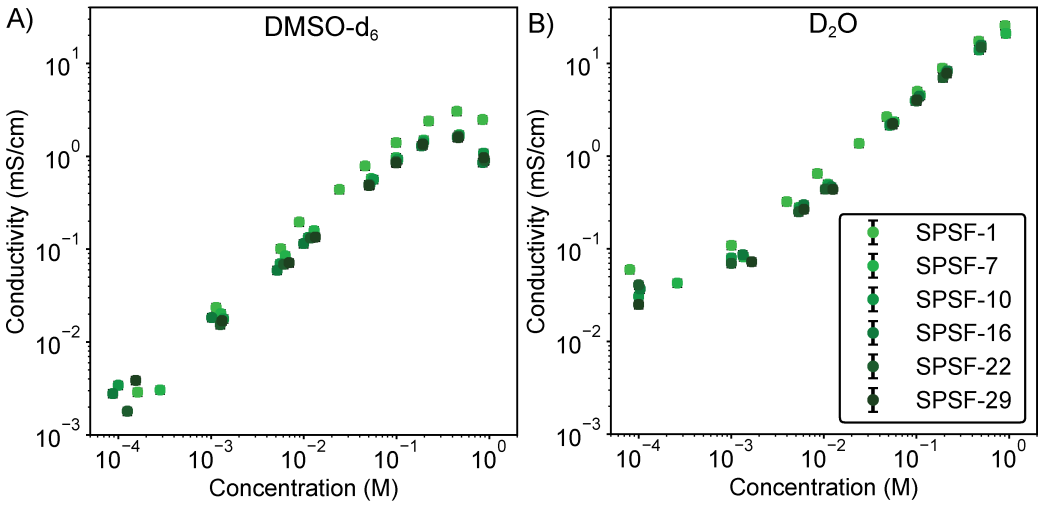

Figure 5.3. Conductivity as a function of concentration in A) DMSO-d_6 and B) D_2O. The legend in B) also applies to A).

Figure 5.4 overlays the diffusion coefficients for the solvent (residual protonated solvent), lithium, and polymer backbone for each polymer and the monomer. In both solutions, it is apparent that there is no molecular weight dependence in the diffusion of either the lithium or solvent, except at high concentration in DMSO-d_6 where the monomer solution has more rapid diffusion for both lithium and solvent. This is somewhat surprising given the vastly more viscous solution in D_2O at the same concentration. Polymer backbone diffusion coefficients in D_2O could only be measured at 0.5M for SPSF-7 and SPSF-10, while no backbone motion could be measured at 1M. At 1M, the backbone NMR peaks are extremely broad and barely visible, indicating minimal molecular reorientation within the NMR tube. Surprisingly, the lithium and solvent diffusion at this concentration was readily observable.

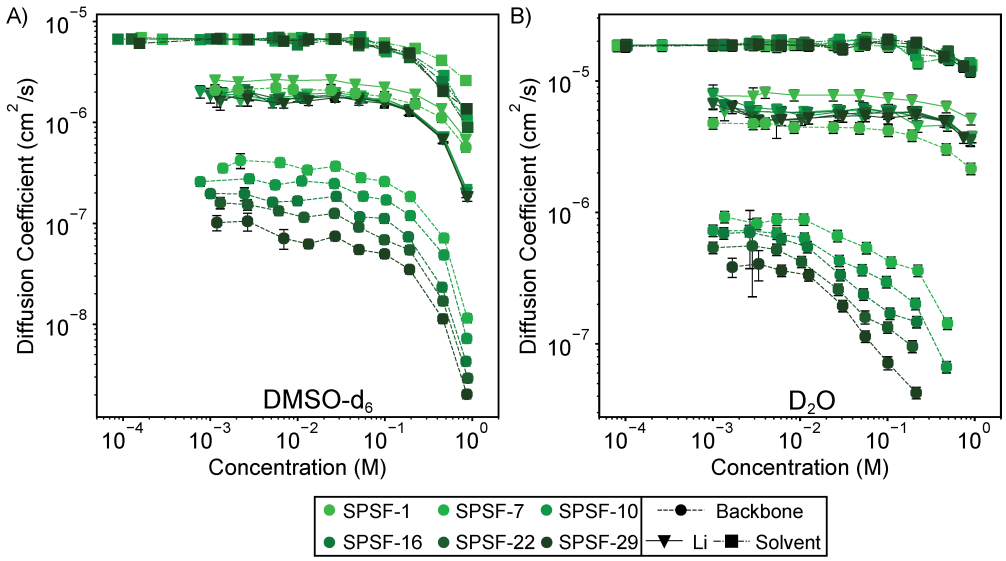

Figure 5.4. Diffusion coefficients, as measured using PFG-NMR, of the solvent, lithium, and backbone as a function of concentration in A) DMSO-d_6 and B) D_2O

V. Discussion

The data presented in the previous section will be discussed first in relation to common scaling arguments, followed by comparison of the polyelectrolyte data to the monomer data, and concluding with design suggestions for polyelectrolyte solutions in battery applications. Scaling theories have been used extensively to describe polyelectrolyte solutions, and thus it is informative to compare the existing literature to the data presented for this system. It should be noted that the short molecular weight of these polymers is well below that assumed for any theory discussed, although their behavior is clearly polymeric. We discuss first the scaling in good backbone solvent DMSO-d_6, followed by the poor backbone solvent D_2O. Conductivity is not expected to follow simple scaling exponent laws, so is not discussed in these scaling sections.[122]

i. Scaling in DMSO-d_6

Figure 5.5 displays the scaling behavior of the specific viscosity ($\frac{\eta-\eta_{solvent}}{\eta_{solvent}}$) as a function of concentration for the monomer and the longest and shortest polymer. The other polymers can be found in the supporting information section, Figure 5.17. Three regimes can be observed, likely corresponding to the semidilute, entangled, and highly concentrated regimes described by Rubinstein.[114] The crossover concentrations appear to be roughly 0.05M and 0.2M for all polymers, and the monomer. The scaling exponent, z, defined as $\eta_{specific} \sim c^z$, for each polymer and the monomer is shown in Figure 5.5D with error bars representing the standard error of the linear fit to the log-log plot. In the first regime, the polymers scale reasonably close to $\sim c^{1/2}$, the classic Fuoss law.[222] In the second, the scaling exponent increases, but does not reach the value of 1.5 predicted by Rubinstein or 1.7 predicted by Muthukumar.[114,115] In the final regime, the scaling exponent appears to increase slightly with molecular weight, approaching, but not reaching the exponent of 3.75 predicted by Rubinstein.

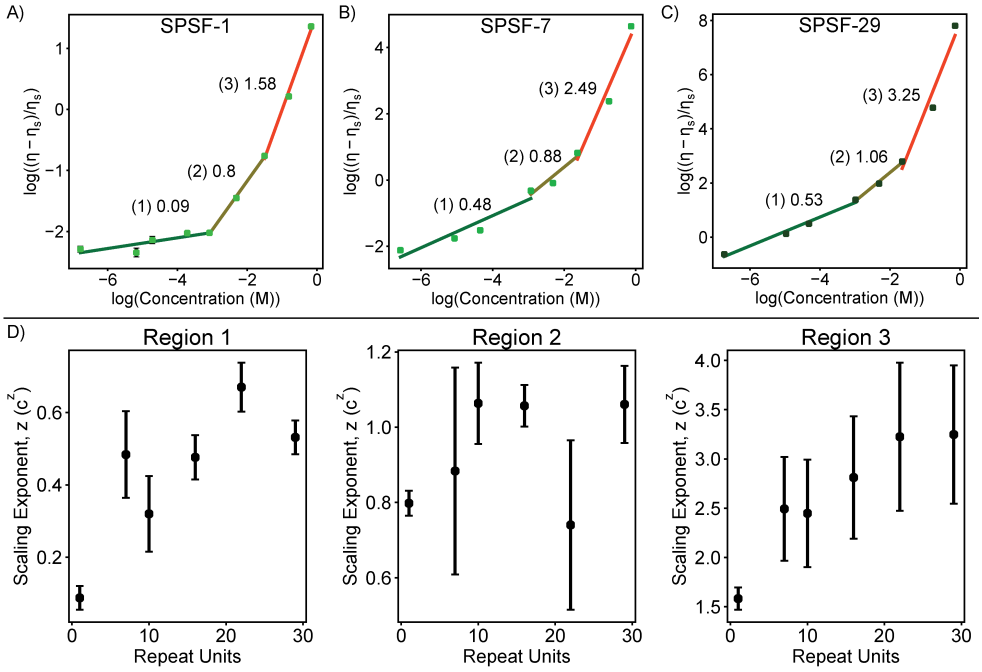

Figure 5.5. Scaling of specific viscosity with concentration for A) the monomer, B) shortest polymer, and C) longest polymer in DMSO-d_6. Numbers on the plot correspond to the slope of the fit line in that region. D) The scaling exponent (slope from A-C) plotted as a function of repeat units for each region.

Figure 5.6 plots the scaling of specific viscosity with N ($\eta_{specific} \sim N^a$), as a function of concentration. Here the monomer is excluded from the fit. In the semidilute range, the scaling exponent increases with concentration, reaching a steady value near 1.25 in the entangled regime. Past this, the exponent again increases. This behavior does not align with existing theory, where a constant value of 1 is expected in the semidilute range, increasing to 3.4 when entangled.[115] The very recent paper of Lopez and Richtering does, however, report an increasing scaling exponent with concentration for many different polymers.[223]

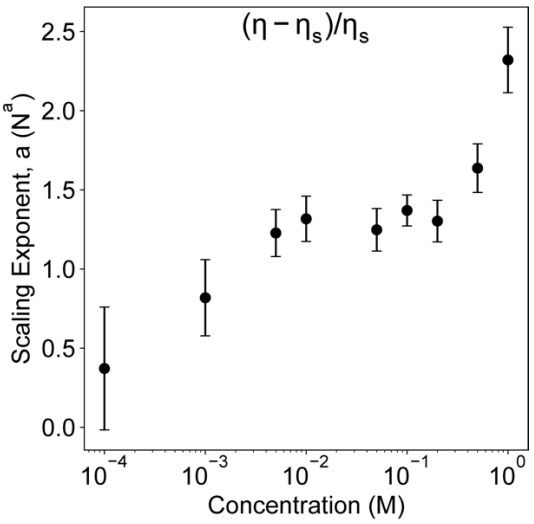

Figure 5.6. Scaling exponent of specific viscosity with molecular weight, as a function of concentration in DMSO-d_6

The regimes apparent in the viscosity data are also apparent in the backbone diffusion coefficient (D_b) data. Figure 5.7 summarizes the scaling of D_b in each regime, as a function of concentration and length. In the semidilute regime, the monomer has no concentration dependence, but the polyions have a slight negative scaling exponent. It is relatively well accepted that there should be no concentration dependence of D_b within the semidilute range, but it should be noted that the slight negative trend seen here is in fact quite similar to that observed originally by Oostwal.[224] Following this, the polyion diffusion decreases more rapidly, approaching the scaling value of -0.5 predicted by Rubinstein for the second regime, and closely aligning with the value of -1.75 in the most concentrated regime.[114] Except at the lowest and highest concentration, in Figure 5.8 the backbone diffusion scales very closely with the expected N^{-1}, although with a slightly more negative exponent. This slightly more negative value is in agreement with the viscosity scaling as slightly more than $\sim N^1$.

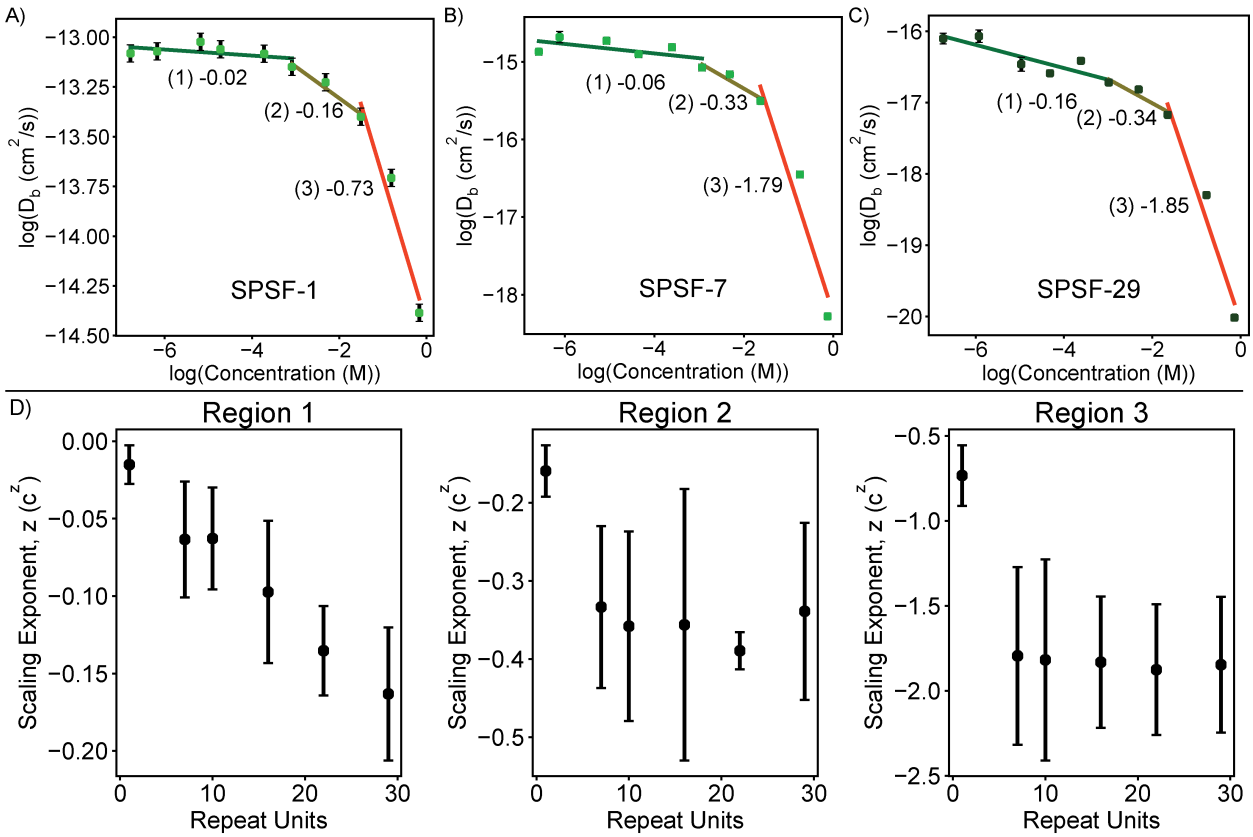

Figure 5.7. Scaling of backbone diffusion coefficient D_b with concentration for A) the monomer, B) shortest polymer, and C) longest polymer in DMSO-d_6. Numbers on the plot correspond to the slope of the fit line in that region. D) The scaling exponent (slope from A-C) plotted as a function of repeat units for each region.

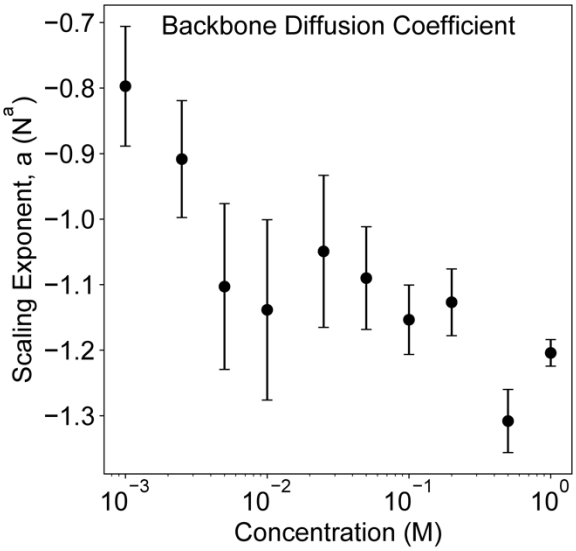

Figure 5.8. Scaling exponent of the backbone diffusion coefficient with molecular weight, as a function of concentration in DMSO-d_6.

The scaling of solvent (D_s) and lithium diffusion (D_{Li}) also follows the regimes described previously, as summarized in Figure 5.9. There are no explicit scaling exponent predictions for either the solvent or lithium diffusion in the literature, although qualitative comparison may be

made to the prior work. We note there is no dependence on molecular weight for the solvent and lithium diffusion in the polyion solutions, which can be clearly observed in Figure 5.4. In the semidilute range, both diffusion coefficients are independent of concentration (Figure 5.9C and D, first panel), while in the entangled regime they appear to scale as approximately $c^{-0.2}$ (Figure 5.9C and D, second panel). At higher concentration, solvent diffusion decreases less rapidly than lithium for all polymers and the monomer. This behavior at high concentration is reminiscent of that observed by Schipper, where normalizing the counterion diffusion to the solvent still produced a decrease in diffusion as concentration increased.[130] Within the semidilute regime, the solvent behavior matches that observed by Schipper, but the lithium behavior is qualitatively different. In their work a nonmonotonic dependence on concentration is observed, with a peak in diffusion coefficient just prior to the downturn at high concentration. The results presented here are in line with the coarse grain results of Chang and Yethiraj, who also noted the discrepancy of their results with Schipper.[132] They explained the difference as arising from different affinities of the counterion for the polyion, with more strongly coupled systems expected to show nonmonotonic behavior. For the system in this work, DMSO solvates lithium ions strongly, and thus weak coupling to the polyion would be expected. The results presented here also appear qualitatively similar to the predictions within some models for conductivity, although here concentration dependence is only expected in poor backbone solvent.[122]

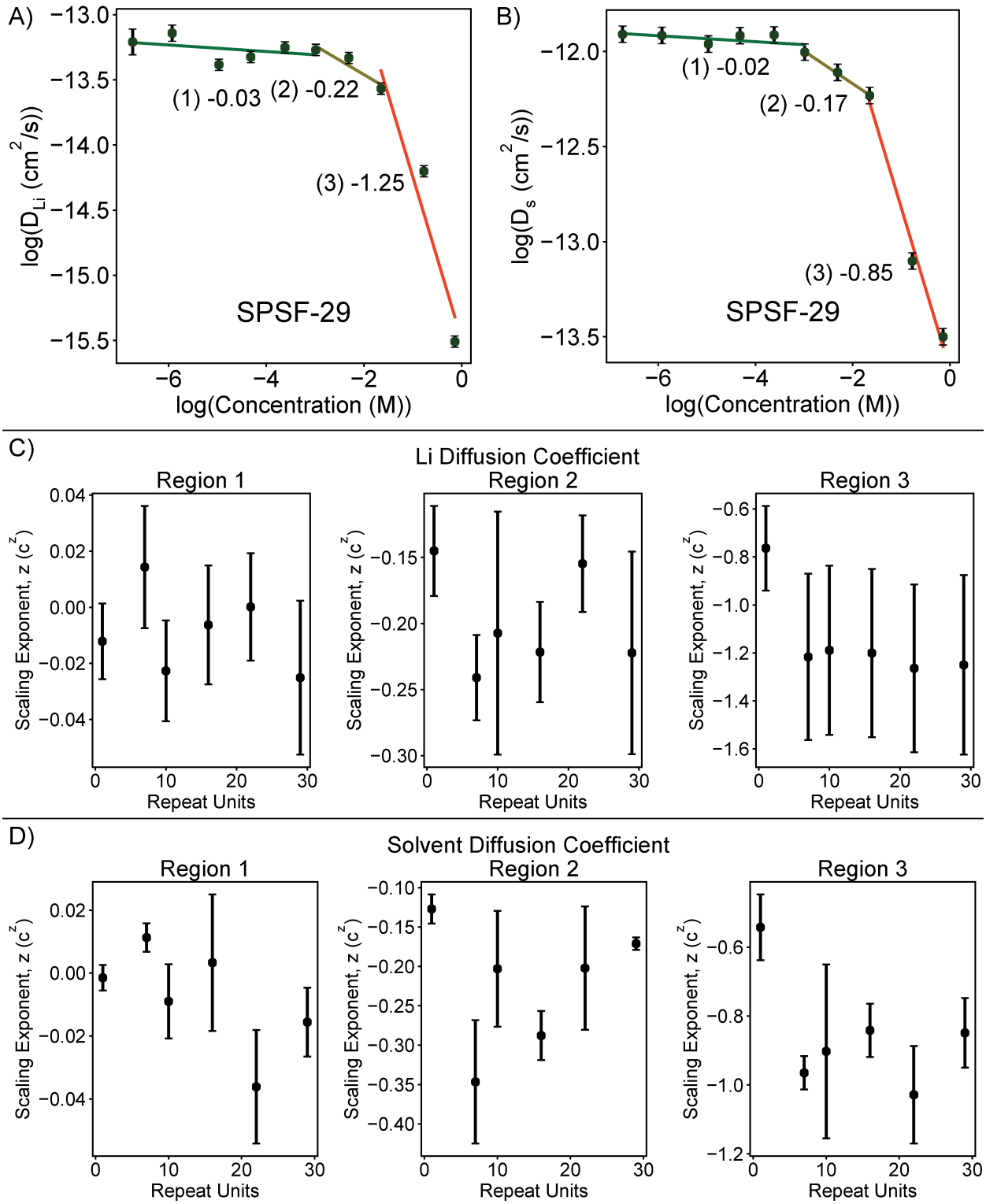

Figure 5.9. A) Scaling of the Li diffusion coefficient (D_{Li}) with concentration for the longest polymer in DMSO-d_6. B) Scaling of the solvent diffusion coefficient (D_S) with concentration for the longest polymer in DMSO-d_6. Numbers on the plot correspond to the slope of the fit line in that region. C) The scaling exponent for Li diffusion (slope from A) plotted as a function of repeat units for each region. D) The scaling exponent for solvent diffusion (slope from B) plotted as a function of repeat units for each region.

ii. Scaling in D_2O

The scaling behavior in the poor backbone solvent D_2O is generally more complex than that in DMSO-d_6 just described. Diffusion of the lithium and the solvent is not well described by a scaling analysis like that for DMSO. Figure 5.10 summarizes the concentration scaling of the backbone diffusion coefficient. The monomer exhibits the same three regimes, with the same transition concentrations as in DMSO. The first regime has a very slight concentration dependence, followed by a steeply decreasing diffusion coefficient. Compared to DMSO, the second and third regimes have scaling exponents approximately half as large. For the polymers, three regimes are also observed, but the transition from semidilute to entangled has shifted lower compared to DMSO-d_6 solutions to 0.01M. In the semidilute range, the polymer diffusion coefficient is very nearly independent of concentration, decreasing slightly more with concentration at the largest molecular weight. The scaling exponent in the second region becomes significantly more negative for the longest polymers, and is larger in magnitude than all of the polymers in DMSO. The third region is only observable in the two shortest polymers, with a steeper drop in diffusion than the second region, though not as steep as the drop in this region in DMSO. Figure 5.11 displays the scaling as a function of repeat units, with a significantly more negative exponent at higher concentrations.

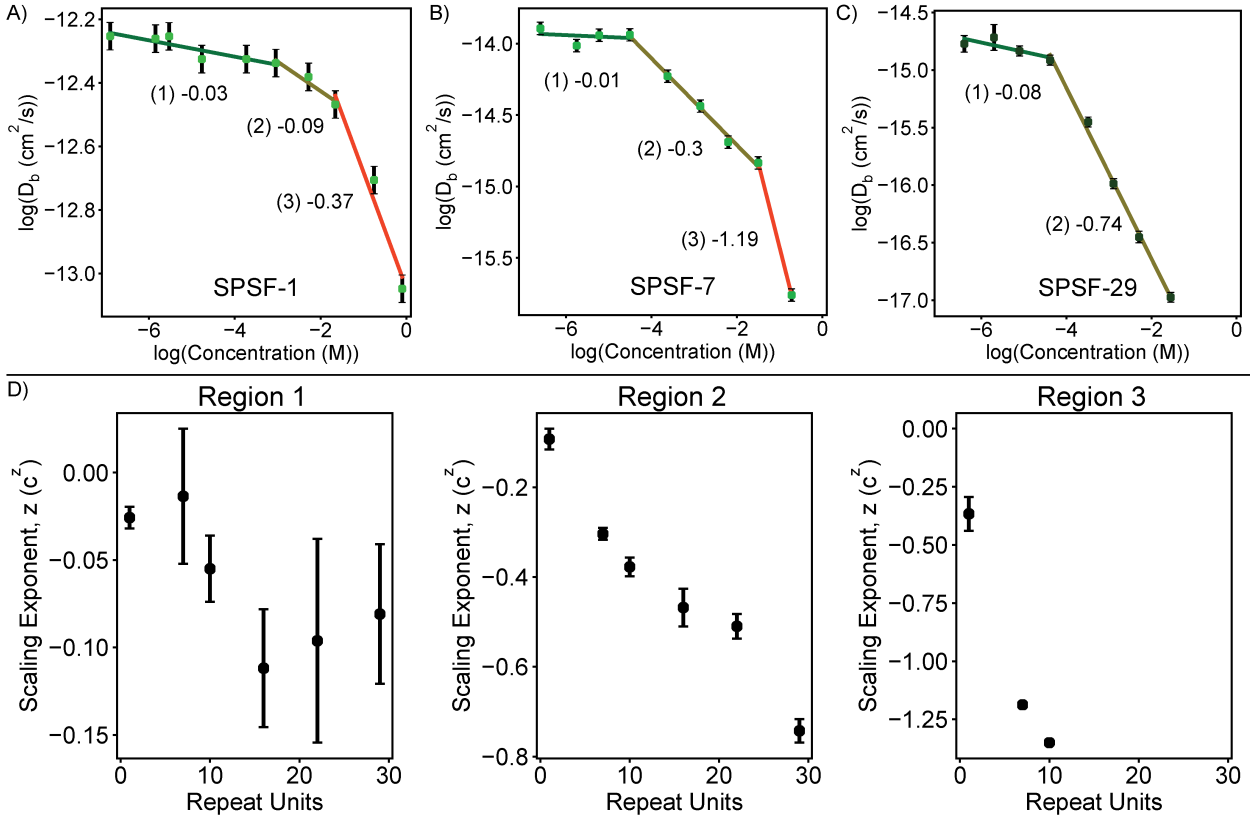

Figure 5.10. Scaling of backbone diffusion coefficient with concentration for A) the monomer, B) shortest polymer, and C) longest polymer in D_2O. Numbers on the plot correspond to the slope of the fit line in that region. D) The scaling exponent (slope from A-C) plotted as a function of repeat units for each region.

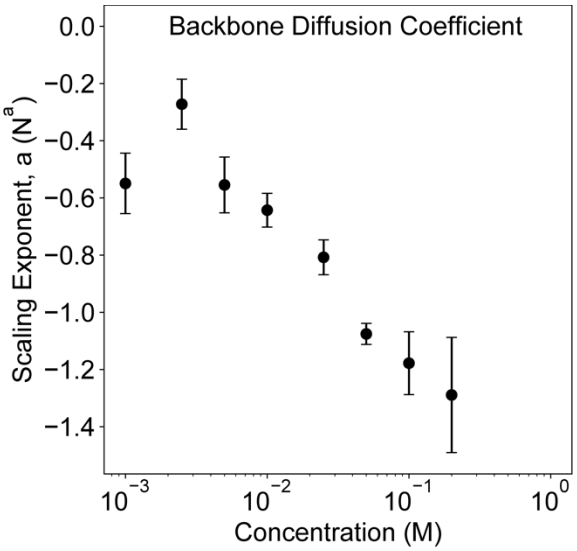

Figure 5.11. Scaling exponent of backbone diffusion with molecular weight, as a function of concentration in D_2O.

Figure 5.12 summarizes the scaling behavior of the specific viscosity for D_2O solutions. Here the regimes observed from the backbone diffusion coefficient analysis are used, although it is clear that the same regimes are not readily apparent here. For the monomer, only two regimes are seen, with a transition around 0.2M. For the polymers, the first region is well described by a power of concentration, but past 0.05M, the fit becomes poorer. In the first region, the scaling exponent increases with repeat units. The same is apparent in the two higher regions, indicating a more significant increase in viscosity as a function of concentration for longer polymers. As a function of length, Figure 5.13, specific viscosity scales more significantly at higher concentration. The scaling exponents in D_2O with concentration and polymer length do not follow the Fuoss law, or Dobrynin's model for hydrophobic polyelectrolytes.[218] Given that this model expects the polyelectrolyte to take on a bead string conformation containing significant microstructure, it is not surprising that this short polymer behaves significantly different.

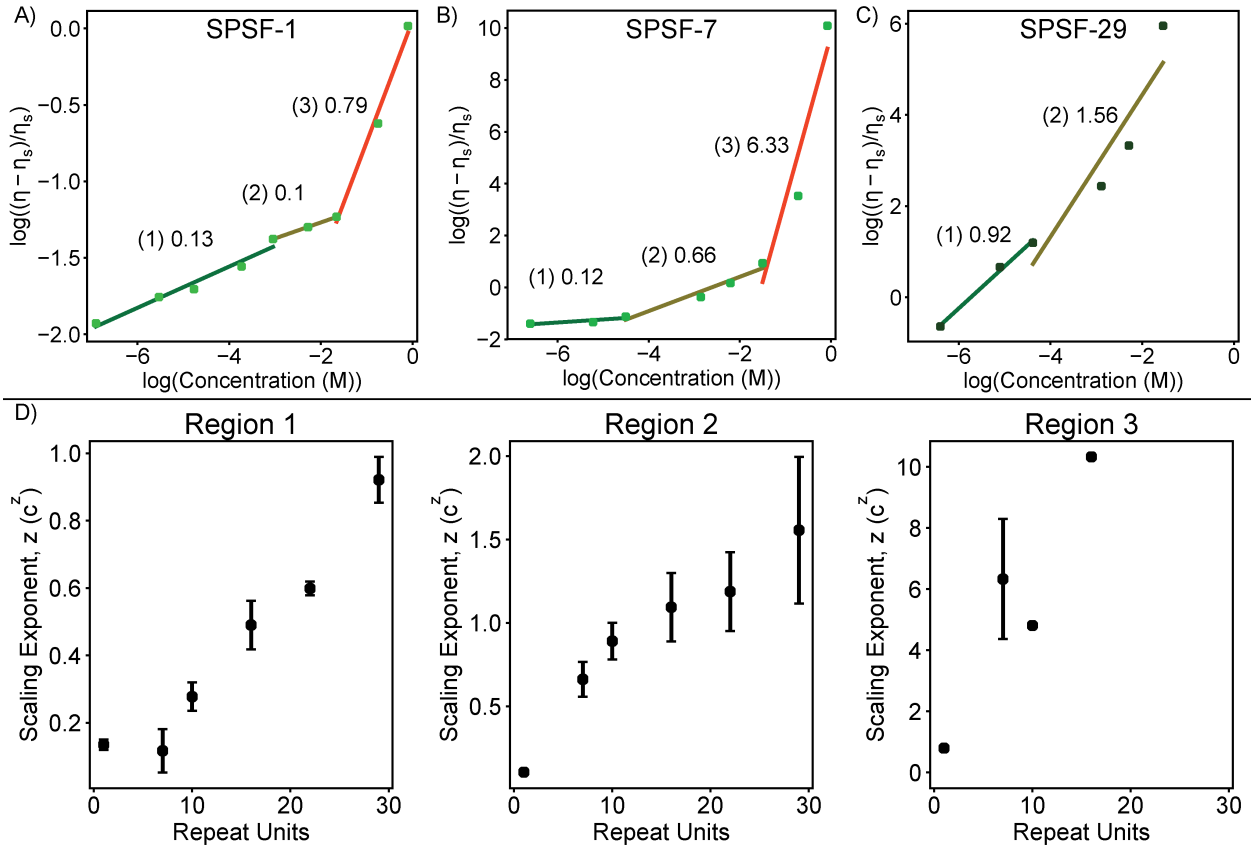

Figure 5.12. Scaling of specific viscosity with concentration for A) the monomer, B) shortest polymer, and C) longest polymer in D_2O. Numbers on the plot correspond to the slope of the fit line in that region. D) The scaling exponent (slope from A-C) plotted as a function of repeat units for each region.

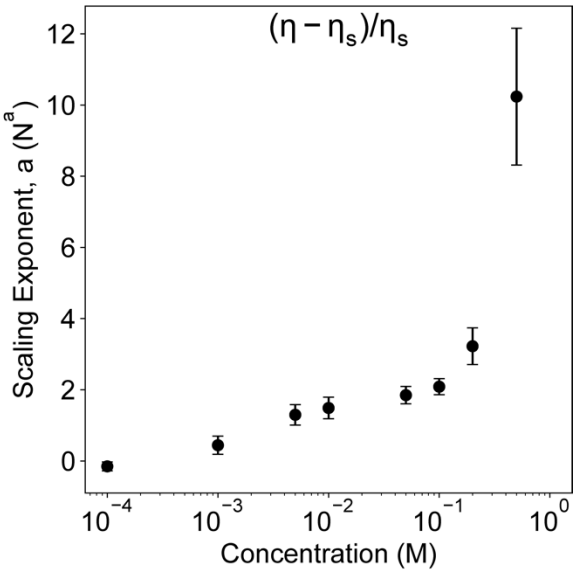

Figure 5.13. Scaling exponent of specific viscosity with molecular weight, as a function of concentration in D_2O.

iii. Comparison to Monomer

Figure 5.14 presents the diffusion coefficient of the solvent and the lithium in each polymer solution divided by the diffusion coefficient of the same species at the same concentration in the monomer solution. For the monomer, this produces a constant value of 1 (as indicated by the straight line on each plot). Deviations from this line in the polymer solutions must come from interactions fundamentally determined by the polymeric nature of the anion, as opposed to electrostatic interactions which the monomer also would have. In both DMSO-d_6 and D_2O solutions, regardless of concentration lithium diffuses slower in the polymer solutions than in the monomer solution (Figure 5.14B and D), likely due to a form of counterion condensation. The relative similarity of $D_{Li}/D_{Li_{monomer}}$ between the two solutions at all but the highest concentrations indicates counterion condensation is relatively similar in the two solvents over the majority of the concentration range. This is in contrast to the results of Smiatek, where condensation is observed to be higher in water than in DMSO for a similar sulfonated polysulfone.[143] For DMSO-d_6 at high concentration, both the solvent and lithium begin to diffuse at a slower rate than in the monomer solution, while in D_2O this is not apparent for either species. This behavior is particularly surprising when viewed in light of the viscosity data in Figure 5.2. For D_2O, the viscosity increases dramatically at high concentration, becoming a gel which barely flows. In DMSO-d_6, however, the solution remains liquid and the bulk viscosity is high, but not gel-like. It would seem that the opposite diffusion coefficient trends would be expected.

These high concentration results clearly suggest that both lithium and solvent more strongly interact with the polyion in DMSO-d_6 solutions than in D_2O. However, the simulation results of Smiatek indicate the opposite is more likely for the counterion. A potential explanation for this discrepancy is also mentioned in Smiatek's report, in that it was noted that counterion condensation in water fluctuated strongly while it did not in DMSO. Our group has recently noted that static analysis of counterions is insufficient to capture their full transport behavior.[225] Others have also noted the importance of dynamic counterion exchange between bound and free ions.[205] It is therefore reasonable to suggest a possible explanation for the difference between DMSO-d_6 and D_2O is that counterions exchange between bound and free states more rapidly in D_2O, allowing their motion over long range even when the polyion becomes entangled and stuck in place. A second hypothesis is that counterions condense significantly more at high concentration in DMSO-d_6 than they do in D_2O, but it is not clear why this would happen and others have suggested the opposite may happen as concentration increases in polyelectrolyte solutions.[226] A further possibility is that the increased affinity of DMSO for the polymer causes a decrease in solvent motion, which in turn is the cause of the decrease in lithium diffusion.

In Smiatek's simulation, the interaction of water and DMSO with the polymer is also studied, finding a stronger binding of DMSO than water to the polymer, though the cumulative number of the two solvents around the polyion is equivalent. This stronger binding of DMSO could explain the decrease in diffusion at high concentration, as the polymer backbone moves significantly more slowly than the monomer. This affinity must also account for the viscosity differences, since DMSO-d_6 solvation of the chain would prevent aggregation of either the charge groups or the polymer backbones. It is reasonable to suggest that the massive increase in viscosity for D_2O is the result of aggregation of the charge groups in clusters or channels where they may be solvated by water while the uncharged backbone is excluded, causing long range motion to slow dramatically. In DMSO-d_6 such phase segregation would not occur. Scattering would be necessary to confirm this, but other groups have noted gels at high concentration for similar

reasons.[227,228] Dobrynin and Rubinstein also described a "gel phase" at high concentrations corresponding to the overlap of necklace beads.[136] It has also been noted that transport in polyelectrolyte gels may be as fast as in solutions.[229]

The results in Figure 5.14 are also somewhat in conflict with the analysis of Schipper and Leyte, and the coarse grain simulations of Chang and Yethiraj. The diffusion trends in both papers mirror the data here, but in both cases the decrease in diffusion at higher concentration is explained by the volume occupied by the polymer, because at these concentrations the electrostatic interactions would be screened. If this were entirely the case, normalizing to the diffusion of the monomer would not entirely account for the decrease in diffusion in the water system. The sulfonated monomer is only half of the actual repeat unit of the polymer, and should therefore occupy less volume than the polymeric repeat unit. As a result, an electrostatic effect must still be important in describing these dynamics. The obstruction argument also would not fully account for the difference between DMSO and water. Simulation or additional theory would likely be required to fully explain the differences observed here.

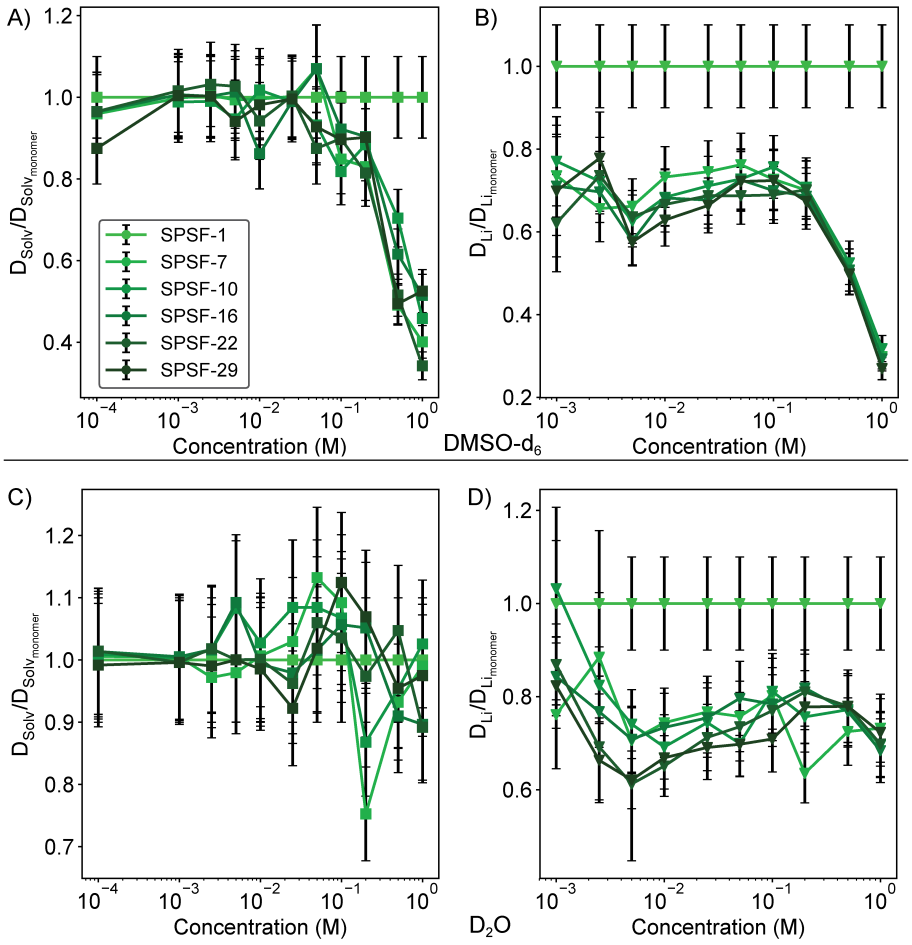

Figure 5.14. Diffusion coefficients of solvent (A and C) and lithium (B and D) normalized to the diffusion coefficient of the same species in the monomer solution for DMSO-d_6 (A and B) and D_2O (C and D). Diffusion in the monomer solutions appears as a straight line at 1 on these plots.

iv. Polyelectrolyte Solution Design

This study can inform the design of high transference number polyelectrolyte solutions for lithium batteries in several ways. Figure 5.15 plots the transport number calculated from NMR diffusion coefficients using equation 5.3.

$$t_{+,NMR} = \frac{D_{Li}}{D_{Li} + 2ND_{backbone}} \qquad 5.3$$

While this equation is not equivalent to the true electrochemical transference number, our group has recently found reasonable agreement between $t_{+,NMR}$ and simulated true transference numbers for polyelectrolyte solutions.[225] A wide range of transport numbers are clearly accessible with this system. The transport number of the monomer is relatively insensitive to concentration, being consistently around 0.4. The polyion solutions, however, have an increasing transport number as a function of concentration. In DMSO-d_6, this is mostly not a function of molecular weight, although the longest polymer consistently has the highest transport number, and at the two highest concentrations studied there is more of a trend towards increasing transport number with repeat units. In D_2O the trend of transport number with molecular weight flips from being negative at low concentration, to positive at high concentration. It should be noted that the transport number is actually 1 for the samples that have gelled, as the diffusion coefficient of the backbone in those samples is essentially 0.

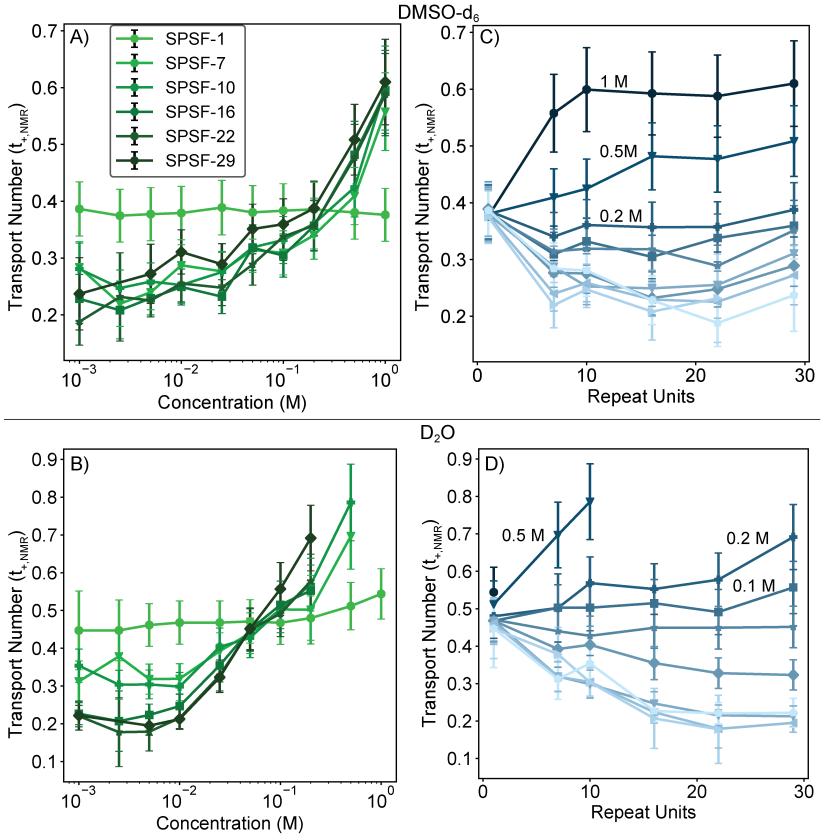

Figure 5.15. Transport number defined in Equation 5.3 in DMSO-d_6 (A and C), and D_2O (B and D). Darker color in C) and D) corresponds to higher concentration. The legend in A) also applies to B). Error bars are propagated from the diffusion measurement.

In Figure 5.16 the transport number is used to calculate the fraction of conductivity that arises from lithium as $\sigma_{Li} = \sigma t_{+_{NMR}}$. Points where σ_{Li} is calculated from an assumed $t_{+_{NMR}}$ of 1 (due to the negligible backbone diffusion) are circled on the figure. This has been suggested as the best parameter to optimize in electrolyte design, as it combines the conductivity and transference number, both of which must be maximized.[230] In DMSO-d_6, the monomer has the highest lithium conductivity over the entire concentration range, while in D_2O the polyelectrolyte solutions have higher lithium conductivity, the difference increasing as a function of molecular weight and concentration. In D_2O it should also be noted that the maximum in conductivity has not yet been reached for any of the studied molecular weights, despite the gelation of samples at this concentration.

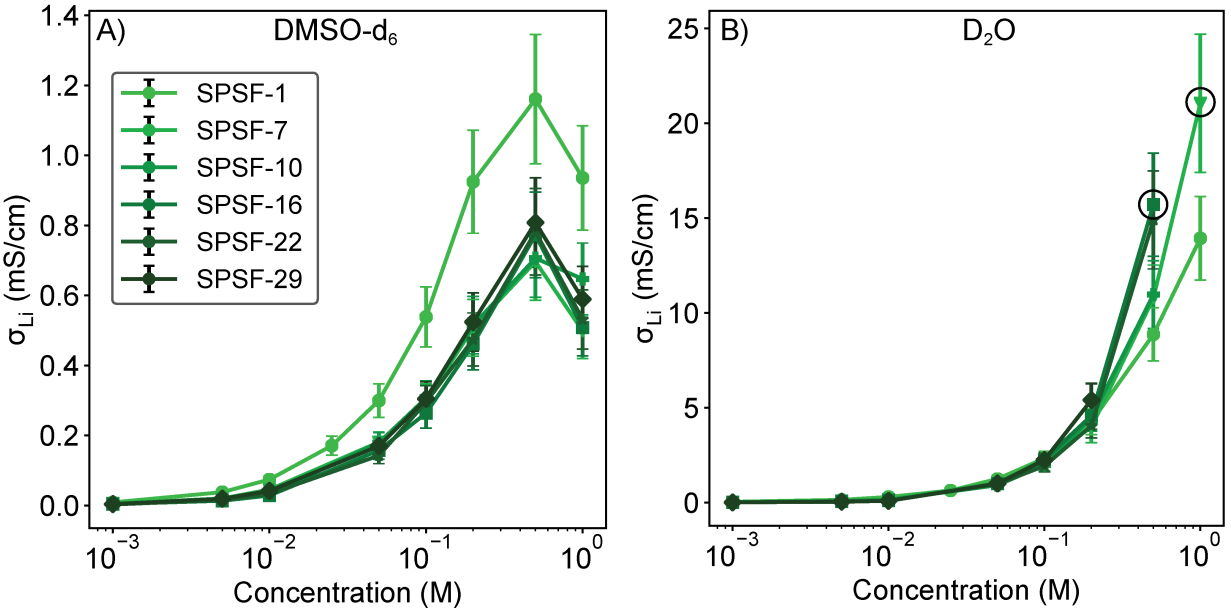

Figure 5.16. Lithium conductivity as a function of concentration for A) DMSO-d_6 and B) D_2O. Points in B) that are circled use an estimated t_{+NMR} of 1 to calculate σ_{Li}

Together, these observations lead to several design recommendations. For a polyelectrolyte in good solvent conditions it is clear that higher transference number is obtained at higher concentration, and that there is only a weak dependence of t_+ on molecular weight. Thus, in good solvent conditions, oligomeric anions could provide the high transference numbers desired, without creating impractically high viscosity. In poor solvent conditions, the highest transference numbers occur in systems that have gelled, effectively coinciding with swollen membranes, although without chemical crosslinking. There have been several studies suggesting in-situ polymerization and crosslinking of membranes as a facile means to create a porous, membrane-containing electrode.[92] Here it is apparent that crosslinking and polymerization may not be necessary, simply evaporating solvent from a polyelectrolyte solution may produce a gel. Prior to the point of gelation, the samples in poor solvent conditions also appear to have a higher transference number as a result of the more strongly negative scaling of the backbone diffusion over a wider range.

The strong concentration dependence of transport number in the polyelectrolyte system is also an interesting point that has not been considered previously. It is not clear how this might impact the formation of concentration gradients in a battery, as most salts are relatively consistent

in anion mobility being higher than cation. Superconcentrated electrolytes do demonstrate some concentration dependence of t_+, but this is not an effect that has been considered from a performance standpoint.[102] An interesting analogy to systems with inherent shutoffs may be drawn, where perhaps the polyelectrolyte solution under a high concentration gradient may provide a spatially varying transference number which either further hinders transport (perhaps providing an inherent shutoff point under extreme conditions) or helps transport by mitigating concentration gradients more strongly with more extreme concentrations.

VI. Summary and Future Work

In this chapter, the transport properties of a sulfonated polysulfone polyelectrolyte solution have been characterized over a range of molecular weights and concentrations for both good and poor solvent conditions. The scaling behavior of these solutions was found to agree in part with many of the existing polyelectrolyte theories, despite not satisfying many of the underlying assumptions (particularly for molecular size). Better agreement was found for the good solvent case, which might be expected given that the poor solvent theories generally assume complex polymer structures that could not be formed in short chains. Comparison of the diffusion coefficients of the lithium and solvent with the same parameters for the solution with the monomer alone found surprising differences from the existing understanding of counterion transport. It is apparent that the higher affinity of the solvent for the polymer backbone in DMSO-d_6 causes a larger decrease in solvent diffusion at higher concentration. Scattering experiments, or more complete rheological characterization, are suggested as means to understand the larger decrease in lithium diffusion at high concentration in the DMSO-d_6 solutions. The transport number of the polyelectrolyte solutions was also determined from the NMR data, suggesting several design recommendations for future polyelectrolyte solutions. Future work in electrophoretic NMR to determine true mobilities as opposed to those estimated from diffusion, combined with simulation of batteries with varying transport properties are likely to provide the most useful information for future design of polyelectrolyte solutions for battery application. The results shown here also raise questions about the transition from polyelectrolyte solution to gel; future work in higher concentration, good solvent systems may provide an interesting comparison.

VII. Supporting Information

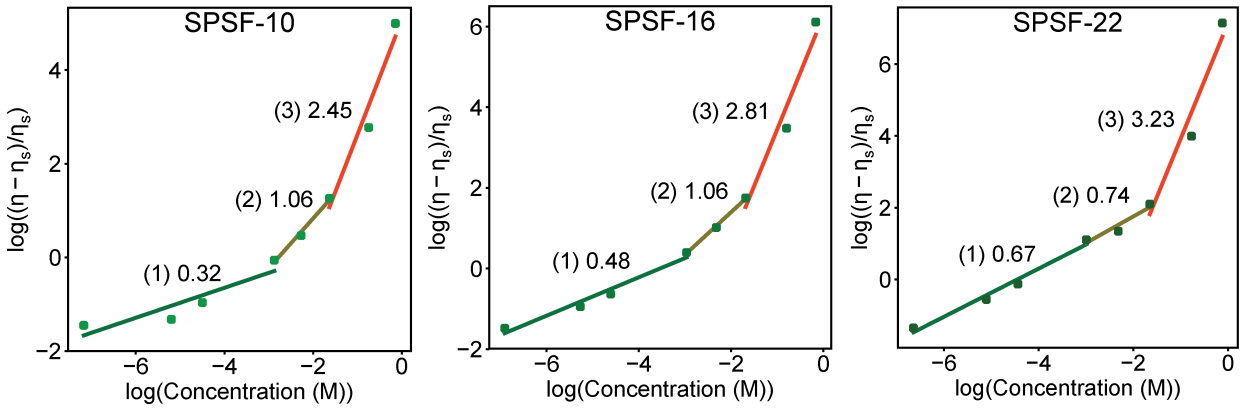

Figure 5.17. Specific viscosity scaling as a function of concentration in DMSO-d_6 for the three polymers not shown in the main text.

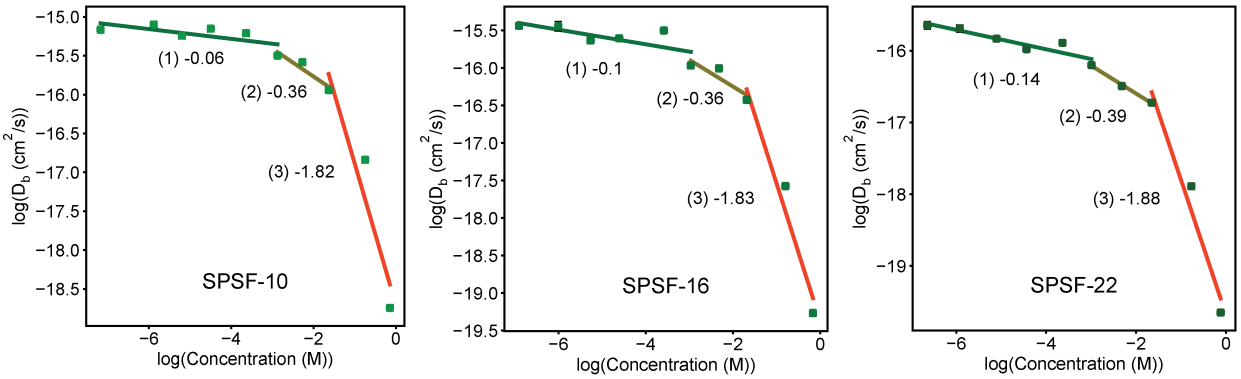

Figure 5.18. Scaling of backbone diffusion coefficient as a function of concentration in DMSO-d_6 for the three polymers not shown in the main text.

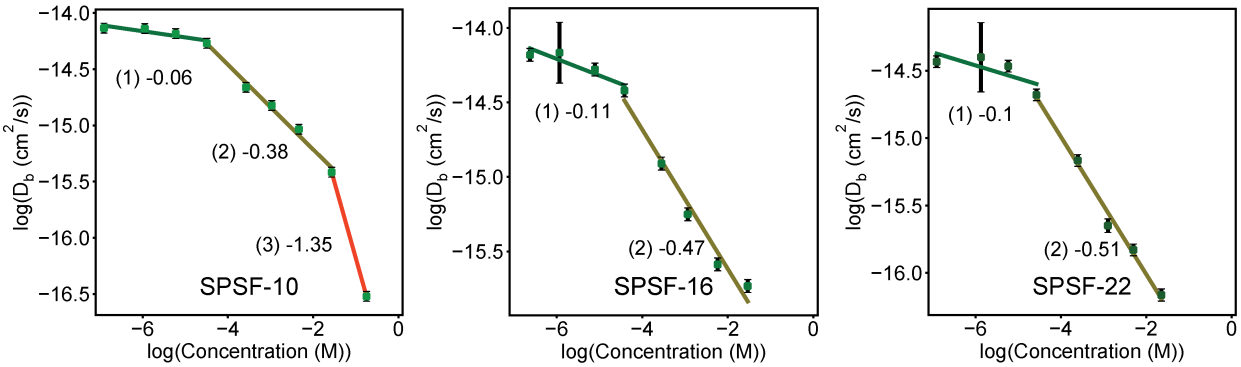

Figure 5.19. Scaling of backbone diffusion coefficient as a function of concentration in D_2O for the three polymers not shown in the main text.

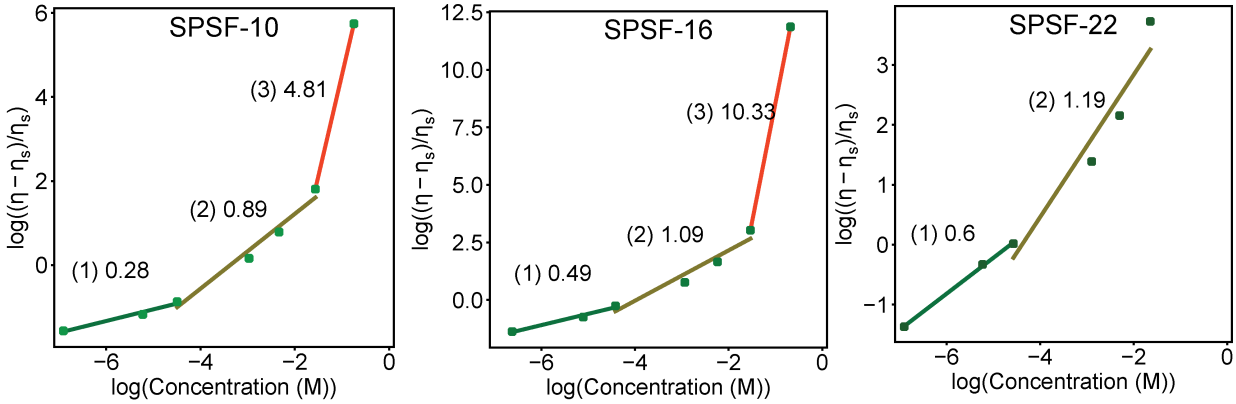

Figure 5.20. Scaling of specific viscosity as a function of concentration in D_2O for the three polymers not shown in the main text.

6. Electrolyte Additives to Enable Nonaqueous Polyelectrolyte Solutions for Lithium Ion Batteries[††]

I. Abstract

Nonaqueous polyelectrolyte solutions, in which a negatively charged macromolecule neutralized by lithium is dissolved in nonaqueous solvents, have shown promise as potential high transference number electrolytes. However, in battery-relevant carbonate solvents (ethylene carbonate/dimethyl carbonate blends), it has been shown that lithium ions do not readily dissociate from easily synthesized sulfonated polymers, despite the solvent's high dielectric constant (~50). In this work, a range of additives are screened to improve conductivity, and we demonstrate that the addition of less than 5 vol% of 15-crown-5 achieves an order of magnitude conductivity increase by selectively improving lithium dissociation. Utilizing the optimized electrolyte, we show that polyelectrolyte solutions may be directly substituted for a standard electrolyte with commercial electrodes in a graphite/$LiFePO_4$ cell, providing further motivation for future study of these new electrolytes.

II. Introduction

Lithium-ion battery electrolytes have been engineered extensively to have high conductivity and form a stable, Li^+-conductive passivation layer on the graphite electrode surface. A key remaining challenge in these electrolytes, however, is engineering control over the relative motion of anions to cations. Lithium is the electroactive species within the battery, but in all commercial electrolytes to date the anion is in fact more mobile than the lithium. This discrepancy is captured by the low cation transference number (t_+) of the electrolyte, defined as the fraction of the total conductivity that arises due to lithium motion in the absence of any concentration gradient.[12] It has been shown that battery rate capability and energy density could be improved with a high t_+ electrolyte (HTNE), even if the total conductivity is reduced relative to the standard electrolyte.[17,18]

Recently, nonaqueous polyelectrolyte solutions, in which a lithium-neutralized negatively charged polymer is fully dissolved in a solvent, have been proposed as potential HTNE's due to the bulky nature of the polyanion.[18,103,105,213] These solutions have been investigated extensively in water due to their relevance to biological systems,[106,112] but significantly less effort has been expended for nonaqueous polyelectrolyte solutions.[140] For a battery application, the preferred solvent is a blend of ethylene carbonate (EC) and a linear carbonate like dimethyl carbonate (DMC). EC has a high dielectric constant and degrades into a stable graphite electrode passivation layer, while DMC is added to reduce the electrolyte melting temperature and lower the viscosity.[15] In the previous chapter, a model sulfonated polysulfone/poly(ethylene glycol) copolymer in this solvent was investigated and it was found that sulfonate groups on the polymer do not readily dissociate in the battery-relevant solvent, leading to very low conductivity when compared with a similar dielectric constant solvent that has been studied more frequently with polyelectrolytes, dimethylsulfoxide (DMSO).[213]

In this chapter, we investigate the possibility of using additives to enable dissociation of the lithium from the sulfonate group within the desired EC/DMC solvent. Additives are key to the performance of all current battery electrolytes, and have been studied extensively both as transport

[††] This chapter was published in *Molecular Systems Design and Engineering*. It is adapted with permission from co-author B.D. McCloskey.[241]

enhancers and for stability.[5,231] Doyle in 2001 studied the possibility of using additives to enable higher conductivity in charged polymer membranes for battery applications, but we know of no study which has ever investigated additives for nonaqueous polyelectrolyte solutions, particularly with the goal of improving lithium ion dissociation and transport.[99] Here we show that preferential lithium binding solvents, particularly crown ethers, are a promising means to enable lithium dissociation from sulfonate groups in EC/DMC, allowing fabrication of a full battery from commercially available electrodes.

III. Experimental Section

i. Materials

Battery grade ethylene carbonate, dimethyl carbonate, lithium bis(trifluoromethylsulfonimide), and tetraglyme were purchased from BASF and used as received. Fluorinated ethylene carbonate was kindly provided by Daikin, and all other additives were purchased from Sigma Aldrich and used as received. The polymer used in this study is a second batch of the polymer used in our prior work and the synthesis and characterization is described there.[213] The structure of the polymer is shown in Scheme 6.1, along with NMR characterization. The peaks noted as A, B, C contain several peaks due to the different possible neighbor monomers and the slight shift that results from these different neighbors. The same is true for the PEG peak, where the peaks noted as "PEG ends" correspond to the PEG monomers at the end of the chain, within the copolymer. The presence of these peaks verifies the incorporation of PEG into the main polymer backbone. This NMR was taken after drying the polymer, and the very small H_2O residual peak (equivalent to the residual H_2O in DMSO-d_6) confirms the polymer is in fact dry. This batch of the polymer has M_n=6.7kDa and a dispersity of 1.6 as measured against poly(ethylene oxide) standards (Sigma Aldrich) in an Agilent 1150 Series GPC with Waters Styragel HR3 and HR4 columns and NMP with 0.05M LiBr as the mobile phase.

Scheme 6.1. Structure of the polymer used in this study, and ^{1}H NMR analysis of the polymer structure. The R group is ~10 mol% of the fluorinated monomer, as a tag for backbone diffusion measurement via ^{19}F NMR.

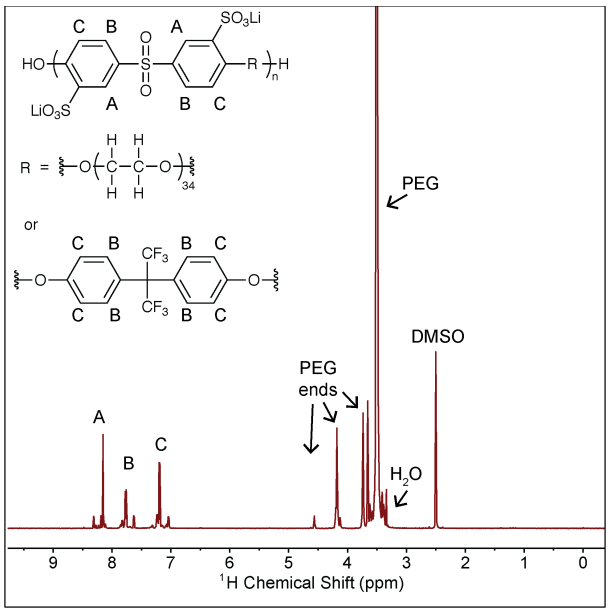

ii. Solution Characterization

Conductivity was measured using a Mettler Toledo InLab 751-4mm conductivity probe in vials kept at 25°C by a dry heating/cooling block inside of an argon glovebox kept below 1ppm water and 10ppm oxygen (Vac Atmospheres). The conductivity probe was calibrated to known standards (Mettler Toledo) at 84 μS/cm, 1413 μS/cm and 12.88 mS/cm. Viscosity was measured with an electromagnetically spinning viscometer (EMS-1000, Kyoto Instruments) using a 2mm aluminum ball at a rotation rate of 1000 rpm and 25°C after the tube was sealed in the glovebox. Error on conductivity is estimated from several repeat measurements on separate samples to be around 10%. Viscosity error bars are taken from 10 repeat measurements of each individual sample.

iii. Nuclear magnetic resonance spectroscopy (NMR) measurements

Diffusion coefficients of each species were measured by pulse field gradient NMR on a Bruker Avance III 500 MHz instrument fitted with a 5mm Z-gradient broadband probe and variable temperature unit maintained at 25°C throughout the measurement. The gradient was calibrated to known values of H_2O in D_2O,[198] H-DMSO in d_6-DMSO,[199] 0.25M LiCl in H_2O,[198] and 4M LiCl in H_2O.[198] A recycle delay of at least $4xT_1$ was utilized for all measurements. Bruker's double stimulated bipolar gradient pulse sequence (dstebpgp3s) was used for all measurements to account for any convection. The signal decay as a function of gradient strength was fit to Equation 6.1, which includes adjustments for a slight change introduced to the pulse program in TopSpin 3.0, as compared with the original paper.[200,202]

$$\frac{I}{I_0} = e^{-\gamma^2 g^2 \delta^2 D\left(\Delta - \frac{5\delta}{3} - 3\tau\right)} \qquad 6.1$$

Here γ is the gyromagnetic ratio, g is the gradient strength, δ is the gradient pulse duration (between 0.1 and 0.2 seconds), D is the diffusion coefficient, Δ is the diffusion delay (between 1 and 3 milliseconds), and τ is the delay for gradient recovery (5 milliseconds). ^{7}Li chemical shift was referenced by adding a flame-sealed melting point capillary filled with 9.7m LiCl in D_2O to the NMR tube after the diffusion measurement.[232] The location of the peak was recorded, and the original ^{7}Li spectra prior to adding the capillary was adjusted to the same location.

iv. Coin Cell Preparation

Graphite (2.64 mAh/cm^2) and $LiFePO_4$ (1.52 mAh/cm^2) electrode sheets were purchased from MTI Corp. and punched to 1.5 cm diameter electrodes inside of an argon glovebox (Vac Atmospheres). These were assembled into a CR2032 coin cell with a quartz fiber (Whatman) separator and 200 μL of the electrolyte of interest. The electrolyte was dropped onto each electrode and the separator was fully soaked before being stacked and crimped closed. The cells were allowed to rest for 12 hours, before cycling at C/20 (0.076 mA/cm^2). 3.8 and 2.0V cutoffs were chosen for charge and discharge, respectively.

IV. Results and Discussion

We select and screen several potential additives to promote lithium dissociation in Figure 6.1. For this screening study, the control solution is 0.1M of the sulfonated polysulfone – co – poly(ethylene glycol) shown in Scheme 6.1. This concentration represents the maximum in conductivity for this polymer in EC/DMC, and the 2:1 ratio is selected due to issues with

crystallization of EC at higher EC contents. Candidate additives are introduced at an equivalent molar ratio of lithium to additive for comparison here. Also shown is the addition of lithium bis(trifluoromethylsulfonimide) (LiTFSI), which was included in our previous study. As shown there, this solution has a conductivity roughly the same as the salt without polymer. The viscosity of the pure polymer solution reported here is lower than the same concentration solution with the previous batch of polymer. This could either be due to slightly lower molecular weight (6.7 kDa vs 8.5 kDa), or perhaps a different order of repeat units that is not easily characterized. The decrease in viscosity with added LiTFSI is reproduced here, though. Representative additives were selected that had a high donor number (DMSO),[233] could coordinate to metal ions (imidazole),[234] or had ether functionality (tetraglyme). Each of these additives indeed improves solution conductivity with minimal viscosity change, but not significantly. Stabilizing additives, vinylene carbonate[235] and fluoroethylene carbonate,[236] have a negligible effect on the conductivity or viscosity. Crown ethers are shown here to have the most impact on the conductivity, again with relatively minimal change in viscosity. The specific crown ethers chosen here are the same previously studied by Doyle,[99] with the addition of dibenzo 24-crown-8 which is a commercially available crown of larger ring size. The magnitude of this impact is particularly apparent in comparison to dioxane and tetraglyme, which have similar functionality, and even water.

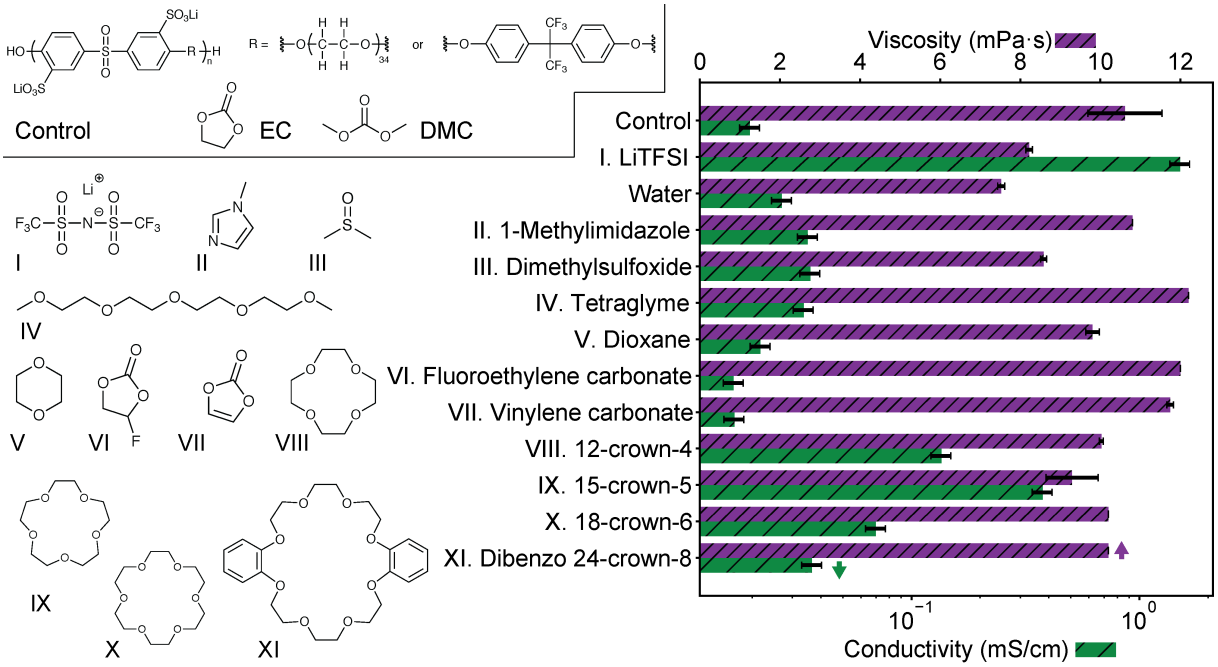

Figure 6.1. Conductivity and viscosity of a range of potential additives to improve conductivity of the control 0.1M polymer in 2:1(vol.) EC:DMC solution. Each additive is introduced at 0.1M, to match the lithium content of the solution. The structure of the polymer, EC and DMC in the control solution are also included.

The trend in conductivity with crown ether size (15-crown-5 > 12-crown-4 > 18-crown-6 > 24-crown-8) mirrors the trend observed by Doyle for EC/DMC swollen Nafion membranes with added crown ether.[99] The close size match of the cavity formed by each crown and the metal ion is likely the cause of this trend as it has long been known that different metal ions bind preferentially to different crown ethers.[237] This is further supported by past calorimetric measurements of crown ether complexation with lithium in several different solvents, which quantify the strength of binding. These measurements correspond directly to the trend in conductivity observed here, with 15-crown-5 having the strongest interaction.[238] As conductivity

must arise from charged species, this suggests addition of crown ether allows lithium to dissociate from the sulfonate group in solution, and the more strongly coordinated species provides a greater degree of dissociation. This ability to improve dissociation and solubility was recognized for battery electrolytes before,[239] but in these cases addition of crown tends to ultimately be detrimental to transport because the lithium/crown complex is bulkier than simply lithium/solvent, lowering the transference number.[15] This is significantly different than the poorly dissociated polyelectrolyte solution case, where the alternative to a crown/lithium complex is coordination with a very bulky slow-moving polymer. Importantly, crown ether additive has not been noted to change electrolyte stability significantly, having been used in the past to enhance the solid interface in PC electrolytes, and appearing to have similar stability as poly(ethylene oxide).[15,240]

In Figure 6.2 we examine the effect of 15-crown-5 (the additive that provided the highest conductivity in our initial additive screening) concentration on the solution conductivity and viscosity. Furthermore, we quantify the influence of water on these measurements given its strong solvation properties (high dielectric constant and Lewis acidity), and its ubiquitous presence as an impurity in nonaqueous solvents. These solutions were prepared by diluting a higher concentration solution to 0.1M Li^+ either by adding EC/DMC or additive, keeping the Li^+ concentration constant. In Figure 6.2A, a clear maximum in conductivity appears near ~4 vol% crown ether, corresponding to a crown to lithium ratio of 2. This conductivity is significantly higher than that observed for a similar ratio of water to lithium (Figure 6.2B). A similar conductivity with water as the additive is not achieved until a much higher water volume. As the amount of crown ether in the solvent increases, conductivity begins to decrease. This could be a result of the slight increase in viscosity at higher concentration (the viscosity of 15-crown-5 alone is 22 mPa·s) or result from the formation of larger solvation structures in solution, such as a single ion with two crown ethers.

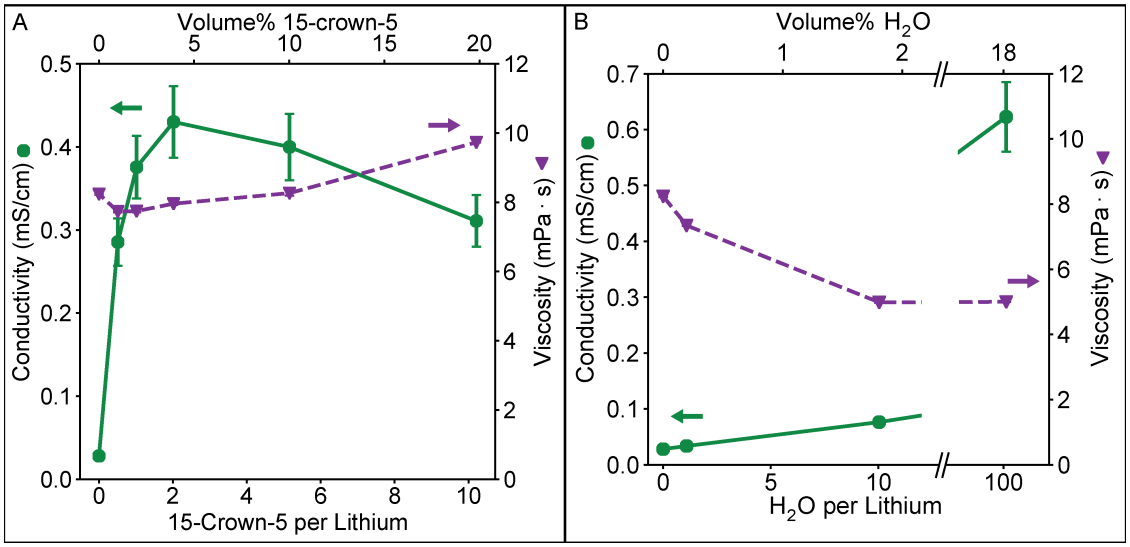

Figure 6.2. Conductivity and viscosity as a function of A) 15-crown-5 content and B) water content in a 0.1M polymer in 2:1(vol.) EC:DMC solution. The total lithium concentration is maintained constant in each solution by diluting from a higher concentration with either 15-crown-5, water, or EC/DMC. Viscosity error bars taken from repeat measurements of the same sample are smaller than the data points in this plot.

The local solution structure and diffusion coefficients of the solution constituents are probed directly through NMR measurements summarized in Figure 6.3. In Figure 6.3A, diffusion coefficients measured through pulse field gradient NMR of EC, lithium, and the polymer backbone clearly demonstrate that the increase in conductivity observed in Figure 6.2A are due to changes

in lithium motion alone. Diffusion coefficients for DMC and the crown ether could not be measured independently as their ^{1}H NMR peaks overlap. The polymer backbone diffusion coefficient is measured via ^{19}F NMR. It should be noted that the lithium diffusion coefficient measured by this technique averages all lithium species in solution. The trend in lithium diffusion coefficient directly aligns with the trend in conductivity in Figure 6.2A, with a maximum in diffusion coefficient observed at 2 crowns per lithium. At higher crown content the decrease in lithium diffusion can be explained by the slight increase in bulk solution viscosity, as the relative decrease in EC diffusion is equivalent to the decrease in lithium diffusion.

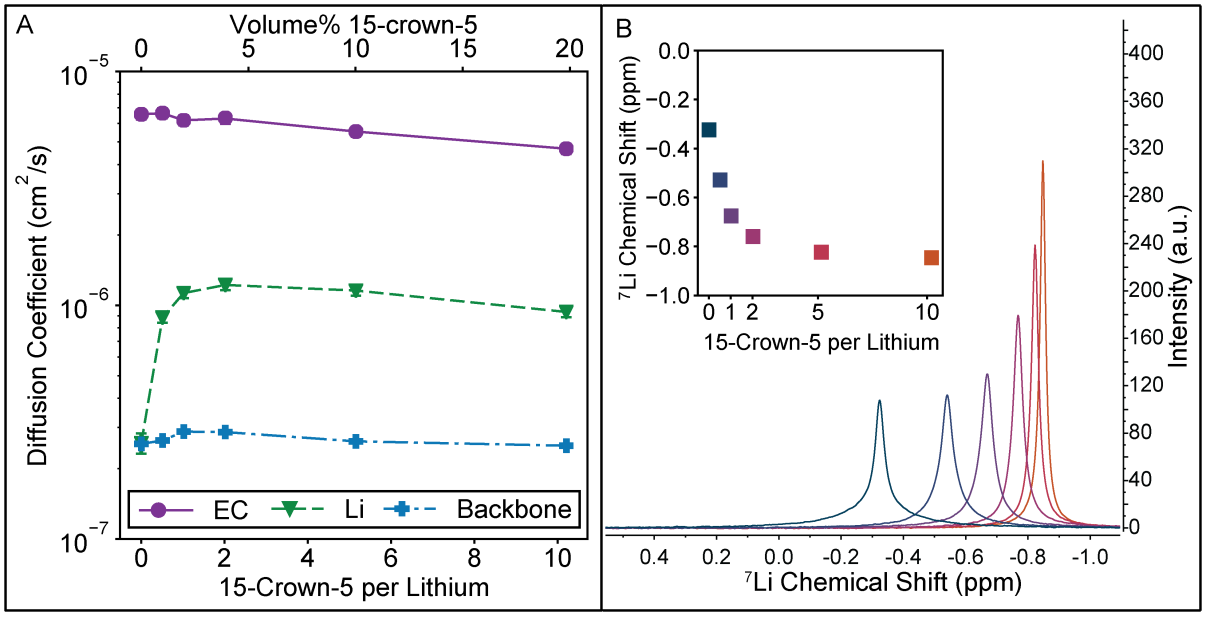

Figure 6.3. A) Diffusion coefficient for EC from the ^{1}H spectra, ^{7}Li diffusion coefficient, and polymer backbone diffusion coefficient measured from the ^{19}F spectra for the set of solutions in Figure 6.2A. Error bars, estimated from the diffusion calibration, are smaller than the data points. B) ^{7}Li spectra for each 15-crown-5 containing solution in Figure 6.2A and inset plot of the ^{7}Li peak location. With increasing crown ether content, the peak narrows and shifts upfield.

The increase in lithium diffusion is accompanied by a narrowing of the NMR peak width, as shown in Figure 6.3B. Here the ^{7}Li spectra of each solution is shown, with the chemical shift referenced to 9.7m LiCl in D_2O.[232] Each of these peaks has a nearly equivalent area. NMR peak width can be a result of numerous interactions in solution, but polymers tend to have broad peaks due to slow molecular reorientation rates in solution. For this system where lithium can either be strongly associated with a polymer or more freely moving in solution, it is reasonable to associate narrowing with an average decrease in association of the lithium with the polymer. ^{7}Li shift has also been used in previous studies on 15-crown-5 solvation with lithium, and the monotonic shift upfield is reminiscent of the trend seen for $LiClO_4$ in propylene carbonate, and other solvents.[238] Importantly, a sharp leveling off of the shift is not observed at a 1:1 ratio, and no change in the shift direction is observed. These observations would be consistent with extremely stable 1:1 complexes, or higher order (2:1) crown complexes. Together these observations on complexation and lithium diffusion indicate that the decrease in conductivity past 2:1 crown per lithium is not due to the formation of larger crown complexes, but instead is likely due to the increased viscosity at higher crown ether content.

As a proof of concept for the optimized electrolyte containing a 2:1 molar ratio of 15-crown-5 to lithium here, we fabricate a battery composed of commercially available electrode components. A graphite anode and $LiFePO_4$ cathode were purchased from MTI Inc. and a coin cell battery was fabricated using a quartz fiber separator. We note that the majority of other proposed novel electrolytes would require optimization of electrode design, as dry polymer electrolytes, swollen charged membranes, and ceramic lithium conductors must be incorporated directly within porous electrodes to achieve high energy density. An advantage of a polyelectrolyte solution is the direct applicability to already available electrode designs. In Figure 6.4, the second charge and discharge curve at C/20 is compared for an electrolyte with no additives, an electrolyte containing stabilizing additives, and the optimized 15-crown-5 containing electrolyte. Combining 15-crown-5 with the stabilizing additives achieves nearly 90% of the full theoretical capacity on the second discharge, while only 20 and 30% are achieved with no additives, or just stabilizing additives, respectively. The difference in capacity can likely be ascribed to the large increase in conductivity when 15-crown-5 is added to the electrolyte, thereby improving Li+ transport through the porous electrode and increasing active material utilization. While cyclability and rate capability are still under study, this initial result clearly demonstrates the ability of additives to enable polyelectrolyte solutions for battery application. A wide variety of sulfonated and other weakly dissociating charged polymers exist, but none have ever been tested for battery applications in solution.

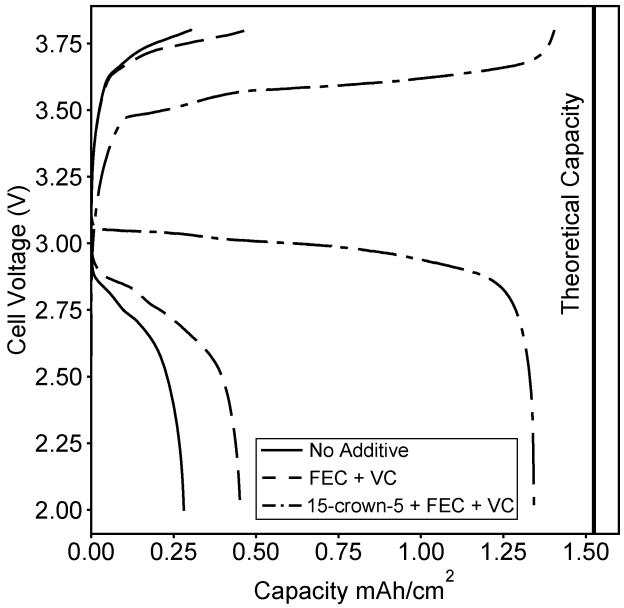

Figure 6.4. Second charge and discharge curves for batteries fabricated with the 0.1M polymer in 2:1(vol.) EC:DMC solution containing no additives, containing stabilizing additives FEC and VC, and containing 15-crown-5 and the stabilizing additives. The calculated theoretical maximum capacity of the cell is also shown.

These results also provide further motivation to fully characterize the transport properties of nonaqueous polyelectrolyte solutions utilizing fully rigorous transport theories and experiments, a significant undertaking. To date, no study has accurately measured the transference number of a lithium containing polyelectrolyte solution experimentally. Computational work in collaboration with our lab has identified a rich assortment of fundamental questions governing transport within these solutions.[225] In particular, the true transference number may vary significantly from any simple estimate due to the complex relationship between diffusion and mobility in these systems.

This complex relationship suggests that a unique opportunity exists with polyelectrolyte solutions to directly tune transference number by varying the fraction of charged groups on the polymer, changing the type of anion, or varying the solvent properties through additive engineering.

V. Conclusions

We have demonstrated that additives, particularly 15-crown-5, enable charge and discharge of a battery fabricated of commercially available electrodes and a polyelectrolyte solution that would otherwise have prohibitively low conductivity. We show that 15-crown-5 selectively solvates lithium ions in solution, allowing much higher diffusivity and thereby increasing solution conductivity. This application of crown ethers allows more direct quantification of crown to lithium ratios as compared with previous studies in membranes and is significantly different from historical applications of crown ethers in batteries which tend to increase solubility at the expense of lithium mobility. While significant work remains in quantifying the effects of crown ethers and polyelectrolytes on battery performance, we believe these initial results should spur further interest in the field. A polyelectrolyte solution could be exchanged directly with existing electrolytes in current cell designs, but also enable direct control over transference number. This could enable faster charge rates and higher energy densities, and provide better fundamental understanding of the effect of transference number on battery performance.

7. Summary and Outlook

This work discussed the creation of a high transference number polymer-based electrolyte, beginning with a fundamental study of conductivity in dry polymer electrolytes and transitioning to design in liquid polyelectrolytes. Chapter 3 employed a new polysulfone-co-poly(ethylene glycol) copolymer which was easily synthesized over a broad composition range to discover a correlation between the activation energy and prefactor in the Vogel-Tammann-Fulcher equation that is typically used to describe temperature-dependent polymer electrolyte conductivity behavior. This correlation sheds light on inherent limitations in dry polymer electrolyte conductivity beyond the single-ion conducting system studied. Primarily, any future design of a polymer electrolyte must consider the inherent tradeoff between charge carrier concentration and ion mobility. This problem has been the subject of much work in recent years, but successfully decoupling ion dynamics from the polymer without an additive, particularly for the small lithium ion has been very challenging. It is likely that discoveries in this field moving forward will be primarily the result of new chemistry, as easily dissociating anions, or anion solvating polymers are the most promising routes forward. An open question remaining specifically from this dissertation is also the fundamental origin of the compensation effect in the VTF equation, and what would dictate how different samples are correlated. Understanding these differences from a computational standpoint could inform the design of systems which are not plagued by the same effects.

The remainder of this dissertation focuses on liquid polyelectrolyte solutions, using different versions of the sulfonated polysulfone polymer. Chapters 4 and 5 are fundamental studies of transport in polyelectrolyte solutions. The first study of a charged polymer dissolved in a carbonate blend solvent demonstrated that sulfonate groups do not readily dissociate from the lithium ion, even in a high dielectric constant solvent, and even if the polymer is fully dissolved. Comparison with DMSO solutions, and with addition of salt, showed some promise for tuning salt addition to adjust conductivity and transference number, though only over a small salt range. In this chapter, NMR peak width is also shown to be a powerful tool to probe dissociation in these electrolytes due to the inherently slow nature of the polyion.

An important question from this work was therefore the relative importance of solvation of the ions versus solvation of the backbone. It is clear that the ions need to be dissociated to provide conductivity, but it is not certain whether the polymer backbone also should be well solvated by the solvent. To investigate this, a study of sulfonated polysulfone in DMSO, a good solvent for both the ions and backbone, and water, a good solvent only for the ions, was presented. This study demonstrated several interesting differences between the two systems. In water, high concentration samples tended to form gel-like phases that would not flow, although these materials had both high conductivity and transference number. In the good solvent, liquid properties are maintained at high concentration, but diffusion of both lithium and the solvent is depressed more strongly by slowing polymer chains than in water. Additional work remains to fully understand the root cause of these observations, with full rheological characterization, scattering, or theory likely necessary.

In the final chapter, a functioning polyelectrolyte solution in carbonate solvents is shown to be achieved when small amounts of 15-crown-5 are added to the electrolyte. A range of different additives were screened for this conductivity enhancement, and crown ethers were shown to provide an order of magnitude increase in conductivity. NMR peak width and diffusion measurements demonstrate this enhancement is due to dissociation of lithium from the sulfonate groups on the polymer. Final proof of concept for polyelectrolyte solutions in batteries is also demonstrated with commercial electrodes. Future work utilizing more readily dissociating anions,

combined with electrophoretic NMR measurements to accurately determine transference number should determine the ultimate potential of polyelectrolyte solutions in battery applications. Combined with theory and computation to understand the atomistic processes occurring, polyelectrolyte solutions show great promise as a means to create the next generation of lithium ion batteries.

8. References

(1) EV-Volumes.com http://www.ev-volumes.com/ (accessed Jun 27, 2019).

(2) Tarascon, J. M.; Armand, M. Issues and Challenges Facing Rechargeable Lithium Batteries. *Nature* 2001, *414* (6861), 359–367.

(3) Armand, M. B.; Tarascon, J.-M. Building Better Batteries. *Nature* 2008, *451* (7179), 652–657.

(4) Goodenough, J. B.; Kim, Y. Challenges for Rechargeable Li Batteries. *Chem. Mater.* 2010, *22* (3), 587–603.

(5) Zhang, S. S. A Review on Electrolyte Additives for Lithium-Ion Batteries. *J. Power Sources* 2006, *162*, 1379–1394.

(6) Hannan, M. A.; Lipu, M. S. H.; Hussain, A.; Mohamed, A. A Review of Lithium-Ion Battery State of Charge Estimation and Management System in Electric Vehicle Applications: Challenges and Recommendations. *Renew. Sustain. Energy Rev.* 2017, *78* (August 2016), 834–854.

(7) Whittingham, M. S. Lithium Batteries and Cathode Materials. *Chem. Rev.* 2004, *104* (607), 4271–4301.

(8) Chan, C. K.; Peng, H.; Liu, G.; McIlwrath, K.; Zhang, X. F.; Huggins, R. A.; Cui, Y. High-Performance Lithium Battery Anodes Using Silicon Nanowires. *Nat. Nanotechnol.* 2008, *3* (1), 31–35.

(9) Qian, J.; Henderson, W. A.; Xu, W.; Bhattacharya, P.; Engelhard, M.; Borodin, O.; Zhang, J.-G. High Rate and Stable Cycling of Lithium Metal Anode. *Nat. Commun.* 2015, *6*, 6362.

(10) Thackeray, M. M.; Kang, S.-H.; Johnson, C. S.; Vaughey, J. T.; Benedek, R.; Hackney, S. A. Li_2MnO_3-Stabilized $LiMO_2$ (M = Mn, Ni, Co) Electrodes for Lithium-Ion Batteries. *J. Mater. Chem.* 2007, *17* (30), 3112.

(11) Obrovac, M. N.; Chevrier, V. L. Alloy Negative Electrodes for Li-Ion Batteries. *Chem. Rev.* 2014, *114* (23).

(12) Newman, J.; Thomas-Alyea, K. E. *Electrochemical Systems*; 2004.

(13) Flamme, B.; Rodriguez Garcia, G.; Weil, M.; Haddad, M.; Phansavath, P.; Ratovelomanana-Vidal, V.; Chagnes, A. Guidelines to Design Organic Electrolytes for Lithium-Ion Batteries: Environmental Impact, Physicochemical and Electrochemical Properties. *Green Chem.* 2017, *19* (8), 1828–1849.

(14) Aurbach, D.; Gamolsky, K.; Markovsky, B.; Gofer, Y.; Schmidt, M.; Heider, U. On the Use of Vinylene Carbonate (VC) as an Additive to Electrolyte Solutions for Li-Ion Batteries. *Electrochim. Acta* 2002, *47* (9), 1423–1439.

(15) Xu, K. Nonaqueous Liquid Electrolytes for Lithium-Based Rechargeable Batteries. *Chem. Rev.* 2004, *104* (10), 4303–4418.

(16) Ue, M. Mobility and Ionic Association of Lithium and Quaternary Ammonium Salts in Propylene Carbonate and γ-Butyrolactone. *J. Electrochem. Soc.* 1994, *141* (12), 3336.

(17) Doyle, M.; Fuller, T. F.; Newman, J. The Importance of the Lithium Ion Transference Number in Lithium/Polymer Cells. *Electrochim. Acta* 1994, *39* (13), 2073–2081.

(18) Diederichsen, K. M.; McShane, E. J.; McCloskey, B. D. Promising Routes to a High Li + Transference Number Electrolyte for Lithium Ion Batteries. *ACS Energy Lett.* 2017, *2* (11), 2563–2575.

(19) Bruce, P. G.; Vincent, C. A. Steady State Current Flow in Solid Binary Electrolyte Cells. *J. Electroanal. Chem. Interfacial Electrochem.* 1987, *225* (1–2), 1–17.

(20) Balsara, N. P.; Newman, J. Relationship between Steady-State Current in Symmetric Cells

and Transference Number of Electrolytes Comprising Univalent and Multivalent Ions. *J. Electrochem. Soc.* 2015, *162* (14), A2720–A2722.
(21) Ma, Y.; Doyle, M.; Fuller, T. F.; Doeff, M. M.; De Jonghe, L. C.; Newman, J. The Measurement of a Complete Set of Transport Properties for a Concentrated Solid Polymer Electrolyte Solution. *J. Electrochem. Soc.* 1995, *142* (6), 1859.
(22) Pesko, D. M.; Timachova, K.; Bhattacharya, R.; Smith, M. C.; Villaluenga, I.; Newman, J.; Balsara, N. P. Negative Transference Numbers in Poly(Ethylene Oxide)-Based Electrolytes. *J. Electrochem. Soc.* 2017, *164* (11), E3569–E3575.
(23) Hayamizu, K.; Aihara, Y.; Arai, S. Pulse-Gradient Spin-Echo 1H, 7Li, and 19F NMR Diffusion and Ionic Conductivity Measurements of 14 Organic Electrolytes Containing $LiN(SO_2CF_3)_2$. *J. Phys. Chem. B* 1999, *103* (3), 519–524.
(24) Valøen, L. O.; Reimers, J. N. Transport Properties of $LiPF_6$-Based Li-Ion Battery Electrolytes. *J. Electrochem. Soc.* 2005, *152* (5), A882.
(25) Hayamizu, K. Temperature Dependence of Self-Diffusion Coefficients of Ions and Solvents in Ethylene Carbonate, Propylene Carbonate, and Diethyl Carbonate Single Solutions and Ethylene Carbonate + Diethyl Carbonate Binary Solutions of $LiPF_6$ Studied by NMR. *J. Chem. Eng. Data* 2012, *57* (7), 2012–2017.
(26) Kato, Y.; Hori, S.; Saito, T.; Suzuki, K.; Hirayama, M.; Mitsui, A.; Yonemura, M.; Iba, H.; Kanno, R. High-Power All-Solid-State Batteries Using Sulfide Superionic Conductors. *Nat. Energy* 2016, *1* (4), 16030.
(27) Bouchet, R.; Maria, S.; Meziane, R.; Aboulaich, A.; Lienafa, L.; Bonnet, J.; Phan, T. N. T.; Bertin, D.; Gigmes, D.; Devaux, D.; et al. Single-Ion BAB Triblock Copolymers as Highly Efficient Electrolytes for Lithium-Metal Batteries. *Nat. Mater.* 2013, *12* (5), 452–457.
(28) Villaluenga, I.; Inceoglu, S.; Jiang, X.; Chen, X. C.; Chintapalli, M.; Wang, D. R.; Devaux, D.; Balsara, N. P. Nanostructured Single-Ion-Conducting Hybrid Electrolytes Based on Salty Nanoparticles and Block Copolymers. *Macromolecules* 2017, *50* (5), 1998–2005.
(29) Murugan, R.; Thangadurai, V.; Weppner, W. Fast Lithium Ion Conduction in Garnet-Type $Li_7La_3Zr_2O_{12}$. *Angew. Chemie - Int. Ed.* 2007, *46* (41), 7778–7781.
(30) Ohtomo, T.; Hayashi, A.; Tatsumisago, M.; Tsuchida, Y.; Hama, S.; Kawamoto, K. All-Solid-State Lithium Secondary Batteries Using the $75Li_2S{\cdot}25P_2S_5$ Glass and the $70Li_2S{\cdot}30P_2S_5$ Glass–Ceramic as Solid Electrolytes. *J. Power Sources* 2013, *233*, 231–235.
(31) Kamaya, N.; Homma, K.; Yamakawa, Y.; Hirayama, M.; Kanno, R.; Yonemura, M.; Kamiyama, T.; Kato, Y.; Hama, S.; Kawamoto, K.; et al. A Lithium Superionic Conductor. *Nat. Mater.* 2011, *10* (9), 682–686.
(32) Aono, H.; Sugimoto, E.; Sadaoka, Y.; Imanaka, N.; Adachi, G. Ionic Conductivity of the Lithium Titanium Phosphate ($Li_{1+X}M_XTi_{2-X}(PO_4)_3$, M = Al, Sc, Y, and La) Systems. *J. Electrochem. Soc.* 1989, *136* (2), 590.
(33) Bruce, P. G.; West, A. R. The A-C Conductivity of Polycrystalline LISICON, $Li_{2+2x}Zn_{1-x}GeO_4$, and a Model for Intergranular Constriction Resistances. *J. Electrochem. Soc.* 1983, *130* (3), 662–669.
(34) Braga, M. H.; Ferreira, J. a.; Stockhausen, V.; Oliveira, J. E.; El-Azab, A. Novel Li_3ClO Based Glasses with Superionic Properties for Lithium Batteries. *J. Mater. Chem. A* 2014, *2* (15), 5470–5480.
(35) Kerman, K.; Luntz, A.; Viswanathan, V.; Chiang, Y.-M.; Chen, Z. Review—Practical Challenges Hindering the Development of Solid State Li-Ion Batteries. *J. Electrochem. Soc.* 2017, *164* (7), A1731–A1744.

(36) McCloskey, B. D. Attainable Gravimetric and Volumetric Energy Density of Li-S and Li-Ion Battery Cells with Solid Separator-Protected Li Metal Anodes. *J. Phys. Chem. Lett.* 2015, *6* (22), 4581–4588.
(37) Liu, W.; Liu, N.; Sun, J.; Hsu, P. C.; Li, Y.; Lee, H. W.; Cui, Y. Ionic Conductivity Enhancement of Polymer Electrolytes with Ceramic Nanowire Fillers. *Nano Lett.* 2015, *15* (4), 2740–2745.
(38) Villaluenga, I.; Wujcik, K. H.; Tong, W.; Devaux, D.; Wong, D. H. C.; DeSimone, J. M.; Balsara, N. P. Compliant Glass-Polymer Hybrid Single Ion-Conducting Electrolytes for Lithium Batteries. *Proc. Natl. Acad. Sci. U. S. A.* 2015, *113* (1), 1520394112-.
(39) Aetukuri, N. B.; Kitajima, S.; Jung, E.; Thompson, L. E.; Virwani, K.; Reich, M. L.; Kunze, M.; Schneider, M.; Schmidbauer, W.; Wilcke, W. W.; et al. Flexible Ion-Conducting Composite Membranes for Lithium Batteries. *Adv. Energy Mater.* 2015, *5* (14), 1–6.
(40) Falco, M.; Ferrari, S.; Appetecchi, G. B.; Gerbaldi, C. Managing Transport Properties in Composite Electrodes/Electrolytes for All-Solid-State Lithium-Based Batteries. *Mol. Syst. Des. Eng.* 2019.
(41) Hallinan, D. T.; Balsara, N. P. Polymer Electrolytes. *Annu. Rev. Mater. Res.* 2013, *43*, 503–525.
(42) Xue, Z.; He, D.; Xie, X. Poly(Ethylene Oxide)-Based Electrolytes for Lithium-Ion Batteries. *J. Mater. Chem. A* 2015, *3* (38), 19218–19253.
(43) MacCallum, J. R.; Vincent, C. *Polymer Electrolyte Reviews*; Elsevier Applied Science, 1989.
(44) Webb, M. A.; Jung, Y.; Pesko, D. M.; Savoie, B. M.; Yamamoto, U.; Coates, G. W.; Balsara, N. P.; Wang, Z.-G.; Miller, T. F. Systematic Computational and Experimental Investigation of Lithium-Ion Transport Mechanisms in Polyester-Based Polymer Electrolytes. *ACS Cent. Sci.* 2015, *1* (4), 198–205.
(45) Timachova, K.; Watanabe, H.; Balsara, N. P. Effect of Molecular Weight and Salt Concentration on Ion Transport and the Transference Number in Polymer Electrolytes. *Macromolecules* 2015, *48* (21), 7882–7888.
(46) Savoie, B. M.; Webb, M. A.; Miller, T. F. Enhancing Cation Diffusion and Suppressing Anion Diffusion via Lewis-Acidic Polymer Electrolytes. *J. Phys. Chem. Lett.* 2017, *8* (3), 641–646.
(47) Wong, D. H. C.; Thelen, J. L.; Fu, Y.; Devaux, D.; Pandya, A. A.; Battaglia, V. S.; Balsara, N. P.; DeSimone, J. M. Nonflammable Perfluoropolyether-Based Electrolytes for Lithium Batteries. *Proc. Natl. Acad. Sci.* 2014, *111* (9), 3327–3331.
(48) Chintapalli, M.; Timachova, K.; Olson, K. R.; Mecham, S. J.; Devaux, D.; DeSimone, J. M.; Balsara, N. P. Relationship between Conductivity, Ion Diffusion, and Transference Number in Perfluoropolyether Electrolytes. *Macromolecules* 2016, *49* (9), 3508–3515.
(49) Shah, D. B.; Nguyen, H. Q.; Grundy, L. S.; Olson, K. R.; Mecham, S. J.; DeSimone, J. M.; Balsara, N. P. Difference between Approximate and Rigorously Measured Transference Numbers in Fluorinated Electrolytes. *Phys. Chem. Chem. Phys.* 2019.
(50) Kobayashi, N.; Uchiyama, M.; Tsuchida, E. Poly[Lithium Methacrylate-Co-Oligo(Oxyethylene)Methacrylate] as a Solid Electrolyte with High Ionic Conductivity. *Solid State Ionics* 1985, *17* (4), 307–311.
(51) Klein, R. J.; Welna, D. T.; Weikel, A. L.; Allcock, H. R.; Runt, J. Counterion Effects on Ion Mobility and Mobile Ion Concentration of Doped Polyphosphazene and Polyphosphazene Ionomers. *Macromolecules* 2007, *40* (11), 3990–3995.

(52) Allcock, H. R.; Welna, D. T.; Maher, A. E. Single Ion Conductors-Polyphosphazenes with Sulfonimide Functional Groups. *Solid State Ionics* 2006, *177* (7–8), 741–747.
(53) Ganapathiappan, S.; Chen, K.; Shriver, D. F. A New Class of Cation Conductors: Polyphosphazene Sulfonates. *Macromolecules* 1988, *21*, 2299–2301.
(54) Bartels, J.; Hess, A.; Shiau, H.-S.; Allcock, H. R.; Colby, R. H.; Runt, J. Synthesis, Morphology, and Ion Conduction of Polyphosphazene Ammonium Iodide Ionomers. *Macromolecules* 2015, *48* (1), 111–118.
(55) Matsumi, N.; Sugai, K.; Ohno, H. Ion Conductive Characteristics of Alkylborane Type and Boric Ester Type Polymer Electrolytes Derived from Mesitylborane. *Macromolecules* 2003, *36* (7), 2321–2326.
(56) Liang, S.; Choi, U. H.; Liu, W.; Runt, J.; Colby, R. H. Synthesis and Lithium Ion Conduction of Polysiloxane Single-Ion Conductors Containing Novel Weak-Binding Borates. *Chem. Mater.* 2012, *24* (12), 2316–2323.
(57) Zhang, H.; Li, C.; Piszcz, M.; Coya, E.; Rojo, T.; Rodriguez-Martinez, L. M.; Armand, M. B.; Zhou, Z. Single Lithium-Ion Conducting Solid Polymer Electrolytes: Advances and Perspectives. *Chem. Soc. Rev.* 2017, *46*, 797–815.
(58) Fujinami, T.; Tokimune, A.; Mehta, M. A.; Shriver, D. F.; Rawsky, G. C. Siloxyaluminate Polymers with High Li+ Ion Conductivity. *Chem. Mater.* 1997, *9* (10), 2236–2239.
(59) Wu Xu; Siow, K. S.; Gao, Z.; Lee, S. Y. Novel Alternating Comblike Copolymer Electrolytes with Single Lithium Ionic Conduction. *Chem. Mater.* 1998, *10* (7), 1951–1957.
(60) Cowie, J. M. G. Novel Single Ion, Comb-Branched Polymer Electrolytes. *Solid State Ionics* 1999, *123* (1–4), 233–242.
(61) Baum, P.; Meyer, W. H.; Wegner, G. Novel Cation Conductors Based on Rigid-Rod Poly(p-Phenylene)S. *Polymer* 2000, *41* (3), 965–973.
(62) Wang, X.; Wang, L.; Li, H.; Tang, X.; Chang, F. Syntheses of Poly(Ethylene Oxide) Polyurethane Ionomers. *J. Appl. Polym. Sci.* 2000, *77* (1), 184–188.
(63) Sadoway, D. R.; Huang, B.; Trapa, P. E.; Soo, P. P.; Bannerjee, P.; Mayes, A. M. Self-Doped Block Copolymer Electrolytes for Solid-State, Rechargeable Lithium Batteries. *J. Power Sources* 2001, *97–98*, 621–623.
(64) Siska, D. P.; Shriver, D. F. Li+ Conductivity of Polysiloxane-Trifluoromethylsulfonamide Polyelectrolytes. *Chem. Mater.* 2001, *13* (9), 4698–4700.
(65) Xu, W.; Williams, M. D.; Angell, C. A. Novel Polyanionic Solid Electrolytes with Weak Coulomb Traps and Controllable Caps and Spacers. *Chem. Mater.* 2002, *14* (1), 401–409.
(66) Azimipour, B.; Reibel, L. C. Radical Copolymerization of Potassium 4-Vinyl Biphenyl-Thermal Behavior and Single-Ion Conductivity of the Copolymer Electrolytes Formed. *Polym. Bull.* 2002, *49*, 225–233.
(67) Snyder, J. F.; Ratner, M. A.; Shriver, D. F. Ion Conductivity of Comb Polysiloxane Polyelectrolytes Containing Oligoether and Perfluoroether Sidechains. *J. Electrochem. Soc.* 2003, *150* (8), A1090.
(68) Sun, X.-G.; Hou, J.; Kerr, J. B. Comb-Shaped Single Ion Conductors Based on Polyacrylate Ethers and Lithium Alkyl Sulfonate. *Electrochim. Acta* 2005, *50* (5), 1139–1147.
(69) Ryu, S.-W.; Trapa, P. E.; Olugebefola, S. C.; Gonzalez-Leon, J. A.; Sadoway, D. R.; Mayes, A. M. Effect of Counter Ion Placement on Conductivity in Single-Ion Conducting Block Copolymer Electrolytes. *J. Electrochem. Soc.* 2005, *152* (1), A158.
(70) Dou, S.; Zhang, S.; Klein, R. J.; Runt, J.; Colby, R. H. Synthesis and Characterization of Poly(Ethylene Glycol)-Based Single-Ion Conductors. *Chem. Mater.* 2006, *18* (18), 4288–

4295.
(71) Fragiadakis, D.; Dou, S.; Colby, R. H.; Runt, J. Molecular Mobility, Ion Mobility and Mobile Ion Concentration in Polyethylene Oxide-Based Polyurethane Ionomers. *Macromolecules* 2008, *41* (15), 5723–5728.
(72) Guhathakurta, S.; Min, K. Lithium Sulfonate Promoted Compatibilization in Single Ion Conducting Solid Polymer Electrolytes Based on Lithium Salt of Sulfonated Polysulfone and Polyether Epoxy. *Polymer* 2010, *51* (1), 211–221.
(73) Feng, S.; Shi, D.; Liu, F.; Zheng, L.; Nie, J.; Feng, W.; Huang, X.; Armand, M.; Zhou, Z. Single Lithium-Ion Conducting Polymer Electrolytes Based on Poly[(4-Styrenesulfonyl)(Trifluoromethanesulfonyl)Imide] Anions. *Electrochim. Acta* 2013, *93*, 254–263.
(74) Doyle, R. P.; Chen, X.; Macrae, M.; Srungavarapu, A.; Smith, L. J.; Gopinadhan, M.; Osuji, C. O.; Granados-Focil, S. Poly(Ethylenimine)-Based Polymer Blends as Single-Ion Lithium Conductors. *Macromolecules* 2014, *47* (10), 3401–3408.
(75) Rojas, A. A.; Inceoglu, S.; Mackay, N. G.; Thelen, J. L.; Devaux, D.; Stone, G. M.; Balsara, N. P. Effect of Lithium-Ion Concentration on Morphology and Ion Transport in Single-Ion-Conducting Block Copolymer Electrolytes. *Macromolecules* 2015, *48* (18), 6589–6995.
(76) Porcarelli, L.; Shaplov, A. S.; Salsamendi, M.; Nair, J. R.; Vygodskii, Y. S.; Mecerreyes, D.; Gerbaldi, C. Single-Ion Block Copoly(Ionic Liquid)s as Electrolytes for All-Solid State Lithium Batteries. *ACS Appl. Mater. Interfaces* 2016, *8* (16), 10350–10359.
(77) Diederichsen, K. M.; Buss, H. G.; McCloskey, B. D. The Compensation Effect in the Vogel–Tammann–Fulcher (VTF) Equation for Polymer-Based Electrolytes. *Macromolecules* 2017, *50* (10), 3831–3840.
(78) Tsuchida, E.; Ohno, H.; Kobayashi, N.; Ishizaka, H. Poly[(ω-Carboxy)Oligo(Oxyethylene) Methacrylate] as a New Type of Polymeric Solid Electrolyte for Alkali-Metal Ion Transport. *Macromolecules* 1989, *22* (4), 1771–1775.
(79) Zhou, G. Bin; Khan, I. M.; Smid, J. Solvent-Free Cation-Conducting Polysiloxane Electrolytes with Pendant Oligo(Oxyethylene) and Sulfonate Groups. *Macromolecules* 1993, *26* (9), 2202–2208.
(80) Okamoto, Y.; Yeh, T. F.; Lee, H. S.; Skotheim, T. A. Design of Alkaline Metal Ion Conducting Polymer Electrolytes. *J. Polym. Sci. Part A Polym. Chem.* 1993, *31* (10), 2573–2581.
(81) Tada, Y.; Sato, M.; Takeno, N.; Nakacho, Y.; Shigehara, K. Attempts at Lithium Single-Ionic Conduction by Anchoring Sulfonate Anions as Terminating Groups of Oligo(Oxyethylene) Side Chains in Comb-Type Polyphosphazenes. *Chem. Mater.* 1994, *6*, 27–30.
(82) Ito, K.; Nishina, N.; Ohno, H. High Lithium Ionic Conductivity of Poly(Ethylene Oxide)s Having Sulfonate Groups on Their Chain Ends. *J. Mater. Chem.* 1997, *7* (8), 1357–1362.
(83) Morris, M. A.; An, H.; Lutkenhaus, J. L.; Epps, T. H. Harnessing the Power of Plastics: Nanostructured Polymer Systems in Lithium-Ion Batteries. *ACS Energy Lett.* 2017, *2* (8), 1919–1936.
(84) Stephan, A. M. Review on Gel Polymer Electrolytes for Lithium Batteries. *Eur. Polym. J.* 2006, *42* (1), 21–42.
(85) Song, J. Y.; Wang, Y. Y.; Wan, C. C. Review of Gel-Type Polymer Electrolytes for Lithium-Ion Batteries. *J. Power Sources* 1999, *77* (2), 183–197.
(86) Appetecchi, G. B.; Croce, F.; Scrosati, B. Kinetics and Stability of the Lithium Electrode in

Poly(Methylmethacrylate)-Based Gel Electrolytes. *Electrochim. Acta* 1995, *40* (8), 991–997.
(87) Manuel Stephan, A.; Nahm, K. S. Review on Composite Polymer Electrolytes for Lithium Batteries. *Polymer* 2006, *47* (16), 5952–5964.
(88) Wang, C.; Zhang, X.-W.; Appleby, A. J. Solvent-Free Composite PEO-Ceramic Fiber/Mat Electrolytes for Lithium Secondary Cells. *J. Electrochem. Soc.* 2005, *152* (1), A205.
(89) Scrosati, B.; Croce, F.; Appetecchi, G. B.; Persi, L. Nanocomposite Polymer Electrolytes for Lithium Batteries. *Nature* 1998, *394* (6692), 456–458.
(90) Bannister, D. J.; Davies, G. R.; Ward, I. M.; McIntyre, J. E. Ionic Conductivities for Poly(Ethylene Oxide) Complexes with Lithium Salts of Monobasic and Dibasic Acids and Blends of Poly(Ethylene Oxide) with Lithium Salts of Anionic Polymers. *Polymer* 1984, *25* (9), 1291–1296.
(91) Hardy, L. C.; Shriver, D. F. Preparation and Electrical Response of Solid Polymer Electrolytes with Only One Mobile Species. *J. Am. Chem. Soc.* 1985, *107* (13), 3823–3828.
(92) Porcarelli, L.; Shaplov, A. S.; Bella, F.; Nair, J. R.; Mecerreyes, D.; Gerbaldi, C. Single-Ion Conducting Polymer Electrolytes for Lithium Metal Polymer Batteries That Operate at Ambient Temperature. *ACS Energy Lett.* 2016, *1* (4), 678–682.
(93) Chen, Y.; Ke, H.; Zeng, D.; Zhang, Y.; Sun, Y.; Cheng, H. Superior Polymer Backbone with Poly(Arylene Ether) over Polyamide for Single Ion Conducting Polymer Electrolytes. *J. Memb. Sci.* 2017, *525* (December 2016), 349–358.
(94) Lu, Q.; Fang, J.; Yang, J.; Yan, G.; Liu, S.; Wang, J. A Novel Solid Composite Polymer Electrolyte Based on Poly(Ethylene Oxide) Segmented Polysulfone Copolymers for Rechargeable Lithium Batteries. *J. Memb. Sci.* 2013, *425–426*, 105–112.
(95) Klein, R. J.; Runt, J. Plasticized Single-Ion Polymer Conductors: Conductivity, Local and Segmental Dynamics, and Interaction Parameters. *J. Phys. Chem. B* 2007, *111* (46), 13188–13193.
(96) Trapa, P. E.; Acar, M. H.; Sadoway, D. R.; Mayes, A. M. Synthesis and Characterization of Single-Ion Graft Copolymer Electrolytes. *J. Electrochem. Soc.* 2005, *152* (12), A2281–A2284.
(97) Lu, Y.; Tikekar, M.; Mohanty, R.; Hendrickson, K.; Ma, L.; Archer, L. A. Stable Cycling of Lithium Metal Batteries Using High Transference Number Electrolytes. *Adv. Energy Mater.* 2015, *5* (9), 1402073.
(98) Oh, H.; Xu, K.; Yoo, H. D.; Kim, D. S.; Chanthad, C.; Yang, G.; Jin, J.; Ayhan, I. A.; Oh, S. M.; Wang, Q. Poly(Arylene Ether)-Based Single-Ion Conductors for Lithium-Ion Batteries. *Chem. Mater.* 2016, *28* (1), 188–196.
(99) Doyle, M.; Lewittes, M. E.; Roelofs, M. G.; Perusich, S. A. Ionic Conductivity of Nonaqueous Solvent-Swollen Ionomer Membranes Based on Fluorosulfonate, Fluorocarboxylate, and Sulfonate Fixed Ion Groups. *J. Phys. Chem. B* 2001, *105* (39), 9387–9394.
(100) Doyle, M.; Wang, L.; Yang, Z.; Choi, S. K. Polymer Electrolytes Based on Ionomeric Copolymers of Ethylene with Fluorosulfonate Functionalized Monomers. *J. Electrochem. Soc.* 2003, *150* (11), D185.
(101) Schaefer, J. L.; Yanga, D. A.; Archer, L. A. High Lithium Transference Number Electrolytes via Creation of 3-Dimensional, Charged, Nanoporous Networks from Dense Functionalized Nanoparticle Composites. *Chem. Mater.* 2013, *25* (6), 834–839.
(102) Suo, L.; Hu, Y.-S.; Li, H.; Armand, M. B.; Chen, L. A New Class of Solvent-in-Salt

Electrolyte for High-Energy Rechargeable Metallic Lithium Batteries. *Nat. Commun.* 2013, *4*, 1481.
(103) Kreuer, K.-D.; Wohlfarth, A.; de Araujo, C. C.; Fuchs, A.; Maier, J. Single Alkaline-Ion (Li^+, Na^+) Conductors by Ion Exchange of Proton-Conducting Ionomers and Polyelectrolytes. *ChemPhysChem* 2011, *12* (14), 2558–2560.
(104) Videa, M.; Xu, W.; Geil, B.; Marzke, R.; Angell, C. A. High Li^+ Self-Diffusivity and Transport Number in Novel Electrolyte Solutions. *J. Electrochem. Soc.* 2001, *148* (12), A1352–A1356.
(105) Buss, H. G.; Chan, S. Y.; Lynd, N. A.; McCloskey, B. D. Nonaqueous Polyelectrolyte Solutions as Liquid Electrolytes with High Lithium Ion Transference Number and Conductivity. *ACS Energy Lett.* 2017, *2* (2), 481–487.
(106) Muthukumar, M. 50th Anniversary Perspective : A Perspective on Polyelectrolyte Solutions. *Macromolecules* 2017, *50* (24), 9528–9560.
(107) Manning, G. S. Limiting Laws and Counterion Condensation in Polyelectrolyte Solutions I. Colligative Properties. *J. Chem. Phys.* 1969, *51* (3), 924–933.
(108) Manning, G. S. Limiting Laws and Counterion Condensation in Polyelectrolyte Solutions II. Self-Diffusion of the Small Ions. *J. Chem. Phys.* 1969, *51* (8), 934–938.
(109) Manning, G. S. Limiting Laws and Counterion Condensation in Polyelectrolyte Solutions. III. An Analysis Based on the Mayer Ionic Solution Theory. *J. Chem. Phys.* 1969, *51* (8), 3249–3252.
(110) Manning, G. S. Counterion Binding in Polyelectrolyte Theory. *Acc. Chem. Res.* 1979, *12* (12), 443–449.
(111) Kamcev, J.; Paul, D. R.; Manning, G. S.; Freeman, B. D. Ion Diffusion Coefficients in Ion Exchange Membranes: Significance of Counterion Condensation. *Macromolecules* 2018, *51* (15), 5519–5529.
(112) Dobrynin, A. V. *Solutions of Charged Polymers*; Elsevier B.V., 2012; Vol. 1.
(113) De Gennes, P. G.; Pincus, P.; Velasco, R. M.; Brochard, F. Remarks on Polyelectrolyte Conformation. *J. Phys.* 1976, *37* (12), 1461–1473.
(114) Rubinstein, M.; Colby, R. H.; Dobrynin, A. V. Dynamics of Semidilute Polyelectrolyte Solutions. *Phys. Rev. Lett.* 1994, *73* (20), 2776–2779.
(115) Muthukumar, M. Dynamics of Polyelectrolyte Solutions. *J. Chem. Phys.* 1997, *107* (7), 2619–2635.
(116) Vink, H. Conductance of Polyelectrolyte Solutions, Anisotropy, and Other Anomalies. In *Physical Chemistry of Polyelectrolytes*; Radeva, T., Ed.; 2001; pp 203–222.
(117) Wandrey, C. Concentration Regimes in Polyelectrolyte Solutions. *Langmuir* 1999, *15* (12), 4069–4075.
(118) Wandrey, C.; Hunkeler, D.; Wendler, U.; Jaeger, W. Counterion Activity of Highly Charged Strong Polyelectrolytes. *Macromolecules* 2000, *33* (19), 7136–7143.
(119) Manning, G. S. On the Interpretation of Conductance Measurements in Salt-Free Polyelectrolyte Solutions with an Application to the Helix-Coil Transition of Poly(D-Glutamic Acid). *Biopolymers* 1970, *9* (12), 1543–1546.
(120) Manning, G. S. Polyelectrolytes. *Annu. Rev. Phys. Chem.* 1972, *23* (1), 117–140.
(121) Bordi, F.; Cametti, C.; Colby, R. H. Dielectric Spectroscopy and Conductivity of Polyelectrolyte Solutions. *J. Phys. Condens. Matter* 2004, *16* (49), R1423–R1463.
(122) Cametti, C. Does Electrical Conductivity of Linear Polyelectrolytes in Aqueous Solutions Follow the Dynamic Scaling Laws? A Critical Review and a Summary of the Key Relations.

Polymers 2014, *6* (4), 1207–1231.
(123) Dobrynin, A. V; Colby, R. H.; Rubinstein, M. Scaling Theory of Polyelectrolyte Solutions. *Macromolecules* 1995, *28* (6), 1859–1871.
(124) Dobrynin, A. V.; Rubinstein, M. Theory of Polyelectrolytes in Solutions and at Surfaces. *Prog. Polym. Sci.* 2005, *30* (11), 1049–1118.
(125) Barrat, J.-L.; Joanny, F. Theory of Polyelectrolyte Solutions. *Adv. Chem.* 1996
(126) Prabhu, V. M. Counterion Structure and Dynamics in Polyelectrolyte Solutions. *Curr. Opin. Colloid Interface Sci.* 2005, *10* (1–2), 2–8.
(127) Manning, G. S. Nonconvective Ionic Flow in Fixed-Charge Systems. *J. Chem. Phys.* 1967, *46* (6), 2324–2333.
(128) Manning, G. S. Molecular Theory of Counterion Conductivity and Self-Diffusion in Polyelectrolyte Solutions. *J. Chem. Phys.* 1967, *47* (6), 2010–2013.
(129) Schipper, F. J. M.; Hollander, J. G.; Leyte, J. C. Counterion Self-Diffusion in Polyelectrolyte Solutions. *J. Phys. Condens. Matter* 1997, *9* (50), 11179–11193.
(130) Schipper, F. J. M.; Leyte, J. C. Mass Transport in Polyelectrolyte Solutions. *J. Phys. Condens. Matter* 1999, *11* (6), 1409–1421.
(131) Schipper, F. J. M.; Hollander, J. G.; Leyte, J. C. The Influence of Screening of the Polyion Electrostatic Potential on the Counterion Dynamics in Polyelectrolyte Solutions. *J. Phys. Condens. Matter* 1998, *10* (41), 9207–9220.
(132) Chang, R.; Yethiraj, A. Brownian Dynamics Simulations of Salt-Free Polyelectrolyte Solutions. *J. Chem. Phys.* 2002, *116* (12), 5284.
(133) Chu, J. C.; Mak, C. H. Inter- and Intrachain Attractions in Solutions of Flexible Polyelectrolytes at Nonzero Concentration. *J. Chem. Phys.* 1999, *110* (5), 2669–2679.
(134) Huizenga, J. R.; Grieger, P. F.; Wall, F. T. Electrolytic Properties of Aqueous Solutions of Polyacrylic Acid and Sodium Hydroxide. I. Transference Experiments Using Radioactive Sodium. *J. Am. Chem. Soc.* 1950, *72* (6), 2636–2642.
(135) Dobrynin, A. V.; Rubinstein, M.; Obukhov, S. P. Cascade of Transitions of Polyelectrolytes in Poor Solvents. *Macromolecules* 1996, *29* (8), 2974–2979.
(136) Dobrynin, A. V.; Rubinstein, M. Counterion Condensation and Phase Separation in Solutions of Hydrophobic Polyelectrolytes. *Macromolecules* 2001, *34* (6), 1964–1972.
(137) Carrillo, J. Y.; Dobrynin, A. V. Detailed Molecular Dynamics Simulations of a Model NaPSS in Water. *J. Phys. Chem. B* 2010, *114* (29), 9391–9399.
(138) Bordi, F.; Cametti, C.; Gili, T. Electrical Conductivity of Aqueous Polyelectrolyte Solutions in the Presence of Counterion Condensation: The Scaling Approach Revisited. *Phys. Rev. E* 2002, *66* (2), 021803.
(139) Hara, M. Polyelectrolytes in Nonaqueous Solution. In *Polyelectrolytes Science and Technology*; Hara, M., Ed.; Marcel Dekker, 1993; pp 193–264.
(140) Hara, M. Polyelectrolytes in Nonaqueous Solutions. In *Physical Chemistry of Polyelectrolytes*; Radeva, T., Ed.; 2001; pp 245–279.
(141) Essafi, W.; Spiteri, M.-N.; Williams, C.; Boue, F. Hydrophobic Polyelectrolytes in Better Polar Solvent. Structure and Chain Conformation As Seen by SAXS and SANS. *Macromolecules* 2009, *42* (24), 9568–9580.
(142) Nishi, K.; Tochioka, S.; Hiroi, T.; Yamada, T.; Kokado, K.; Kim, T. H.; Gilbert, E. P.; Sada, K.; Shibayama, M. Structural Analysis of Lipophilic Polyelectrolyte Solutions and Gels in Low-Polar Solvents. *Macromolecules* 2015, *48* (11), 3613–3621.
(143) Smiatek, J.; Wohlfarth, A.; Holm, C. The Solvation and Ion Condensation Properties for

Sulfonated Polyelectrolytes in Different Solvents—a Computational Study. *New J. Phys.* 2014, *16* (2), 025001.
(144) Johnson, R. N.; Farnham, A. G.; Clendinning, R. A.; Hale, W. F.; Merriam, C. N. Poly(Aryl Ethers) by Nucleophilic Aromatic Substitution. I. Synthesis and Properties. *J. Polym. Sci. Part A-1 Polym. Chem.* 1967, *5* (9), 2375–2398.
(145) Viswanathan, R.; Johnson, B. C.; McGrath, J. E. Synthesis, Kinetic Observations and Characteristics of Polyarylene Ether Sulphones Prepared via a Potassium Carbonate DMAC Process. *Polymer* 1984, *25* (12), 1827–1836.
(146) Wang, F.; Hickner, M. A.; Ji, Q.; Harrison, W. L.; Mecham, J. B.; Zawodzinski, T. A.; McGrath, J. E. Synthesis of Highly Sulfonated Poly(Arylene Ether Sulfone) Random(Statistical) Copolymers via Direct Polymerization. *Macromol. Symp.* 2001, *175* (1), 387–396.
(147) Wang, F.; Hickner, M.; Kim, Y. S.; Zawodzinski, T. A.; McGrath, J. E. Direct Polymerization of Sulfonated Poly(Arylene Ether Sulfone) Random (Statistical) Copolymers: Candidates for New Proton Exchange Membranes. *J. Memb. Sci.* 2002, *197* (1–2), 231–242.
(148) Ting, Y.; Hancock, L. Preparation of Polysulfone/Poly (Ethylene Oxide) Block Copolymers. *Macromolecules* 1996, *9297* (96), 7619–7621.
(149) Kim, H. W.; Park, H. B. Gas Diffusivity, Solubility and Permeability in Polysulfone–Poly(Ethylene Oxide) Random Copolymer Membranes. *J. Memb. Sci.* 2011, *372* (1–2), 116–124.
(150) Mecham, J. B. Direct Polymerization of Sulfonated Poly (Arylene Ether) Random Copolymers and Poly (Imide) Sulfonated Poly (Arylene Ether) Segmented Copolymers : New Candidates for Proton Exchange Membrane Fuel Cell Material Systems, 2001.
(151) Harrison, W. L.; Wang, F.; Mecham, J. B.; Bhanu, V. A.; Hill, M.; Kim, Y. S.; McGrath, J. E. Influence of the Bisphenol Structure on the Direct Synthesis of Sulfonated Poly(Arylene Ether) Copolymers. I. *J. Polym. Sci. Part A Polym. Chem.* 2003, *41* (14), 2264–2276.
(152) Newman, J.; Thomas, K. E.; Hafezi, H.; Wheeler, D. R. Modeling of Lithium-Ion Batteries. *J. Power Sources* 2003, *119–121*, 838–843.
(153) Chazalviel, J.-N. Electrochemical Aspects of the Generation of Ramified Metallic Electrodeposits. *Phys. Rev. A* 1990, *42* (12), 7355–7367.
(154) Zhou, W.; Wang, S.; Li, Y.; Xin, S.; Manthiram, A.; Goodenough, J. B. Plating a Dendrite-Free Lithium Anode with a Polymer/Ceramic/Polymer Sandwich Electrolyte. *J. Am. Chem. Soc.* 2016, *138* (30), 9385–9388.
(155) Zheng, H.; Li, J.; Song, X.; Liu, G.; Battaglia, V. S. A Comprehensive Understanding of Electrode Thickness Effects on the Electrochemical Performances of Li-Ion Battery Cathodes. *Electrochim. Acta* 2012, *71*, 258–265.
(156) Tsuchida, E.; Kobayashi, N.; Ohno, H. Single-Ion Conduction in Poly[(Oligo(Oxyethylene) Methacrylate)-Co-(Alkali-Metal Methacrylates)]. *Macromolecules* 1988, *21*, 96–100.
(157) Armand, M. B. The History of Polymer Electrolytes. *Solid State Ionics* 1994, *69* (3–4), 309–319.
(158) Park, M.; Zhang, X.; Chung, M.; Less, G. B.; Sastry, A. M. A Review of Conduction Phenomena in Li-Ion Batteries. *J. Power Sources* 2010, *195* (24), 7904–7929.
(159) Zhang, S.; Dou, S.; Colby, R. H.; Runt, J. Glass Transition and Ionic Conduction in Plasticized and Doped Ionomers. *J. Non. Cryst. Solids* 2005, *351* (33), 2825–2830.

(160) Roach, D. J.; Dou, S.; Colby, R. H.; Mueller, K. T. Nuclear Magnetic Resonance Investigation of Dynamics in Poly(Ethylene Oxide)-Based Lithium Polyether-Ester-Sulfonate Ionomers. *J. Chem. Phys.* 2012, *136* (1), 014510.
(161) Fragiadakis, D.; Dou, S.; Colby, R. H.; Runt, J. Molecular Mobility and Li^+ Conduction in Polyester Copolymer Ionomers Based on Poly(Ethylene Oxide). *J. Chem. Phys.* 2009, *130* (6), 064907.
(162) Meziane, R.; Bonnet, J.-P.; Courty, M.; Djellab, K.; Armand, M. B. Single-Ion Polymer Electrolytes Based on a Delocalized Polyanion for Lithium Batteries. *Electrochim. Acta* 2011, *57*, 14–19.
(163) Inceoglu, S.; Rojas, A. A.; Devaux, D.; Chen, X. C.; Stone, G. M.; Balsara, N. P. Morphology–Conductivity Relationship of Single-Ion-Conducting Block Copolymer Electrolytes for Lithium Batteries. *ACS Macro Lett.* 2014, *3* (6), 510–514.
(164) Chen, Q.; Bao, N.; Wang, J.-H. H.; Tunic, T.; Liang, S.; Colby, R. H. Linear Viscoelasticity and Dielectric Spectroscopy of Ionomer/Plasticizer Mixtures: A Transition from Ionomer to Polyelectrolyte. *Macromolecules* 2015, *48* (22), 8240–8252.
(165) Gu, G. Y.; Bouvier, S.; Wu, C.; Laura, R.; Rzeznik, M.; Abraham, K. M. 2-Methoxyethyl (Methyl) Carbonate-Based Electrolytes for Li-Ion Batteries. *Electrochim. Acta* 2000, *45* (19), 3127–3139.
(166) Costa, L.; Gad, A. M.; Camino, G.; Cameron, G. G.; Qureshi, M. Y. Thermal and Thermooxidative Degradation of Poly(Ethylene Oxide)-Metal Salt Complexes. *Macromolecules* 1992, *25* (20), 5512–5518.
(167) Gorecki, W.; Jeannin, M.; Belorizky, E.; Roux, C.; Armand, M. B. Physical Properties of Solid Polymer Electrolyte PEO(LiTFSI) Complexes. *J. Phys. Condens. Matter* 1995, *7* (7).
(168) Klein, R. J.; Zhang, S.; Dou, S.; Jones, B. H.; Colby, R. H.; Runt, J. Modeling Electrode Polarization in Dielectric Spectroscopy: Ion Mobility and Mobile Ion Concentration of Single-Ion Polymer Electrolytes. *J. Chem. Phys.* 2006, *124* (14), 144903.
(169) Sinha, K.; Maranas, J. K. Segmental Dynamics and Ion Association in PEO-Based Single Ion Conductors. *Macromolecules* 2011, *44* (13), 5381–5391.
(170) Linert, W. The Isokinetic Relationship. VII. Statistical Analyses and Examples for Unimolecular Reaction Systems. *Inorganica Chim. Acta* 1988, *141* (2), 233–242.
(171) Yelon, A.; Movaghar, B.; Branz, H. M. Origin and Consequences of the Compensation (Meyer-Neldel) Law. *Phys. Rev. B* 1992, *46* (19), 12244–12250.
(172) Yelon, A.; Movaghar, B.; Crandall, R. S. Multi-Excitation Entropy: Its Role in Thermodynamics and Kinetics. *Reports Prog. Phys.* 2006, *69* (4), 1145–1194.
(173) Liu, L.; Guo, Q. X. Isokinetic Relationship, Isoequilibrium Relationship, and Enthalpy-Entropy Compensation. *Chem. Rev.* 2001, *101* (3), 673–695.
(174) Widenhorn, R.; Rest, A.; Bodegom, E. The Meyer-Neldel Rule for a Property Determined by Two Transport Mechanisms. *J. Appl. Phys.* 2002, *91* (10 I), 6524–6528.
(175) Wieczorek, W. Entropy Effects on Conductivity of the Blend-Based and Composite Polymer Solid Electrolytes. *Solid State Ionics* 1992, *53–56*, 1064–1070.
(176) Wieczorek, W. Temperature Dependence of Conductivity of Mixed-Phase Composite Polymer Solid Electrolytes. *Mater. Sci. Eng. B* 1992, *15* (2), 108–114.
(177) Geise, G. M.; Paul, D. R.; Freeman, B. D. Fundamental Water and Salt Transport Properties of Polymeric Materials. *Prog. Polym. Sci.* 2014, *39* (1), 1–24.
(178) Hickner, M. A. Ion-Containing Polymers : New Energy & Clean Water New Generations of Materials Are Being Sought as Solid-State. *Mater. Today* 2010, *13* (5), 34–41.

(179) Chintapalli, M.; Le, T. N. P.; Venkatesan, N. R.; Mackay, N. G.; Rojas, A. A.; Thelen, J. L.; Chen, X. C.; Devaux, D.; Balsara, N. P. Structure and Ionic Conductivity of Polystyrene-Block -Poly(Ethylene Oxide) Electrolytes in the High Salt Concentration Limit. *Macromolecules* 2016, *49* (5), 1770–1780.
(180) Devaux, D.; Bouchet, R.; Glé, D.; Denoyel, R. Mechanism of Ion Transport in PEO/LiTFSI Complexes: Effect of Temperature, Molecular Weight and End Groups. *Solid State Ionics* 2012, *227*, 119–127.
(181) Barrie, P. J. The Mathematical Origins of the Kinetic Compensation Effect: 1. the Effect of Random Experimental Errors. *Phys. Chem. Chem. Phys.* 2012, *14* (1), 318–326.
(182) Barrie, P. J. The Mathematical Origins of the Kinetic Compensation Effect: 2. the Effect of Systematic Errors. *Phys. Chem. Chem. Phys.* 2012, *14* (1), 327.
(183) Dunstan, D. J. The Role of Experimental Error in Arrhenius Plots: Self-Diffusion in Semiconductors. *Solid State Commun.* 1998, *107* (4), 159–163.
(184) Kirchheim, R.; Huang, X. Y. A Relationship between Prefactor and Activation Energy for Diffusion. *Phys. Status Solidi* 1987, *144* (1), 253–257.
(185) Mano, J. F.; Pereira, E. Data Analysis with the Vogel−Fulcher−Tammann−Hesse Equation. *J. Phys. Chem. A* 2004, *108* (49), 10824–10833.
(186) Mogurampelly, S.; Borodin, O.; Ganesan, V. Computer Simulations of Ion Transport in Polymer Electrolyte Membranes. *Annu. Rev. Chem. Biomol. Eng.* 2016, *7* (1), 349–371.
(187) Lu, M.; Runt, J.; Painter, P. An Infrared Spectrocopic Study of a Polyester Copolymer Ionomer Based on Poly(Ethylene Oxide). *Macromolecules* 2009, *42* (17), 6581–6587.
(188) Page, K. A.; Park, J. K.; Moore, R. B.; Sakai, V. G. Direct Analysis of the Ion-Hopping Process Associated with the α-Relaxation in Perfluorosulfonate Ionomers Using Quasielastic Neutron Scattering. *Macromolecules* 2009, *42* (7), 2729–2736.
(189) Xu, K.; Lam, Y.; Zhang, S. S.; Jow, T. R.; Curtis, T. B. Solvation Sheath of Li^+ in Nonaqueous Electrolytes and Its Implication of Graphite/Electrolyte Interface Chemistry. *J. Phys. Chem. C* 2007, *111* (20), 7411–7421.
(190) Winter, M.; Besenhard, J. O. J.; Spahr, M. E.; Novák, P. Insertion Electrode Materials for Rechargeable Lithium Batteries. *Adv. Mater.* 1998, *10* (10), 725–763.
(191) Cheng, X.; Pan, J.; Zhao, Y.; Liao, M.; Peng, H. Gel Polymer Electrolytes for Electrochemical Energy Storage. *Adv. Energy Mater.* 2018, *8* (7), 1702184.
(192) Tu, Z.; Choudhury, S.; Zachman, M. J.; Wei, S.; Zhang, K.; Kourkoutis, L. F.; Archer, L. A. Designing Artificial Solid-Electrolyte Interphases for Single-Ion and High-Efficiency Transport in Batteries. *Joule* 2017, 1–13.
(193) Zhao, C.-Z.; Zhang, X.-Q.; Cheng, X.-B.; Zhang, R.; Xu, R.; Chen, P.-Y.; Peng, H.-J.; Huang, J.-Q.; Zhang, Q. An Anion-Immobilized Composite Electrolyte for Dendrite-Free Lithium Metal Anodes. *Proc. Natl. Acad. Sci.* 2017, *114* (42), 11069–11074.
(194) Nagasawa, M. *Physical Chemistry of Polyelectrolyte Solutions*; 2015.
(195) *Physical Chemistry of Polyelectrolytes*; Radeva, T., Ed.; 2001.
(196) Muthukumar, M. Theory of Counter-Ion Condensation on Flexible Polyelectrolytes: Adsorption Mechanism. *J. Chem. Phys.* 2004, *120* (19), 9343–9350.
(197) Hara, M.; Wu, J.; Lee, A. H. Solution Properties of Ionomers. 2. Simple Salt Effect. *Macromolecules* 1989, *22* (2), 754–757.
(198) Holz, M.; Weingartner, H. Calibration in Accurate Spin-Echo Self-Diffusion Measurements Using ^1H and Less-Common Nuclei. *J. Magn. Reson.* 1991, *92* (1), 115–125.
(199) Holz, M.; Mao, X.; Seiferling, D.; Sacco, A. Experimental Study of Dynamic Isotope

Effects in Molecular Liquids: Detection of Translation-rotation Coupling. *J. Chem. Phys.* 1996, *104* (2), 669–679.
(200) Jerschow, A.; Müller, N. Suppression of Convection Artifacts in Stimulated-Echo Diffusion Experiments. Double-Stimulated-Echo Experiments. *J. Magn. Reson.* 1997, *125* (2), 372–375.
(201) Wu, D. H.; Chen, A. D.; Johnson, C. S. An Improved Diffusion-Ordered Spectroscopy Experiment Incorporating Bipolar-Gradient Pulses. *Journal of Magnetic Resonance, Series A*. 1995, pp 260–264.
(202) Sinnaeve, D. The Stejskal-Tanner Equation Generalized for Any Gradient Shape-an Overview of Most Pulse Sequences Measuring Free Diffusion. *Concepts Magn. Reson. Part A* 2012, *40A* (2), 39–65.
(203) Gering, K. L. Prediction of Electrolyte Conductivity: Results from a Generalized Molecular Model Based on Ion Solvation and a Chemical Physics Framework. *Electrochim. Acta* 2017, *225*, 175–189.
(204) Krachkovskiy, S. A.; Bazak, J. D.; Fraser, S.; Halalay, I. C.; Goward, G. R. Determination of Mass Transfer Parameters and Ionic Association of $LiPF_6$: Organic Carbonates Solutions. *J. Electrochem. Soc.* 2017, *164* (4), A912–A916.
(205) Jia, P.; Yang, Q.; Gong, Y.; Zhao, J. Dynamic Exchange of Counterions of Polystyrene Sulfonate. *J. Chem. Phys.* 2012, *136* (8), 084904.
(206) Bordi, F.; Cametti, C.; Gili, T. Electrical Conductivity of Polyelectrolyte Solutions in the Presence of Added Salt: The Role of the Solvent Quality Factor in Light of a Scaling Approach. *Phys. Rev. E* 2003, *68* (1), 011805.
(207) Vink, H. Investigation of Local Viscosity in Polymer Solutions by Means of Electrolytic Conductivity. *Polymer* 1982, *23* (1), 6–9.
(208) Timachova, K.; Chintapalli, M.; Olson, K. R.; Mecham, S. J.; DeSimone, J. M.; Balsara, N. P. Mechanism of Ion Transport in Perfluoropolyether Electrolytes with a Lithium Salt. *Soft Matter* 2017, *13* (32), 5389–5396.
(209) MacGregor, W. S. The Chemical and Physical Properties of DMSO. *Ann. N. Y. Acad. Sci.* 1967, *141* (1), 3–12.
(210) Naejus, R.; Lemordant, D.; Coudert, R.; Willmann, P. Excess Thermodynamic Properties of Binary Mixtures Containing Linear or Cyclic Carbonates as Solvents at the Temperatures 298.15 K and 315.15 K. *J. Chem. Thermodyn.* 1997, *29* (12), 1503–1515.
(211) Hall, D. S.; Self, J.; Dahn, J. R. Dielectric Constants for Quantum Chemistry and Li-Ion Batteries: Solvent Blends of Ethylene Carbonate and Ethyl Methyl Carbonate. *J. Phys. Chem. C* 2015, *119* (39), 22322–22330.
(212) Abbrent, S.; Greenbaum, S. Recent Progress in NMR Spectroscopy of Polymer Electrolytes for Lithium Batteries. *Curr. Opin. Colloid Interface Sci.* 2013, *18* (3), 228–244.
(213) Diederichsen, K. M.; Fong, K. D.; Terrell, R. C.; Persson, K. A.; McCloskey, B. D. Investigation of Solvent Type and Salt Addition in High Transference Number Nonaqueous Polyelectrolyte Solutions for Lithium Ion Batteries. *Macromolecules* 2018, *51* (21), 8761–8771.
(214) Nakamura, I.; Shi, A. C.; Wang, Z. G. Ion Solvation in Liquid Mixtures: Effects of Solvent Reorganization. *Phys. Rev. Lett.* 2012, *109* (25), 1–5.
(215) Pliego, J. R.; Riveros, J. M. The Cluster−Continuum Model for the Calculation of the Solvation Free Energy of Ionic Species. *J. Phys. Chem. A* 2001, *105* (30), 7241–7247.
(216) Lundberg, R. D.; Bailey, F. E.; Callard, R. W. Interactions of Inorganic Salts with

Poly(Ethylene Oxide). *J. Polym. Sci. Part A-1 Polym. Chem.* 1966, *4* (6), 1563–1577.
(217) Schipper, F. J. M.; Kassapidou, K.; Leyte, J. C. Polyelectrolyte Effects on Counterion Self-Diffusion. *J. Phys. Condens. Matter* 1997, *9* (3), 765–765.
(218) Dobrynin, A. V; Rubinstein, M. Hydrophobic Polyelectrolytes. *Macromolecules* 1999, *32* (3), 915–922.
(219) Cowie, J. M. G. *Polymers: Chemistry and Physics of Modern Materials*; 1991.
(220) Stait-Gardner, T.; Anil Kumar, P. G.; Price, W. S. Steady State Effects in PGSE NMR Diffusion Experiments. *Chem. Phys. Lett.* 2008, *462* (4–6), 331–336.
(221) Zubkov, M.; Stait-Gardner, T.; Price, W. S.; Stilbs, P. Steady State Effects in a Two-Pulse Diffusion-Weighted Sequence. *J. Chem. Phys.* 2015, *142* (15).
(222) Fuoss, R. M. Viscosity Function for Polyelectrolytes. *J. Polym. Sci.* 1948, *3* (4), 603–604.
(223) Lopez, C. G.; Richtering, W. Viscosity of Semidilute and Concentrated Nonentangled Flexible Polyelectrolytes in Salt-Free Solution. *J. Phys. Chem. B* 2019.
(224) Oostwal, M. G.; Blees, M. H.; De Bleijser, J.; Leyte, J. C. Chain Self-Diffusion in Aqueous Salt-Free Solutions of Sodium Poly(Styrenesulfonate). *Macromolecules* 1993, *26* (26), 7300–7308.
(225) Fong, K. D.; Self, J.; Diederichsen, K. M.; Wood, B. M.; McCloskey, B. D.; Persson, K. A. Ion Transport and the True Transference Number in Nonaqueous Polyelectrolyte Solutions for Lithium Ion Batteries. *ACS Cent. Sci.* 2019, 10.1021/acscentsci.9b00406.
(226) Colby, R. H.; Boris, D. C.; Krause, W. E.; Tan, J. S. Polyelectrolyte Conductivity. *J. Polym. Sci. Part B Polym. Phys.* 1997, *35* (17), 2951–2960.
(227) Hara, M.; Wu, J.; Lee, A. H. Effect of Intra- and Intermolecular Interactions on Solution Properties of Sulfonated Polystyrene Ionomers. *Macromolecules* 1988, *21* (7), 2214–2218.
(228) Truzzolillo, D.; Bordi, F.; Cametti, C.; Sennato, S. Counterion Condensation of Differently Flexible Polyelectrolytes in Aqueous Solutions in the Dilute and Semidilute Regime. *Phys. Rev. E* 2009, *79* (1), 011804.
(229) Sasaki, S.; Schipper, F. J. M. Coupled Diffusion of Segments and Counterions in Polyelectrolyte Gels and Solutions. *J. Chem. Phys.* 2001, *115* (9), 4349–4354.
(230) Zheng, Q.; Pesko, D. M.; Savoie, B. M.; Timachova, K.; Hasan, A. L.; Smith, M. C.; Miller, T. F.; Coates, G. W.; Balsara, N. P. Optimizing Ion Transport in Polyether-Based Electrolytes for Lithium Batteries. *Macromolecules* 2018, *51* (8), 2847–2858.
(231) Xu, K. Electrolytes and Interphases in Li-Ion Batteries and Beyond. *Chem. Rev.* 2014, *114* (23), 11503–11618.
(232) Harris, R. K.; Becker, E. D.; Cabral de Menezes, S. M.; Granger, P.; Hoffman, R. E.; Zilm, K. W. Further Conventions for NMR Shielding and Chemical Shifts (IUPAC Recommendations 2008). *Pure Appl. Chem.* 2008, *80* (1), 59–84.
(233) Cataldo, F. A Revision of the Gutmann Donor Numbers of a Series of Phosphoramides Including Tepa. *Eur. Chem. Bull* 2015, *4* (2), 92–97.
(234) Schauser, N. S.; Sanoja, G. E.; Bartels, J. M.; Jain, S. K.; Hu, J. G.; Han, S.; Walker, L. M.; Helgeson, M. E.; Seshadri, R.; Segalman, R. A. Decoupling Bulk Mechanics and Mono- and Multivalent Ion Transport in Polymers Based on Metal–Ligand Coordination. *Chem. Mater.* 2018, *30* (16), 5759–5769.
(235) Simon, B.; Boeuve, J.-P. Rechargeable Lithium Electrochemical Cell. 5626981, 1997.
(236) McMillan, R.; Slegr, H.; Shu, Z. .; Wang, W. Fluoroethylene Carbonate Electrolyte and Its Use in Lithium Ion Batteries with Graphite Anodes. *J. Power Sources* 1999, *81–82*, 20–26.
(237) Pedersen, C. J. Cyclic Polyethers and Their Complexes with Metal Salts. *J. Am. Chem. Soc.*

1967, *89* (26), 7017–7036.
(238) Smetana, A. J.; Popov, A. I. Lithium-7 Nuclear Magnetic Resonance and Calorimetric Study of Lithium Crown Complexes in Various Solvents. *J. Solution Chem.* 1980, *9* (3), 183–196.
(239) Morita, M.; Hayashida, H.; Matsuda, Y. Effects of Crown Ether Addition to Organic Electrolytes on the Cycling Behavior of the TiS_2 Electrode. *J. Electrochem. Soc.* 1987, *134* (9), 2107.
(240) Nagasubramanian, G.; Attia, A. I.; Halpert, G. Effects of 12-Crown-4 Ether on the Electrochemical Performance of CoO_2 and TiS_2 Cathodes in Li Polymer Electrolyte Cells. *J. Electrochem. Soc.* 1992, *139* (11), 3043.
(241) Diederichsen, K. M.; McCloskey, B. D. Electrolyte Additives to Enable Nonaqueous Polyelectrolyte Solutions for Lithium Ion Batteries. *Mol. Syst. Des. Eng.* 2019, 10.1039/C9ME00067D.